MEMBRANE TECHNOLOGY FOR OSMOTIC POWER GENERATION BY PRESSURE RETARDED OSMOSIS

WAN CHUNFENG
(B.Eng. (1st class Hons.), NUS)

A THESIS SUBMITTED
FOR THE DEGREE OF DOCTOR OF PHILOSOPHY
DEPARTMENT OF CHEMICAL AND
BIOMOLECULAR ENGINEERING
NATIONAL UNIVERSITY OF SINGAPORE

2016

Supervisor:
Professor Neal Chung Tai-Shung

Examiners:
Associate Professor Chen Shing Bor
Associate Professor Hong Liang
Professor Scott Husson, Clemson University

Declaration

I hereby declare that this dissertation is my original work and it has been written by me in its entirety. I have duly acknowledged all the sources of information which have been used in the dissertation.

This dissertation has also not been submitted for any degree in any university previously.

WAN CHUNFENG

Wan Chunfeng

11 Sep 2016

Date

Acknowledgement

This dissertation would not have been possible without the help of many people who in one way or another contributed their invaluable assistance in the progress and completion of this study.

First and foremost, my deepest gratitude to my supervisor Prof. Chung Tai-Shung who brought me into the broad area of membrane research with his consistent guidance and encouragement throughout my PhD period. He was always approachable whenever I had problems. An even more valuable treasure is his knowledge, enthusiasm and dedication that educated me over the last four years about what qualifies a researcher.

NUS Department of Chemical and Biomolecular Engineering, for providing the financial, administrative and facility support for my PhD study.

This research grant is supported by the Singapore National Research Foundation under its Environment and Water Research Programme and administered by Public Utility Board (PUB), under the following projects “Membrane Development for Osmotic Power Generation, Part 1. Materials Development and Membrane Fabrication” (1102-IRIS-11-01) and NUS grant no. R-279-000-381-279 and “Membrane Development for Osmotic Power Generation, Part 2. Module Fabrication and System Integration” (1102-IRIS-11-01) and NUS grant no. R-279-000-382-279.

My lovely lab mates including Dr. Gang Han, Dr. Sui Zhang, Dr. Xue Li, Dr. Junying Xiong Dr. Na Peng, Dr. Hangzheng Chen, Mr. Tianshi Yang, Mr. Zhenlei Cheng, Miss Bofan Li, Miss Wenxiao Gai and Mr. Fengjiang Fu for their kind help.

Table of Contents

Summary

Pressure retarded osmosis (PRO) is a promising technology to produce clean and sustainable osmotic energy from salinity gradient. During my PHD work, robust TFC hollow fiber membranes with high power density were developed. It can generate a power density of 27 W/m^2 at 20 bar using 1 M NaCl solution and DI water as feeds. We further studied the engineering and science on how to fabricate TFC hollow fiber pilot-scale modules including the formation of inner-selective polyamide layers and the repair of leakages. TFC-PES hollow fiber modules with 30% and 50% packing densities have been successfully fabricated, showing peak power densities of 20.0 W/m^2 and 19.4 W/m^2, respectively, at 20 bar using 1 M NaCl solution.

However, fresh water is scarce in Singapore. I explored alternative sources of feed solutions and draw solutions. For the first time, seawater brine from the TuaSpring desalination plant and wastewater retentate from the NEWater plant were used in a state-of-the-art TFC-PES hollow fiber membrane PRO process. It is projected that 25.6-40.7 million kWh/day of energy can be recovered globally, if the brines from SWRO are used as the draw solution and diluted to the seawater level in a PRO system. It is found that the highest power density dropped from 27 W/m^2 to 4.6 W/m^2 when wastewater retentate was used as the feed solution. Fouling on the porous substrate induced by the wastewater retentate was identified as the main cause of reduction in power density. Both ultrafiltration (UF) and nanofiltration (NF) pretreatment were employed to mitigate fouling from the wastewater retentate, and the power densities were

boosted to 6.6 W/m^2 and 8.9 W/m^2, respectively, beyond the power density of 5 W/m^2 proposed by Statkraft for the PRO process to be economical.

Detailed SWRO-PRO integrated processes were designed and presented. The governing mathematical models that describe both the mass transport on a module level and the energy flow on a system level were developed to evaluate the performances of the SWRO-PRO processes. The specific energy consumptions of three SWRO-involved processes; namely, (1) SWRO without a pressure exchanger, (2) SWRO with a pressure exchanger, and (3) SWRO with pressure exchangers and PRO are compared. The results show that the specific energy consumptions for the above three processes are 5.51, 1.79 and 1.08 kWh/(m^3 of desalinated water) for a 25% recovery SWRO plant; and 4.13, 2.27 and 1.14 kWh/(m^3 of desalinated water) for a 50% recovery SWRO plant.

The operating profit of SWRO-PRO is also studied by calculating the profit generated for every m^3 of seawater entering the process because maximizing the operating profit is the uttermost objective of the SWRO-PRO process. A strategy has been proposed to maximize the operating profit of the SWRO-PRO process while maintaining the highest power density of the PRO membranes. We concluded that integration of SWRO with PRO will not only effectively reduce the specific energy consumption of desalination by up to 35% but also increase the operating profit up to 100%.

List of Tables

List of Figures

Chapter 1: Introduction and background

1.1 Water and energy crisis

Freshwater and energy are crucial for human well-being and sustainable socio-economic development. Inadequate access to water and energy has become one of the most pervasive global problems due to the rapid increase in consumption and depletion in their reserves. Demand for freshwater and energy will continue to increase significantly in the near future to meet the needs of growing populations and economics, changing lifestyles and evolving consumption patterns, greatly amplifying existing pressures on limited natural resources and on ecosystems. It is projected that the global freshwater demand, in terms of water withdrawal, will increase by 55%, and more than 40% of the global population will live under great water stress by 2050. The global energy demand is expected to grow by more than 33% and the electricity demand is expected to grow by 70% by 2035 [1-3].

Water and energy are closely interlinked and co-dependent. Water is essential for energy generation, primarily for cooling power plants and fuel production. Energy comes from different resources and can be produced in different ways, approximately 90% of which are water intensive. On the other hand, energy powers machines for water production, transportation and distribution. Growing population, rapid industrialization and stringent requirements for water quality have driven higher energy for clean water production. The current energy consumptions to produce potable water vary from 0.37 – 0.48 kWh/m^3 to desalinate surface and groundwater to 2.58 – 8.50 kWh/m^3 to desalinate

seawater [3]. Lower energies are required to produce freshwater from surface and groundwater. However, they only constitute 0.5% of the total water on Earth. Various research technologies to convert saline water, which constitutes 97.5% of the global water resources, into drinking water are being explored [4].

The most widely used method of seawater desalination is seawater reverse osmosis (SWRO), where seawater is pushed through a semi-permeable membrane under high pressures to produce clean water. SWRO can desalinate seawater with significantly less energy than conventional distillations. In the last decade, SWRO dominated the growth of desalination capacity outside Middle East [5]. According to International Desalination Association, the total capacity of SWRO would increase from 24.73 million m^3/day in 2013 to 36.33 million m^3/day in 2016 [5]. Though the current seawater reverse osmosis (SWRO) process is highly energy-efficient, it still consumes a large amount of energy to pressurize and pump water [6-8]. SWRO also receives social resistance because the disposal of its concentrated brine has negative impacts on the environments [6-8]. Development of high-efficiency pumps and high-efficiency energy recovery devices (ERD) have significantly reduced the specific energy consumption (SEC) of desalination towards its thermodynamic minimum [6-8]. Growing demand for limited water supplies places increasing pressure on water intensive energy producers to seek alternative approaches, especially in areas where energy is competing with other major water users (agriculture, manufacturing, drinking water and sanitation services for cities). There are many opportunities for the joint development and management of water and energy infrastructure and technologies that maximize co-benefits and

minimize negative trade-offs. An array of opportunities exists to co-produce energy and water services and to exploit the benefits of synergies, such as combined power and desalination plants, combined heat and power plants, using alternative water sources for thermal power plant cooling, and even energy recovery from sewerage water.

1.2 Pressure Retarded Osmosis

Osmotic energy, as known as salinity-gradient energy, is the energy released when waters with different salinities are mixed, like rivers and oceans. The average salt concentration of seawater is 3.5% by weight, approximately equivalent to a 0.58 M NaCl solution, corresponding to an osmotic pressure of around 27 bar. The concentrations of the concentrated brine from reverse osmosis (RO) desalination plants usually range from 50 to 75 g/L, corresponding to the osmotic pressures from 40 to 65 bar [9, 10]. Approximately 0.70-0.75 kWh of energy is released when 1 m^3 of fresh water flows into the sea [11, 12]. More energy will be extracted if salt solutions with higher concentrations are used. For example, the maximum extractable energy from the mixing of 1 m^3 of fresh water with the Great Salt Lake and the Dead Sea are 10.4 and 14.1 kWh, respectively [13]. The worldwide potential of osmotic energy is reported to be 1650 TWh per year, or equivalent to approximately half the current hydropower generation [11].

Several processes, such as pressure retarded osmosis (PRO) [14], reverse electro-dialysis (RED) [15], capacitive mixing [16] and hydrogel swelling [17], are proposed to harvest the osmotic energy. PRO is the most widely investigated

process because of its greater efficiency, higher power density and potential integration with other processes. PRO extracts the Gibbs free energy of mixing by allowing water to spontaneously flow through a semi-permeable membrane from a low-salinity feed solution to a high-salinity draw solution against a hydraulic pressure [18-20]. The Gibbs free energy is converted to the hydraulic pressure of the diluted brine that can be further converted to mechanical energy by a pressure exchanger (PX) [21, 22] or electrical energy by a hydro-turbine [11, 23-25].

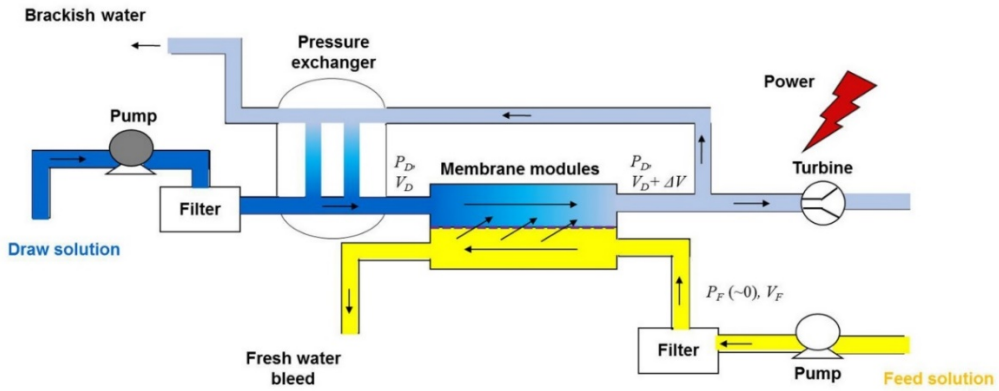

Figure 1.1 An illustration of the electrical power production by the PRO process. The system is coupled with pressure exchangers to recover the energy.

To achieve continuous and steady power generation by the PRO process, practical PRO systems can be designed as shown in Figure 1.1 [9, 23, 24]. Firstly, the concentrated draw solution, characterized by the volumetric flow rate V_D and osmotic pressure π_D, is pumped into the flow channel. The hydraulic pressure is boosted to P_D before the draw solution enters the membrane module. In the meantime, the low concentration feed solution with a volumetric flow rate of V_F and an osmotic pressure of π_F, enters the other side of the membrane module. A low hydraulic pressure of P_F (usually can be considered as 0) is applied to drive the flow. Water permeates through the membrane from the feed to the draw solution at a volumetric flux of ΔV, and is immediately pressurized.

The draw flow is diluted to be brackish water, with a hydraulic pressure of P_D and a volumetric flow rate of $V_D + \Delta V$. Part of the flow (ΔV) goes into the hydroturbine to generate electricity, and the other part (V_D) may go to a pressure exchanger to transfer the energy to the incoming fresh draw solution.

It was reported that osmotic energy could indeed be harvested under the PRO principles. However, due to the expensive and low-efficiency membranes at that time, research was slowed down in the 80s and 90s [26]. From the 1990s, membranes for desalination and wastewater treatment have advanced rapidly and have been widely commercialized. In 2009, Statkraft in Norway built the first PRO prototype plant using the commercial reverse osmosis (RO) membranes [11, 27]. The plant was shut down in 2013 partly due to the lack of effective commercial PRO membranes and extensive pretreatment needed to minimize membrane fouling [28].

Recently, the SWRO-PRO integrated process has received increasing attention [21, 22, 25, 29-32]. In the Japan Megaton Water Project, a PRO system where a maximum power density of 13.3 W/m^2 at a hydraulic pressure difference of approximately 27 bar was developed using the SWRO brine as the draw solution and freshwater as the feed [25, 33]. In this prototyped plant, hydro-turbines were used to harvest the osmotic energy. In 2014, Sarp et al. [21] and Prante et al. [22] independently proposed two modeled SWRO-PRO processes, where the high-pressure diluted seawater brine from PRO was used to pressurize the seawater feed to SWRO through a PX. Comparing with the conventional seawater-freshwater PRO process, the SWRO-PRO integrated process offers a

number of advantages [34]: (1) a higher power density is possible due to the increased difference in osmotic pressure; (2) the seawater brine has been pretreated in the SWRO system and will cause less fouling in the PRO system; (3) even though the pretreatment of the feed solution to the PRO system is still required, the overall pretreatment units can be significantly downsized if the brine is diluted to the seawater level in PRO and recycled to SWRO. Nonetheless, to take full advantages of the synergic SWRO-PRO process, strategic co-location of the SWRO plant and low salinity water sources is required during urban planning [35].

1.3 Research Objectives

Freshwater is scarce in Singapore, due to the absence of natural aquifer [13]. In this PhD work, alternative feed pairs to the PRO system are explored. The wastewater retentate (referred to as WWRe thereafter) from the wastewater plant has a salinity close to that of river water, and can be potentially used as the feed solution for a PRO process [16, 17]. Since the seawater brine (referred to as SWBr thereafter) has a higher salinity than that of seawater, theoretically more osmotic energy can be harvested by mixing the SWBr and the WWRe [2, 16-22]. Both the SWBr and WWRe streams are often regards as waste streams. The feasibility to use the waste streams for PRO power generation is investigated and potential challenges are addressed.

(1) The first challenge to use WWRe as the feed solution is the severe fouling from WWRe, which causes significant reduction in the PRO water flux and power density. Various pretreatment methods are

employed to mitigate fouling and recover the PRO membrane performance.

(2) Since the SWBr has a higher salinity and osmotic pressure, novel PRO membrane with stronger mechanical properties and PRO performance are need. By tuning the water content in the polymer dope and optimizing the interfacial polymerization, robust Thin film composite (TFC) – polyethersulfone (PES) PRO membrane with high pure water permeability, low salt permeability, small structural parameter and therefore high power density is develop.

(3) The newly developed TFC-PES hollow fiber membrane is further scaled up to 1-inch and 2-inch semi-pilot scale module to evaluate its performance on a larger scale. The protocol to develop a structured hollow fiber bundle with high packing density and to synthesize a more defect-free TFC layer on the hollow fiber substrate module is established. The semi-pilot scale module is aimed to achieve >90% of the lab scale hollow fiber module.

(4) Use SWBr as the draw solution promotes the integration of PRO with SWRO and use the osmotic energy to compensate and reduce the energy consumption of seawater desalination. Various designs of the PRO-SWRO integrated processes are designed and investigated. The design focus on both the material and energy flow between PRO and SWRO.

(5) Model that describes the internal concentration polarization, external concentration polarization, and reverse salt flux is developed to accurately describe the water and salt transfer in the PRO membrane.

(6) Model that describes the material balance and energy balance of the integrated PRO and SWRO process is developed to investigate potential material and energy integration between PRO and SWRO.

(7) Ultimately, the potential energy saving and OpEx saving by integrating PRO with SWRO is calculated. What's more, the integrated process is optimized for minimal specific energy consumption and OpEx.

References:

[1] UN-Water, Water security & the global water agenda: a UN-Water analytical Brief, UN-Water, 2013.

[2] UN-Water, UN-Water Strategy 2014-2020, UN-Water, 2013.

[3] UNWWAP, The United Nations world water development report 2014: water and energy, UN-Water, 2014.

[4] J. Kucera, Desalination: water from water, Wiley, New York, 2014.

[5] GWI, Desalination market 2010, GWI, 2010.

[6] L.F. Greenlee, D.F. Lawler, B.D. Freeman, B. Marrot, P. Moulin, Reverse osmosis desalination: water sources, technology, and today's challenges, Water research 43 (2009) 2317-2348.

[7] S. Liyanaarachchi, L. Shu, S. Muthukumaran, V. Jegatheesan, K. Baskaran, Problems in seawater industrial desalination processes and potential sustainable solutions: a review, Reviews in Environmental Science and Bio/Technology 13 (2013) 203-214.

[8] B. Peñate, L. García-Rodríguez, Current trends and future prospects in the design of seawater reverse osmosis desalination technology, Desalination 284 (2012) 1-8.

[9] S.E. Skilhagen, J.E. Dugstad, R.J. Aaberg, Osmotic power – power production based on the osmotic pressure difference between waters with varying salt gradients, Desalination 220 (2008) 476-482.

[10] A. Achilli, A.E. Childress, Pressure retarded osmosis: from the vision of Sidney Loeb to the first prototype installation – review, Desalination 261 (2010) 205-211.

[11] T. Thorsen, T. Holt, The potential for power production from salinity gradients by pressure retarded osmosis, Journal of Membrane Science 335 (2009) 103-110.

[12] N.Y. Yip, M. Elimelech, Thermodynamic and energy efficiency analysis of power generation from natural salinity gradients by pressure retarded osmosis, Environmental Science & Technology 46 (2012) 5230-5239.

[13] F. Helfer, C. Lemckert, Y.G. Anissimov, Osmotic power with pressure retarded osmosis: theory, performance and trends – a review, Journal of Membrane Science 453 (2014) 337-358.

[14] G. Han, S. Zhang, X. Li, T.S. Chung, Progress in pressure retarded osmosis (PRO) membranes for osmotic power generation, Progress in Polymer Science 51 (2015) 1-27.

[15] M. Tedesco, C. Scalici, D. Vaccari, A. Cipollina, A. Tamburini, G. Micale, Performance of the first reverse electrodialysis pilot plant for power production from saline waters and concentrated brines, Journal of Membrane Science 500 (2016) 33-45.

[16] M. Marino, L. Misuri, R. Ruffo, D. Brogioli, Electrode kinetics in the “capacitive mixing” and “battery mixing” techniques for energy production from salinity differences, Electrochimica Acta 176 (2015) 1065-1073.

[17] X. Zhu, W. Yang, M.C. Hatzell, B.E. Logan, Energy recovery from solutions with different salinities based on swelling and shrinking of hydrogels, Environmental Science & Technology 48 (2014) 7157-7163.

[18] B.E. Logan, M. Elimelech, Membrane-based processes for sustainable power generation using water, Nature 488 (2012) 313-319.

[19] T.S. Chung, S. Zhang, K.Y. Wang, J.C. Su, M.M. Ling, Forward osmosis processes: yesterday, today and tomorrow, Desalination 287 (2012) 78-81.

[20] A. Achilli, T.Y. Cath, A.E. Childress, Power generation with pressure retarded osmosis: an experimental and theoretical investigation, Journal of Membrane Science 343 (2009) 42-52.

[21] S. Sarp, I.H. Yeo, Y.G. Park, Membrane based desalination apparatus with osmotic energy recovery and membrane based desalination method with osmotic energy recovery, GS Engineer & Construction Corp, Korea, (2014).

[22] J.L. Prante, J.A. Ruskowitz, A.E. Childress, A. Achilli, RO-PRO desalination: an integrated low-energy approach to seawater desalination, Applied Energy 120 (2014) 104-114.

[23] S. Loeb, Production of energy from concentrated brines by pressure-retarded osmosis : I. preliminary technical and economic correlations, Journal of Membrane Science 1 (1976) 49-63.

[24] S. Loeb, F.V. Hessen, D. Shahaf, Production of energy from concentrated brines by pressure-retarded osmosis : II. experimental results and projected energy costs, Journal of Membrane Science 1 (1976) 249-269.

[25] K. Saito, M. Irie, S. Zaitsu, H. Sakai, H. Hayashi, A. Tanioka, Power generation with salinity gradient by pressure retarded osmosis using concentrated brine from SWRO system and treated sewage as pure water, Desalination and Water Treatment 41 (2012) 114-121.

[26] G.D. Mehta, S. Loeb, Performance of permasep B-9 and B-10 membranes in various osmotic refions and at high osmotic pressures, Journal of Membrane Science 4 (1979) 335-349.

[27] K. Gerstandt, K.V. Peinemann, S.E. Skilhagen, T. Thorsen, T. Holt, Membrane processes in energy supply for an osmotic power plant, Desalination 224 (2008) 64-70.

[28] A.P. Straub, A. Deshmukh, M. Elimelech, Pressure-retarded osmosis for power generation from salinity gradients: is it viable?, Energy & Environmental Science 9 (2016) 31-48.

[29] J. Kim, J. Lee, J.H. Kim, Overview of pressure-retarded osmosis (PRO) process and hybrid application to sea water reverse osmosis process, Desalination and Water Treatment 43 (2012) 193-200.

[30] J. Kim, M. Park, S.A. Snyder, J.H. Kim, Reverse osmosis (RO) and pressure retarded osmosis (PRO) hybrid processes: model-based scenario study, Desalination 322 (2013) 121-130.

[31] A. Achilli, J.L. Prante, N.T. Hancock, E.B. Maxwell, A.E. Childress, Experimental results from RO-PRO: a next generation system for low-energy desalination, Environmental Science & Technology 48 (2014) 6437-6443.

[32] M.H. Sharqawy, S.M. Zubair, J.H. Lienhard, Second law analysis of reverse osmosis desalination plants: an alternative design using pressure retarded osmosis, Energy 36 (2011) 6617-6626.

[33] A. Tanioka, Energy recovery by pressure retarded osmosis using concentrated brine from SWRO and treated waste water, http://www.megatonwater.com/ (2014).

[34] T.S. Chung, X. Li, R.C. Ong, Q. Ge, H. Wang, G. Han, Emerging forward osmosis (FO) technologies and challenges ahead for clean water and clean energy applications, Current Opinion in Chemical Engineering 1 (2012) 246-257.

[35] V.S. Sim, Q. She, T.H. Chong, C.Y. Tang, A.G. Fane, W.B. Krantz, Strategic co-location in a hybrid process involving desalination and pressure retarded osmosis (PRO), Membranes 3 (2013) 98-125.

Chapter 2: Mass transport, thermodynamics and membranes

2.1. Mass transfer across the PRO membranes

For an ideal semi-permeable membrane, the water permeation flux, J_w, is proportional to the driving force across the membrane and the pure water permeability (A) of the membrane [1, 2].

$$J_w = A(\Delta\pi - \Delta P) \tag{2.1}$$

However, the realistic membranes are usually asymmetric and imperfect. As shown in Figure 2.1, typical PRO membranes consist of a thin skin layer to reject salts and a thick porous layer to provide the mechanical support. Solutions within the support layer are sheltered from the shear and turbulence in the bulk crossflow solution. As a result, solute diffusion is hindered in this layer and hence its concentration is different from the bulk solution. This is referred to as internal concentration polarization (ICP). Depending on the orientation of the membrane, the operating mode can be either AL-DS where the draw solution faces the active layer, or AL-FS where the draw solution faces the support. In the AL-DS mode, the feed solutes are carried into the supporting layer by the water permeation flow and are left beneath the dense layer when water permeates through. As a result, the solute concentration beneath the dense layer is higher than that in the bulk feed. Similarly, in the AL-FS mode, the solute concentration near the inner side of the dense layer is lower than the bulk. In both cases, the effective osmotic driving force is greatly reduced. It is noted that since in the AL-FS mode the dilutive ICP is more severe for the high concentration draw solution compared to the AL-DS mode, AL-DS is most

widely applied for PRO processes. Thus, all discussions in the later context of this chapter is referred to the AL-DS or PRO mode [3].

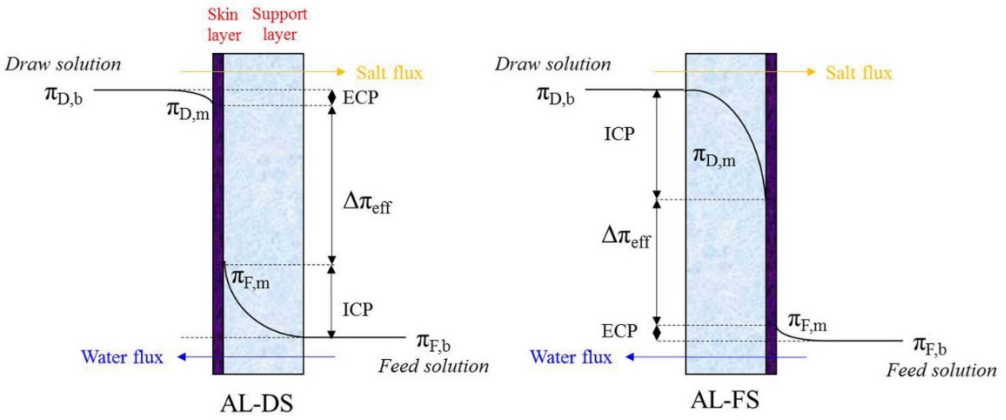

Figure 2.1 Concentration profiles in (a) AL-DS and (b) AL-FS orientated membranes.

Meanwhile, due to the imperfection of the skin layer, solutes leak from the draw solution to the feed. This is usually referred to as solute reverse flux. It causes the loss of solutes and osmolality in the draw solution. Moreover, the leaked salts are concentrated on the inner surface of the dense layer due to ICP, leading to a further decrease in the effective driving force. Another deviation from the ideal scenario is the external concentration polarization (ECP). In PRO, significant ECP may occur on the surface of the skin layer when convective water permeation flow drags solutes away from the surface, leaving the local salt concentration lower than the bulk.

Due to the combined effects of ICP, salt reverse flux and ECP, the effective osmotic pressure differential is much lower than in the ideal case. Therefore, eqn. 2.1 should be re-written as the following [3]:

$$J_w = A(\Delta\pi_{eff} - \Delta P) \tag{2.2}$$

where $\Delta\pi_{eff}$ is the effective osmotic pressure difference across the active layer of the membrane.

Lee et al. were the first to develop a model to project the performance of the PRO membrane by taking into consideration of the ICP and salt reverse flux effects [3].

$$\Delta\pi_{eff} = \frac{\pi_{D,b} - \pi_{F,b}\exp(\frac{J_w S}{D})}{1+\frac{B}{J_w}[\exp(\frac{J_w S}{D})-1]} \tag{2.3}$$

where $\pi_{D,b}$ is the bulk osmotic pressure of the draw solution, $\pi_{F,b}$ is the bulk osmotic pressure of the feed solution, D is the solute diffusivity, B is the salt permeability and S is the structural parameter of the support layer defined as follows.

$$S = \frac{\tau\lambda}{\varepsilon} \tag{2.4}$$

where τ, ε and λ are the tortuosity, porosity and thickness of the membrane support, respectively.

It can be seen from eqn. 2.3 that the effective osmotic pressure difference is reduced by both the ICP in the support layer as represented by the term $\exp(\frac{J_w S}{D})$, and the salt reverse leakage from the draw solution to the feed side, which is further deteriorated by the coupling with ICP, as is expressed by the term $\frac{B}{J_w}[\exp\left(\frac{J_w S}{D}\right) - 1]$. The reverse salt flux J_s can be calculated from the following equation.

$$J_s = \frac{B}{iRT}\left(\frac{J_w}{A} + \Delta P\right) \tag{2.5}$$

The Lee's model is extended to eqn. 2.6 by incorporating ECP within the draw solution side. The loss of draw solutes caused by salt reverse leakage and its effects on ECP in the draw side are taken into account [4]:

$$\Delta\pi_{eff} = \frac{\pi_{D,b}\exp(-\frac{J_w}{k}) - \pi_{F,b}\exp(\frac{J_w S}{D})}{1 + \frac{B}{J_w}[\exp(\frac{J_w S}{D}) - \exp(-\frac{J_w}{k})]} \tag{2.6}$$

where k is the mass transfer coefficient of the draw solution as defined below:

$$k = \frac{ShD}{d_h} \tag{2.7}$$

where d_h is the hydraulic diameter of the flow channel, Sh is the Sherwood number.

A simplified equation, which ignores the effect of draw solute loss on ECP is also used [5].

$$\Delta\pi_{eff} = \frac{\pi_{D,b}\exp(-\frac{J_w}{k}) - \pi_{F,b}\exp(\frac{J_w S}{D})}{1 + \frac{B}{J_w}[\exp(\frac{J_w S}{D}) - 1]} \tag{2.8}$$

The power density W is a measure of the energy generated per unit time and unit membrane area. It is an important performance index of the PRO membranes and systems. Power density can be calculated as the product of water flux and the hydraulic pressure difference.

$$W = J_w \Delta P \tag{2.9}$$

In the ideal case,

$$W = A(\Delta\pi - \Delta P)\Delta P \tag{2.10}$$

It achieves a maximum of $A\Delta\pi^2/4$ when $\Delta P=\Delta\pi/2$. However, complicated by the effects of ICP, ECP and reverse salt flux in reality, the maximal power density may occur at $\Delta P>\Delta\pi/2$ or $\Delta P<\Delta\pi/2$ [6].

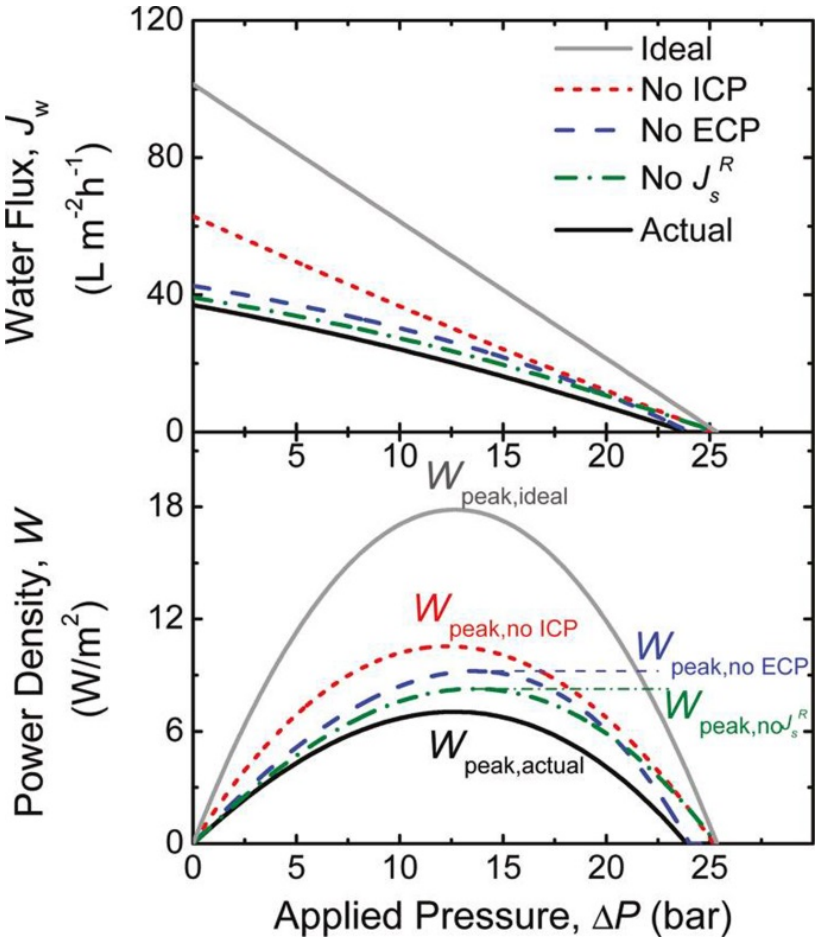

Figure 2.2 An illustration of the water flux and power density curves against hydraulic pressure in the PRO process. The effects of ECP, ICP and salt reverse diffusion on membrane performance are also demonstrated [5].

Figure 2.2 shows a theoretical illustration of the typical water flux and power density curves against hydraulic pressure in the PRO process [5]. The osmotic pressure difference between the feed and draw solutions is around 25 bar. It is seen that in the ideal case, the water flux decreases linearly against ΔP as a result of the decrement in driving force. The flux is reduced to zero when the applied pressure equals the osmotic pressure differential. Meanwhile, the power density

shows a firstly increasing and then decreasing trend. The ideal peak power density is achieved at one half of the osmotic pressure difference, or 12 – 13 bar, as predicted. However, the actual water flux and power density are much lower due to the combined effects of salt reverse flux, ECP and ICP. Three scenarios where salt reverse flux, ECP and ICP are assumed negligible are simulated respectively. An increment in water flux is immediately seen and the most substantial change is observed when ICP is neglected. It indicates that ICP is the most serious flux-reduction factor for PRO membrane processes.

2.2. Thermodynamic limits of the PRO process

While mass transfer defines how fast water moves across the membrane or how high the power density is, the thermodynamics determines the total amount of water that can be transported or the total amount of energy that can be generated.

PRO harvests the Gibbs free energy when mixing two solutions with different salinities. The Gibbs free energy released during mixing of two solutions can be calculated as follows [7, 8].

$$-\Delta G = RT\{[\sum C_i \ln(\gamma_i C_i)]_M - \phi_A[\sum C_i \ln(\gamma_i C_i)]_A - \phi_B[\sum C_i \ln(\gamma_i C_i)]_B\} \quad (2.11)$$

where C_i is the mole concentration and γ_i is the activity coefficient of species i in the solution, Φ is the total moles (or volume) of the solution to the total moles (or volume) of the system. For an ideal mixing of strong electrolyte solutions of low salt concentrations, the above equation can be simplified as follows:

$$-\Delta G = iRT[C_D^f V_D^f \ln(C_D^f) - C_D^0 V_D^0 \ln(C_D^0) + C_F^f V_F^f \ln(C_F^f) - C_F^0 V_F^0 \ln(C_F^0)] \quad (2.12)$$

where ΔG is the Gibbs free energy of mixing, C_F^0 and C_F^f are the concentrations of the feed solution before and after mixing, respectively; C_D^0 and C_D^f are the concentrations of the draw solution before and after mixing, respectively; V_F^0 and V_F^f are the flowrates of the feed solution before and after mixing, respectively; V_D^0 and V_D^f are the flowrates of the draw solution before and after mixing, respectively.

In a reversible PRO mixing process, the theoretical maximum amount of energy that can be harvested is equal to the Gibbs free energy of mixing. However, in the actual application of PRO, a constant hydraulic pressure, ΔP, is applied to the draw solution side. The osmotic pressure difference between the feed solution and the draw solution diminishes as the draw solution gets diluted and the feed solution gets concentrated. A thermodynamic equilibrium is reached and no more mixing happens when $\Delta\pi$ is reduced to ΔP. The degree of mixing is limited by the hydraulic pressure applied. Moreover, energy is lost to overcome the hydraulic resistance of the membrane. Therefore, the total amount of work that can be harvested from a constant-pressure PRO process, $W_{\Delta P}$, is less than that from a reversible mixing process [7, 8]. Yip et al. developed the following model to calculate the amount of extractable work in a constant-pressure PRO process [8].

$$W_{\Delta P} = iRT[\frac{C_D^0 V_D^0}{V_D^0 + \Delta V} - \frac{C_F^0 V_F^0}{V_F^0 - \Delta V}]\Delta V \qquad (2.13)$$

where ΔV is the total permeate volume. Based on this model, the maximum amount of energy can be extracted is as follows.

$$W_{\Delta P,\max} = iRT\left(\frac{V_F^0 V_D^0}{V_F^0 + V_D^0}\right)\left(\sqrt{C_D^0} - \sqrt{C_F^0}\right)^2 \quad (2.14)$$

Figure 2.3 presents the amount of energy that can be harvested, unutilized or lost due to friction [8]. The upper area represents the frictional losses of energy to over the hydraulic resistance of the membrane. The area enclosed by ΔV and ΔP is the amount of energy that can be harvested in a constant-pressure PRO process. With the progress of mixing, the draw solution is continuously diluted. Mixing stops when the osmotic pressure difference drops down to the value of ΔP. This leaves a great portion of osmotic energy that cannot be utilized.

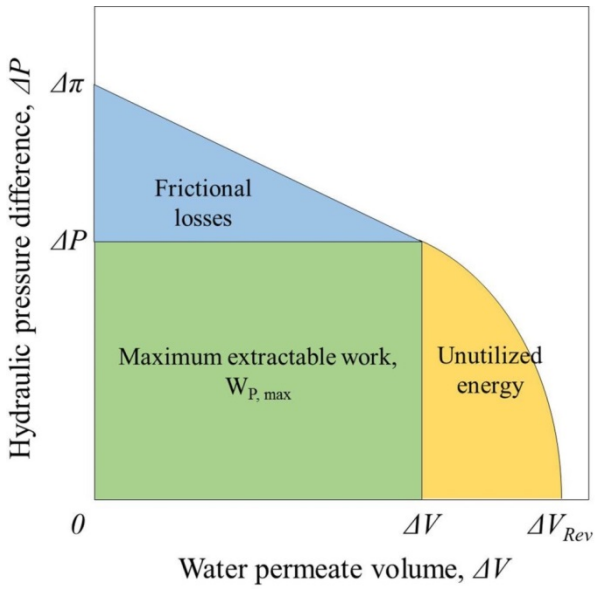

Figure 2.3 Maximum extractable work, unutilized energy and frictional losses. Redrawn from [8].

Theoretical calculation of a river water-seawater constant-pressure PRO system, represented by 1.5 and 600 mM NaCl solutions respectively, reveals that ideally the maximum extractable work is 0.75 kWh m^{-3} (per initial feed volume) when 1 m^3 of fresh water is mixed with an infinite amount of seawater. The extractable work decreases linearly when the volumetric ratio of feed and draw solutions is

reduced. In reality, as PRO progresses, the osmotic pressure difference decreases due to the dilution of draw solution and the concentration of feed solution. The effective driving force diminishes and the water flux stops before the mixing energy is fully utilized. As a result, the maximum extractable energy is reduced [8].

The mixing energy defined in eqn. 2.10 is based on the initial volume of the fresh water. Since both the fresh water and seawater requires pretreatment and pumping, specific energy is defined to characterize the energy production over the total volume of the feed and draw solutions:

$$SE = \frac{\Delta V \Delta P}{V_D^0 + V_F^0} \tag{2.15}$$

The maximum specific energy is 0.192 kWh m^{-3} for river water and seawater only if the flow rates of both solutions are designed properly [9, 10].

Osmotic energy is converted to useful works when the pressurized draw solution with increased flowrate is discharged through an energy recovery device (ERD) [11, 12] or a hydro-turbine [1, 2]. The hydro-turbine converts the osmotic energy to electricity with an efficiency of 80%-85% [1, 2]. Pressure exchanger is a highly efficient ERD that can convert 90%-96% of the pressure of the high-pressure stream to the low-pressure stream, and therefore has received increasing interests in PRO application [13,14].

2.3. Design of PRO membranes

As the heart of PRO processes, PRO membranes have received great attentions and significant progresses have been made since Loeb and Mehta tested

commercial RO membranes for PRO applications in the 70s [15]. There are mainly three key parameters determining the applications and performance of a hollow fiber membrane; namely, (1) the chemistry, mechanical and physicochemical properties of the membrane material, (2) the thickness of the functional separation or selective layer and its substructure morphology, and (3) the effective mean pore size and pore size distribution as well as the surface charge characteristics [16]. In addition to govern the intrinsic permeability and selectivity of the fiber, the physicochemical properties of the material play important roles in determining the spinnability and mechanical strengths, the inherent hydrophilicity/hydrophobicity, fouling tendency for aqueous separations, bio-compatibility for medical uses, and chemical resistance and stability for applications in harsh environments.

Once a potential material with proper physicochemical properties is chosen for membrane development, membrane scientists should molecularly design the hollow fiber membrane with a desirable pore size, narrow pore size distribution, ultrathin selective layer and open-cell substructure morphology. Figure 2.4 shows a typical dry-jet wet hollow fiber spinning line for the preparation of polymeric hollow fibers via non-solvent induced phase inversion. The hollow fiber spinning process usually consists of the following steps: (1) metering the spinning dope and bore fluid simultaneously by precision pumps separately, (2) conveying the spinning solutions through a spinneret under shear and possibly converging flows, (3) internal coagulation taking place when the bore fluid meets the polymer dope exiting from the spinneret, (4) solvent evaporation from the outer nascent membrane surface during the air-gap region, (5) moisture

induced early phase separation in the outer nascent membrane surface during the air-gap region, (6) stretch by gravity and elongation forces induced by the take-up unit, (7) fully phase inversion or solidification induced by the external non-solvent coagulation bath system, and (8) solvent exchange or additional post-treatments to remove residual solvents or prevent pores from collapsing.

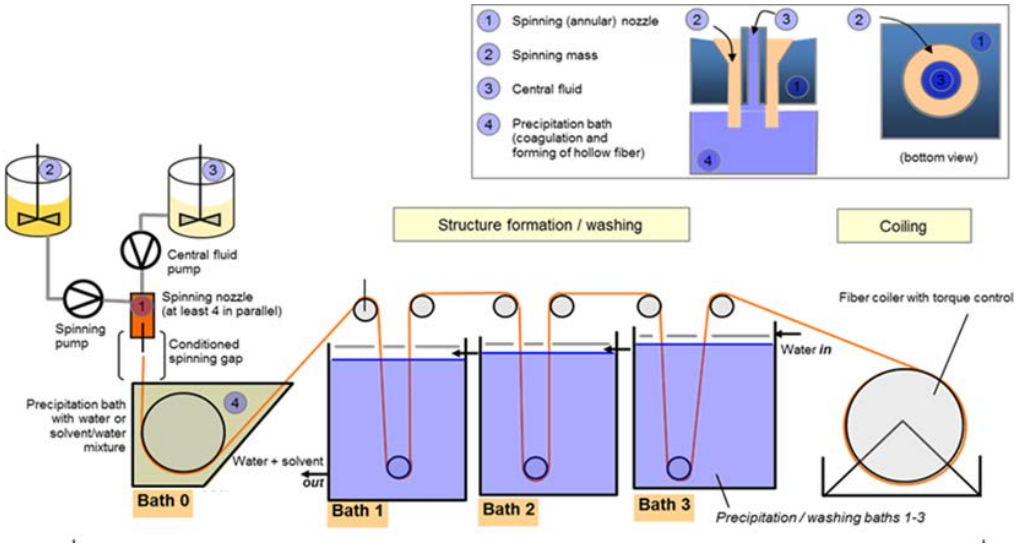

Figure 2.4: Drawing of a dry-jet wet spinning line for the preparation of polymeric hollow fibers via non-solvent induced phase inversion

Depending on the fabrication methods, two types of polymeric membranes have been successfully developed for PRO applications; namely, (1) integrally-skinned hollow fibers made from direct phase inversion and (2) thin-film composite (TFC) hollow fibers made from interfacial polymerization. Direct phase inversion involves the aforementioned non-solvent induced phase separation and subsequently forms the integrally-skinned membranes in one step. TFC membranes are generally prepared in two steps. Firstly, a porous hollow fiber substrate is prepared by means of a non-solvent induced phase inversion process and then a thin selective layer is deposited on top by

interfacial polymerization. As a result, a cross-linked aromatic polyamide selective skin is synthesized on the substrate surface [17-22].

2.3.1. Integrally-skinned PRO hollow fiber membranes

Integrally-skinned asymmetric hollow fiber membranes can be prepared by a direct dry-jet wet spinning process in one step. This type of membranes features simplified and convenient fabrication processes. The membrane company Toyobo in Japan developed a series of PRO hollow fiber membranes from cellulose triacetate (CTA) through the direct phase inversion method [23-35]. However, the details have not been disclosed. According to the reported literatures, the developed CTA fibers have an outer selective layer with an inner diameter and outer dimeter of approximately 0.1 mm and 0.2 mm, respectively. Several hundred thousands of the hollow fibers are wound in a crisscross pattern onto a perforated central tube to form a hollow fiber module [23-35]. The main problem of these integrally-skinned hollow fiber membranes is their relatively low permeability, salt rejection, and PRO performance.

2.3.2. Thin-film composite (TFC) PRO hollow fiber membranes

In the last decades, thin-film composite (TFC) membranes gained increasing considerations due to their higher water fluxes and higher power densities. Most TFC membranes are formed in-situ onto the surface of micoporous substrates via interfacial polymerization of aromatic diamine such as piperazine (PIP) and m-phenylenediamine (MPD) with acid chloride monomers such as such as trimesoyl chloride (TMC) and isophthaloyl chloride (IPC).

In order to develop effective PRO membranes, two strategies have been focused: (1) the improvements of water permeability and selectivity of TFC membranes during the formation of polyamide layers and novel post-treatment processes, and/or (2) the development of novel substrates that possess a small structural parameter and sufficient mechanical robustness. The morphology and mechanical properties of the microporous substrate are particularly important because they directly determine the quality of the polyamide layer, structural parameter, and mechanical stability of the TFC membrane under PRO operations.

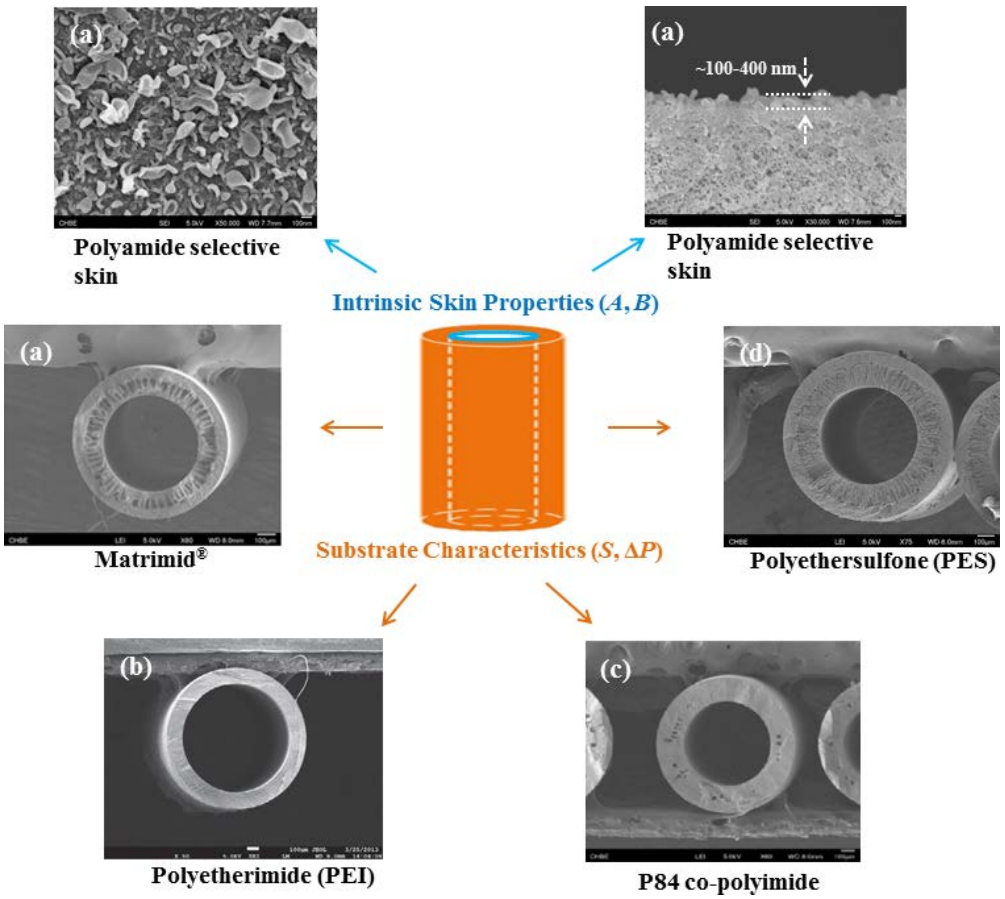

Figure 2.5 morphology of the state-of-the-art TFC hollow fiber membranes

Currently, most TFC membranes for PRO applications are inner-selective with a polyamide selective skin interfacially polymerized onto the inner surface of

fiber substrates. Figure 2.5 displays the morphology of the state-of-the-art TFC PRO hollow fiber membranes with an inner-selective skin. They have a similar polyamide selective layer, but their support fibers are made from different polymers [26-29]. The microscopic structures and morphology of the supporting fibers are also different. Currently, membranes with an *A* of up to 6 L m^{-2} h^{-1} bar^{-1}, a *B* of less than 1 L m^{-2} h^{-1}, a *S* of less than 500 μm and robust mechanical strength are readily available in the lab scale.

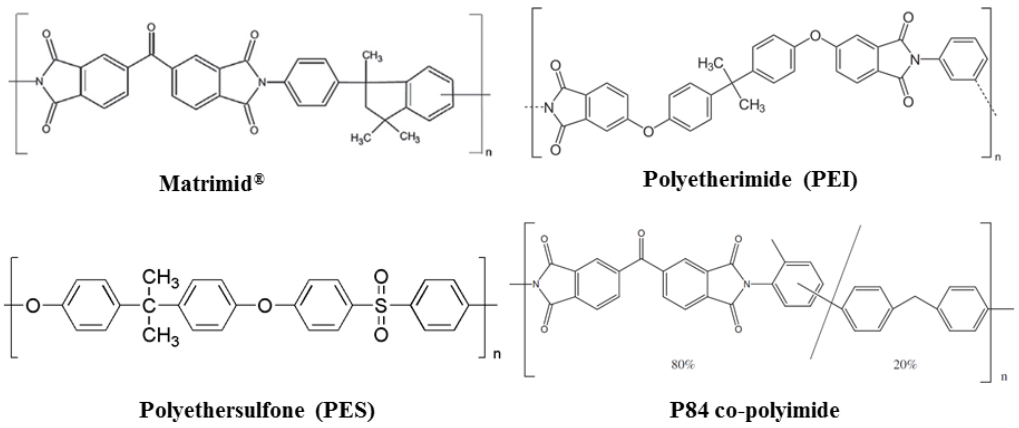

Figure 2.6 Structures of polymers used to fabricate hollow fiber substrates

The mechanical stability of the substrates determines the overall strength of the TFC hollow fiber membrane. Figure 2.6 shows the chemical structures of the polymers that have been employed to fabricate hollow fiber substrates for PRO applications. They are all intrinsically robust materials consisting of mechanically strong benzene rings. In addition to the membrane materials, the microstructure across the hollow fiber substrate should be carefully designed with a balanced asymmetry. The pore size on the inner surface should be small with a narrow pore size distribution to ensure the mechanical stability of the selective layer under high pressures. If the substrate has widely distributed pores,

it may result in a defective TFC layer with a high salt reverse flux and severe ICP under high PRO pressures [29]. In order to reduce ICP, the hollow fiber substrate should have a highly porous support layer, but be sufficiently interconnected to re-distribute the stresses and stabilize the membrane. The fiber dimension and wall thickness also significantly influence the strength and performance of the TFC-PRO membranes. The development of high performance inner selective TFC PRO hollow fiber membranes is at the interface of membrane materials science and engineering, osmotic energy and power generation. Breakthroughs in membrane materials, and hollow fiber fabrication guided by fundamental materials science, chemical engineering are essential to produce patentable and marketable high-performance membranes.

References

[1] S. Loeb, Production of energy from concentrated brines by pressure-retarded osmosis: I. preliminary technical and economic correlations, Journal of Membrane Science 1 (1976) 49-63.

[2] S. Loeb, F.V. Hessen, D. Shahaf, Production of energy from concentrated brines by pressure-retarded osmosis: II. experimental results and projected energy costs, Journal of Membrane Science 1 (1976) 249-269.

[3] J.G. Lee, Y.D. Kim, S.M. Shim, B.G. Im, W.S. Kim, Numerical study of a hybrid multi-stage vacuum membrane distillation and pressure-retarded osmosis system, Desalination 363 (2015) 82-91.

[4] N.Y. Yip, A. Tiraferri, W.A. Phillip, J.D. Schiffman, L.A. Hoover, Y.C. Kim, M. Elimelech, Thin-film composite pressure retarded osmosis membranes for sustainable power generation from salinity gradients, Environmental Science & Technology 45 (2011) 4360-4369.

[5] A. Achilli, T.Y. Cath, A.E. Childress, Power generation with pressure retarded osmosis: an experimental and theoretical investigation, Journal of Membrane Science 343 (2009) 42-52.

[6] S. Zhang, T.S. Chung, Minimizing the instant and accumulative effects of salt permeability to sustain ultrahigh osmotic power density, Environmental Science & Technology 47 (2013) 10085-10092.

[7] B.J. Feinberg, G.Z. Ramon, E.M. Hoek, Thermodynamic analysis of osmotic energy recovery at a reverse osmosis desalination plant, Environmental Science & Technology 47 (2013) 2982-2989.

[8] N.Y. Yip, M. Elimelech, Thermodynamic and energy efficiency analysis of power generation from natural salinity gradients by pressure retarded osmosis, Environmental Science & Technology 46 (2012) 5230-5239.

[9] S. Lin, A.P. Straub, M. Elimelech, Thermodynamic limits of extractable energy by pressure retarded osmosis, Energy & Environmental Science 7 (2014) 2706.

[10] A.P. Straub, A. Deshmukh, M. Elimelech, Pressure-retarded osmosis for power generation from salinity gradients: is it viable?, Energy & Environmental Science 9 (2016) 31-48.

[11] S. Sarp, Z. Y. Li, J. Saththasivam, Pressure retarded osmosis (PRO): past experiences, current developments, and future prospects, Desalination 389 (2016) 2-14.

[12] C. Aydiner, U. Sen, S. Topcu, D. Sesli, D. Ekinci, A.D. Altınay, B. Ozbey, D.Y. Koseoglu-Imer, B. Keskinler, Techno-economic investigation of water recovery and whey powder production from whey using UF/RO and FO/RO integrated membrane systems, Desalination and Water Treatment 52 (2013) 123-133.

[13] G. Migliorini, E. Luzzo, Seawater reverse osmosis plant using the pressure exchanger for energy recovery: a calculation model, Desalination 165 (2004) 289-298.

[14] R.L. Stover, Seawater reverse osmosis with isobaric energy recovery devices, Desalination 203 (2007) 168-175.

[15] G.D. Mehta, S. Loeb, Performance of permasep B-9 and B-10 membranes in various osmotic refions and at high osmotic pressures, J. Membr. Sci. 4 (1979) 335-349.

[16] Yilmaz, L. and McHugh, A.J., Analysis of nonsolvent-solvent-polymer phase diagrams and their relevance to membrane formation modelling. J. Appl. Polym. Sci., 1986. 31: p. 997-1018.

[17] Cadotte, J. E., Petersen, R.J., Larson, R.E., and Erickson, E.E., A new thin-film composite seawater reverse osmosis membrane. Desalination 1980. 32: p. 25-31.

[18] Han, G.; Cheng, Z., and Chung, T.S., Thin-film composite (TFC) hollow fiber membrane with double-polyamide active layers for internal concentration polarization and fouling mitigation in osmotic processes. J. Membr. Sci., 2017. 523: p. 497-504.

[19] Han, G., Zhao, B., Fu, F., Chung, T.S., Weber, M., Staudt, C., and Maletzko, C., High performance thin-film composite membranes with mesh-reinforced hydrophilic sulfonated polyphenylenesulfone (sPPSU) substrates for osmotically driven processes. J. Membr. Sci., 2015. 502: p. 84-93.

[20] Ghosh, A.K. and Hoek, E.M.V., Impacts of support membrane structure and chemistry on polyamide–polysulfone interfacial composite membranes. J Membr Sci, 2009. 336: p. 140-8.

[21] Kong, C.L., Kanezashi, M., Yamomoto, T., Shintani, T., and Tsuru, T., Controlled synthesis of high performance polyamide membrane with thin dense layer for water desalination. J Membr Sci 2010. 362: p. 76-80.

[22] Ghosh, A.K., Jeong, B.H., Huang, X.F., and Hoek, E.M.V., Impacts of reaction and curing conditions on polyamide composite reverse osmosis membrane properties. J Membr Sci, 2008. 311: p. 34-45.

[23] Kumano, A., Marui, K., and Terashima, Y., Hollow fiber type PRO module and its characteristics. Desalination, 2016. 389: p. 149-154.

[24] Saito, K., Irie, M., Zaitsu, S., Sakai, H., Hayashi, H., and Tanioka, A., Power generation with salinity gradient by pressure retarded osmosis using concentrated brine from SWRO system and treated sewage as pure water. Desalination and Water Treatment, 2012. 41: p. 114-121.

[25] Kurihara, M., Sakai, H., Tanioka, A., and Tomioka, H., Role of pressure-retarded osmosis (PRO) in the mega-ton water project. Desalination and Water Treatment, 2016. 57: p. 26518-26528.

[26] Chou, S., Wang, R., and Fane, A.G., Robust and high performance hollow fiber membranes for energy harvesting from salinity gradients by pressure retarded osmosis. J. Membr. Sci., 2013. 448: p. 44-54.

[27] Han, G. and Chung, T.S., Robust and high performance pressure retarded osmosis hollow fiber membranes for osmotic power generation. AIChE J, 2014. 60: p. 1107-1119.

[28] Li, X. and Chung, T.S., Thin-film composite P84 co-polyimide hollow fiber membranes for osmotic power generation. Appl Energy, 2014. 114: p. 600-610.

[29] Zhang, S., Sukitpaneenit, P., and Chung, T.S., Design of robust hollow fiber membranes with high power density for osmotic energy production. Chem Eng J, 2014. 241: p. 457-465.

Chapter 3: Experimental and methodology

3.1. Materials

Radel® A polyethersulfone (PES, Solvay Advanced Polymer, L.L.C., GA), N-methyl-2-pyrrolidone (NMP, > 99.5%, Merck), polyethylene glycol 400 (PEG, Mw = 400 g/mol, Sigma-Aldrich) and deionized (DI) water were used as the polymer, solvent, and non-solvent additive, respectively, for the fabrication of hollow fiber substrates. A 50/50 wt% mixture of glycerol (Industrial grade, Aik Moh Pains & Chemicals Pte. Ltd., Singapore) and DI water was used for the post-treatment of as-spun hollow fiber membranes. Trimesoyl chloride (TMC, >98%, Tokyo Chemical Industry, Co. Ltd., Japan), *m*-phenylenediamine (MPD, > 99%, Sigma-Aldrich), sodium dodecyl sulphate (SDS, >97%, Fluka) and hexane (>99.9%, Fisher Chemicals) were used for interfacial polymerization. Sodium chloride (NaCl, 99.5%, Merck) was used for the membrane transport characterizations and PRO performance tests. Epoxy (KSbond, Kuo Seng Enterprise, Taiwan) was purchased to cast the tubesheets of the hollow fiber modules.

3.2. Fabrication of the TFC-PES hollow fiber membranes

A dry-jet wet spinning process with the aid of co-extrusion through a dual layer spinneret, as presented in Figure 3.1, was employed to spin the PES hollow fiber substrates [1-3]. The spinning solutions and conditions have been described previously with minor modifications to ensure dope stability and improve membrane performance [4-6]. The detailed spinning parameters are shown in Table 3.1. The as-spun hollow fiber substrates were rinsed with tap water for 2

days to remove the residual solvent. The hollow fiber membranes were then posted by soaking in a 50/50 wt% glycerol/water solution for 2 days before drying in the air at room temperature. Finally, a lab-scale module with three pieces of hollow fiber substrates was made.

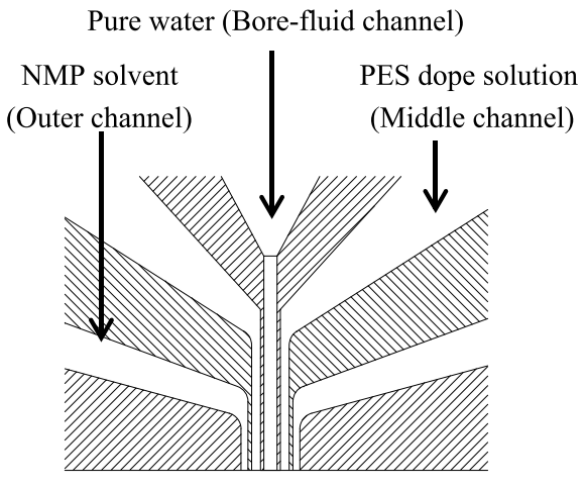

Figure 3.1 Schematic representation of the dual-layer spinneret and its dimensions employed in this study.

Spinning Parameters	PES Membrane Substrate
Bore fluid	Deionized Water
Dope composition (wt%)	20-22/36-39/36-39/1-4 (PES/PEG/NMP/Water)
Outer channel	NMP
External coagulant	Water
Outer flow rate (ml/min)	0.03 – 0.1
Inner dope flow rate (ml/min)	2.0 – 3.0
Bore fluid flow rate (ml/min)	0.8 – 1.2
Air gap length (cm)	1 – 3
Take up speed (m/min)	1 - 5
Dual layer spinneret dimension (mm)	Outer OD = 1.6 mm, Inner OD = 1.3 mm, ID = 1.14 mm

Table 3.1 Dope composition and spinning conditions of PES hollow fiber supports

The TFC-PES hollow fiber membranes were prepared via interfacial polymerization [1-4]. Firstly, a 2 wt% MPD aqueous solution containing 0.1 wt%

SDS was fed into the lumen side of hollow fibers for 3 min at a flow rate of 4.25 ml/min. After that the excessive MPD residual solution was removed by purging air for 5 min using a compressed air gun. Then a hexane solution with 0.15 wt% TMC was brought into contact with the MPD absorbed on the inner surface of the membrane at a flow rate of 2.50 ml/min for 5 min to form a thin polyamide layer. The resultant TFC-PES membranes were purged with air for 1 min to remove the residual hexane solution.

3.3. Measurements of pure water permeability (PWP or A) and salt permeability (B) of the TFC-PES membranes

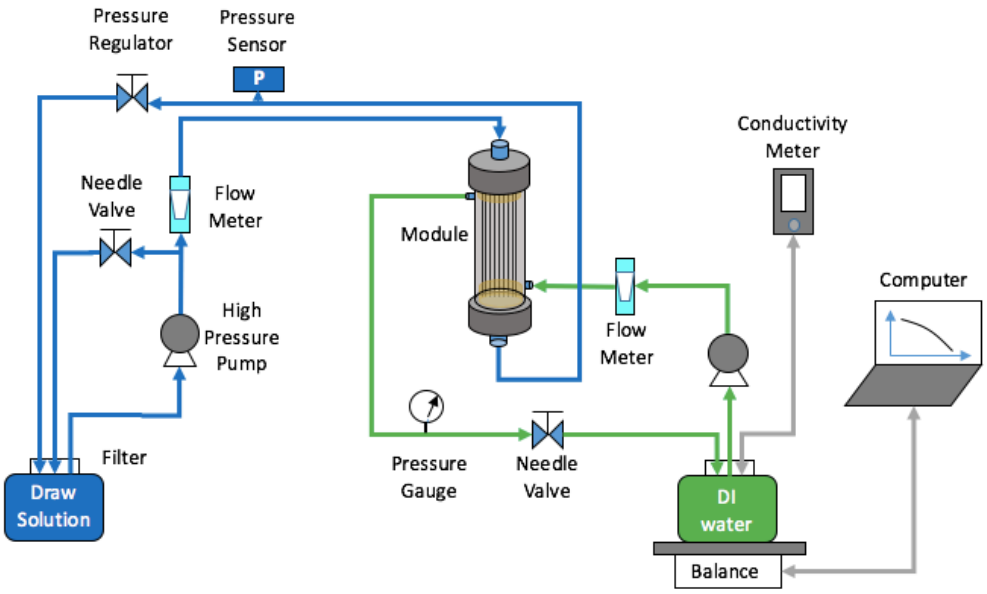

Figure 3.2 Schematic drawing of the PRO setup to test hollow fiber modules

The pure water permeability (A) and the salt permeability (B) of the TFC-PES hollow fiber modules were measured under the RO mode using the PRO setup in Figure 3.2 [6, 7].

The lumen side of the modules were pressurized with DI water and permeate was collected from the shell side. Before the tests, the TFC-PES membranes were pressurized from inside out at 20 bar using DI water for 30 min. After that, DI water was pumped into the lumen side of the hollow fiber membranes at 5 bar, 10 bar, 15 bar and 20 bar, respectively. The permeate from the shell side was collected and the PWP or A (LMH/bar) was calculated as:

$$A = \frac{\Delta V}{A_m \Delta t \Delta P_h} \tag{3.1}$$

where ΔV is the volumetric change of permeate collected over a period of Δt (h) during the test, A_m (m^2) is the effective permeation area, and ΔP_h (bar) is the transmembrane pressure difference.

The membrane rejections (R) to NaCl at 5 bar, 10 bar, 15 bar and 20 bar were obtained by using a 1000 ppm NaCl solution as the feed at the flow rate of 0.2 ml/min. The conductivities of the permeate and feed were measured to calculate R using the following equation [4]:

$$R = (1 - \frac{C_p}{C_f}) \times 100\% \tag{3.2}$$

where C_f and C_p refer to the concentrations of the feed and permeate, respectively. Salt permeability B (LMH) was then calculated using the following equation [4]:

$$B = \frac{1 - R}{R} (\Delta P_h - \Delta \pi) A \tag{3.3}$$

3.4. Osmotic power generation via the PRO process

PRO tests were conducted under the PRO mode using the PRO setup in Figure 3.2 [6, 7] with the SWBr facing the inner selective skin and the WWRe facing

the outer substrates of the TFC-PES hollow fiber membranes. After being conditioned at 20 bar with DI water for 30 min, the SWBr was pumped into the lumen side of the membrane at a flow rate of 0.2 L/min, and the WWRe was pumped into the shell side at a flow rate of 0.2 L/min. While the WWRe was maintained at the atmospheric pressure, the pressure of the SWBr was increased from the atmospheric pressure to 20 bar at an increment of 5 bar. The mass of the feed solution (i.e., WWRe) was recorded every second for 30 min using a digital data logging system. The details of operating conditions and module designs are summarized in Table 3.2.

Module Parameters		Operating Conditions	
Number of fibers	3	Temperature (˚C)	25
Fiber id (micron)	575	SWBr flowrate (L/min)	0.2
Fiber od (micron)	1025	SWBr pressure (bar)	0-20
Fiber length (cm)	15	WWRe flowrate (L/min)	0.2
Packing density	2.50%	WWRe pressure (bar)	0

Table 3.2 Summary of module parameters and operating conditions

The water permeation flux J_w (LMH) was calculated from the volumetric change of the feed solution.

$$J_W = \frac{\Delta V_f}{A_m \Delta t} \tag{3.4}$$

where ΔV_f is the volumetric change of the feed solution over a period of Δt (h) during the test.

The salt concentration in the feed solution was determined from a conductivity-concentration calibration curve. The reverse salt flux from the draw solution to the feed solution, J_s (gMH), was calculated from the following equation:

$$J_s = \frac{\Delta(C_f V_f)}{A_m \Delta t} \tag{3.5}$$

where C_f and V_f are the salt concentration and volume of the feed solution, respectively. The theoretical osmotic power density, W, was calculated from

$$W = \frac{J_w \Delta P_h}{36} \tag{3.6}$$

The denominator of 36 is to convert the unit from L·bar/(m^2·hr) to W/m^2.

References

[1] G. Han, T.S. Chung, Robust and high performance pressure retarded osmosis hollow fiber membranes for osmotic power generation, AIChE J. 60 (2014) 1107-1119.

[2] G. Han, P. Wang, T.S. Chung, Highly robust thin-film composite pressure retarded osmosis (PRO) hollow fiber membranes with high power densities for renewable salinity-gradient energy generation, Environ. Sci. Technol. 47 (2013) 8070-8077.

[3] P. Sukitpaneenit, T.S. Chung, High performance thin-film composite forward osmosis hollow fiber membranes with macrovoid-free and highly porous structure for sustainable water production, Environ. Sci. Technol. 46 (2012) 7358-7365.

[4] S. Zhang, P. Sukitpaneenit, T.-S. Chung, Design of robust hollow fiber membranes with high power density for osmotic energy production, Chem. Engin. J. 241 (2014) 457-465.

[5] S. Zhang, T.S. Chung, Minimizing the instant and accumulative effects of salt permeability to sustain ultrahigh osmotic power density, Environ. Sci. Technol. 47 (2013) 10085-10092.

[6] C.F. Wan, B. Li, T. Yang, T.S. Chung, Design and fabrication of inner-selective thin-film composite (TFC) hollow fiber modules for pressure retarded osmosis (PRO), Sep. Purif. Technol. 172 (2017) 32-42.

[7] X. Li, S. Zhang, F. Fu, T.S. Chung, Deformation and reinforcement of thin-film composite (TFC) polyamide-imide (PAI) membranes for osmotic power generation, J. Membr. Sci. 434 (2013) 204-217.

Chapter 4: Osmotic power generation by pressure retarded osmosis using seawater brine as the draw solution and wastewater retentate as the feed

4.1. Introduction

Osmotic energy from salinity gradient is a promising sustainable energy [1-5]. Pressure retarded osmosis (PRO) is one of the technologies to extract osmotic energy by allowing water to flow through a semi-permeable membrane from a low-salinity feed solution to a high-salinity draw solution against an applied hydraulic pressure [5-7]. The majority of PRO researches are focused on mixing of seawater and river water [7-12], from which up to 2.6 TW osmotic energy is projected to be produced globally [1]. However, the seawater-river water PRO system has a low energy density due to its low osmotic pressure difference [2-10]. It would become less economically feasible when substantial pretreatments are required to mitigate biofouling in both feed streams [2-5].

Freshwater is scarce in of Singapore, due to the absence of natural aquifer [13]. Four National Taps – local catchment water, imported water, reclaimed water from local waste (branded as NEWater) and desalinated water – are essential to secure water from alternative sources in Singapore [13, 14]. The five NEWater plants have a combined productivity of 273,000 m^3/d [14]. The NEWater plants receive treated wastewater effluent and further treat it with a three-stage process: microfiltration (MF), reverse osmosis (RO) and ultraviolet (UV) disinfection [15]. The wastewater retentate (referred to as WWRe thereafter) from the RO process has a salinity close to that of river water, and can be potentially used as the feed solution for a PRO process [16, 17]. The TuaSpring desalination plant

is the largest membrane-based seawater desalination facility in Singapore, with a capacity of 318,500 m^3/day [14]. It utilizes an ultrafiltration (UF) process for pretreatment and a two-stage RO process for desalination [18]. Since the seawater brine (referred to as SWBr thereafter) has a higher salinity than that of seawater, theoretically more osmotic energy can be harvested by mixing the SWBr and the WWRe [2, 16-22].

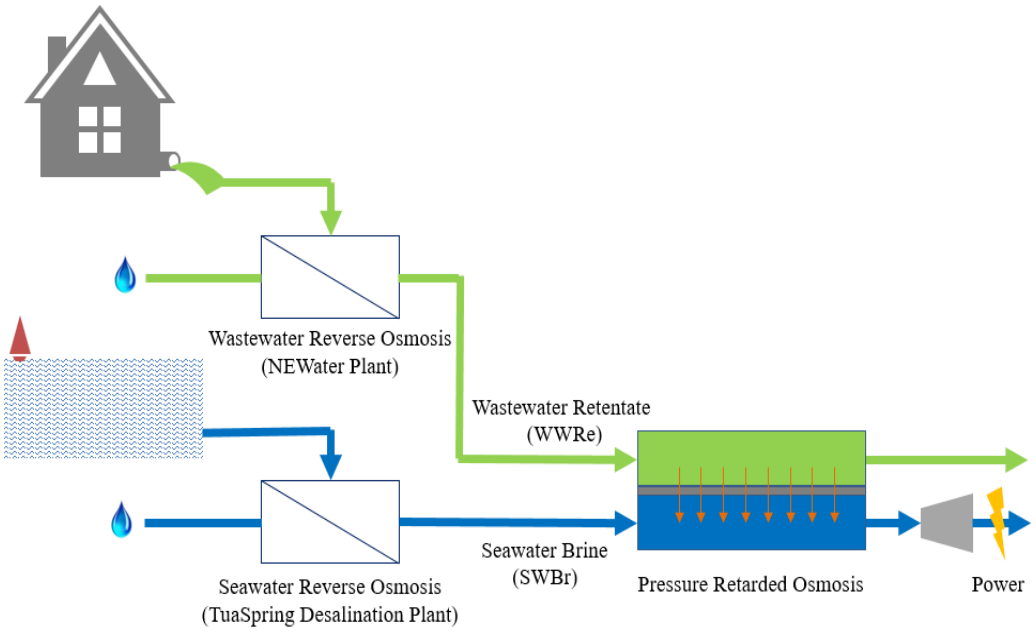

Figure 4.1 Illustration of osmotic power generation through pressure retarded osmosis (PRO) utilizing SWBr as draw solution and WWRe as feed solution

In this study, the SWBr from the first-stage RO in the TuaSpring desalination plant (the second-stage RO brine was not available for collection at the moment of this study) and the WWRe from the NEWater plant were used as the draw and feed solutions, respectively, in a state-of-the-art hollow fiber membrane PRO process in Figure 4.1. The SWRr-WWRe PRO process has the following advantages: 1) partially recover the energy consumed in the seawater reverse osmosis (SWRO) process [16, 17, 19], and 2) dilute the SWBr to mitigate the environmental impact of discharging the concentrate brine [23]. The feasibility

of such PRO process is investigated in a lab-scale setup, and potential challenges are discussed.

4.2. Experiment

4.2.1. Pretreatment of the WWRe

NADIR® UH050 flat-sheet UF and CSM® NE2540-70 flat-sheet NF membranes, whose characteristics are presented in Table 4.1, were installed on a dead-end permeation cell. The WWRe was then filled into the permeation cell and pressured to 1 bar and 2.5 bar in the UF and NF processes, respectively. The filtrates were collected and ready for further tests.

Membrane Characteristics	Membrane Code	
	UH050	NE2540-70
Material	Polyethersulfone	Polyamide
PWP (LMH/bar)	83.3	4.32
MWCO (Da)	50,000	200
NaCl Rejection (%)	N.A.	40-70
$MgSO_4$ Rejection (%)	N.A.	99.5

Table 4.1 Characteristics of the UH050 UF and NE2540-70 NF membranes

4.2.2. Characterization of the SWBr, original WWRe, WWRe UF and NF filtrates

The osmolality, pH, and total organic carbon (TOC) of both the SWBr and the WWRe were measured by an osmometer (model 3250, Advanced Instruments, Inc.), a pH meter (Accumet AP84, Fisher Scientific, Co.) and a TOC analyzer (TOC ASI5000A, Shimadzu, Corp.), respectively.

A 100 ml hexane solution was used to extract the substances from 300 ml WWRe, and was subsequently concentrated to 10 ml. The concentrate was then sent for nominal mass analysis (micrOTOFQII, Brucker, Corp.).

Moreover, the original WWRe and the filtrates from the UF and NF processes were sent for inductively coupled plasma (ICP) analysis (Dual-view Optima 5300 DV ICP-OES system, PerkinElmer Optoelectronics, Pte Ltd.) and ion chromatography (IC) analysis (940 Professional IC Vario, Metrohm, Pte Ltd.) to determine the concentrations of metal cations and anions in the solutions, respectively.

4.3. Simulation

4.3.1. Fluid dynamics and material transport along the axial direction of the membrane in the PRO process

Under the current operating conditions, there was a significant hydraulic resistance for the draw solution to flow inside the hollow fiber membranes. It has been experimentally verified that the Hagen-Poiseuille equation provides a good approximation of pressure loss over a wide range of flow conditions inside the hollow fiber membranes [24]:

$$\Delta P_{Lumen} = \frac{128 \nu Q_D L}{\pi d^4} \tag{4.1}$$

where ν and Q_D are the kinematic viscosity and volumetric flow rate of the draw solution, respectively; L and d are the effective length and inner diameter of the hollow fiber membranes, respectively. On the other hand, the pressure loss on the shell side can be calculated from the Ergun Equation [25]:

$$\Delta P_{Shell} = \frac{\rho L V_s^2 \phi}{d_p (1-\phi)^3} \left(\frac{150 \phi \mu}{d_p V_s \rho} + 1.75 \right) \tag{4.2}$$

where ρ, V_s and μ are the density, superficial velocity and dynamic viscosity of the feed solution, respectively; d_p is the hydraulic diameter of the hollow fibers

and ϕ is the packing density of the module. Due to the low packing density ($\phi \rightarrow 0$) inside the module, the pressure drop of the feed solution along the shell side can be neglected.

As shown in Figure 4.2, a counter-current flow configuration was employed in the tests. The flow direction of the feed solution was arbitrarily chosen as the positive direction.

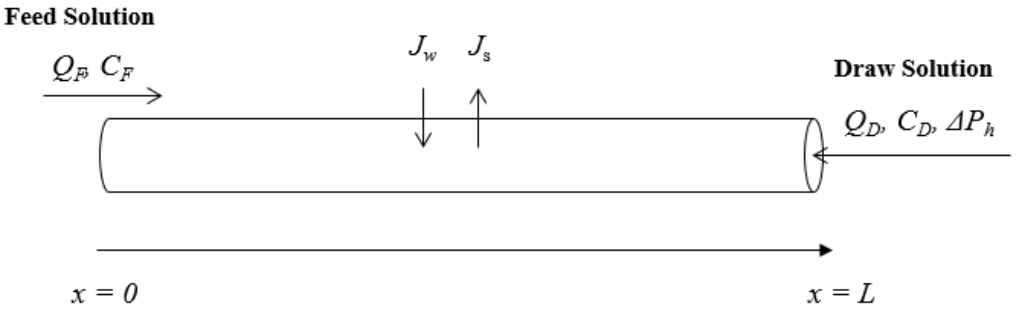

Figure 4.2 Schematic drawing of the PRO process in a single hollow fiber. The feed solution at atmospheric pressure, flowing in the positive direction, enters the shell side at x=0 with a flow rate of Q_F and a salt concentration of C_F. The draw solution at a hydraulic pressure of ΔP_h, flowing in the negative direction, enters the hollow fiber at x=L with a flow rate of Q_D and a salt concentration of C_D. Water flux, J_w, is driven from the feed to the draw solution, while the reverse salt flux, J_s, diffuses from the draw to the feed solution.

$$\frac{dQ_F}{dx} = -J_w(\pi d) \tag{4.3}$$

$$\frac{d(Q_F C_F)}{dx} = J_s(\pi d) \tag{4.4}$$

$$\frac{dQ_D}{dx} = -J_w(\pi d) \tag{4.5}$$

$$\frac{d(Q_D C_D)}{dx} = J_s(\pi d) \tag{4.6}$$

$$\frac{d\Delta P_h}{dx} = \frac{128\nu Q_D}{\pi d^4} \tag{4.7}$$

The sign of Eq. 4.3 & 4.5 is negative and the signs of Eq. 4.4 & 4.6 are positive because the draw solution flow in the opposite direction of the feed solution. The computational flow diagram is demonstrated in Figure 4.3. Eq. 4.3-4.7 are integrated from the entry of the feed solution ($x=0$) to the exit of the feed solution ($x=L$), as shown in Figure 4.2, using the finite element method, with the boundary conditions $Q_F(0) = Q_F$, $C_F(0) = C_F$, $Q_D(L) = Q_D$, $C_D(L) = C_D$ and $\Delta P_h(L) = \Delta P_h$. Initial guesses are given to $Q_D(0)$, $C_D(0)$ and $\Delta P_h(0)$, and iterations of trial and error are carried out until the relative errors of $Q_D(L)$, $C_D(L)$ and $\Delta P_h(L)$ are less than 10^{-6}. The operating conditions of the PRO system are summarized in Table 4.2.

Module Parameters		Operating Conditions	
Number of fibers	3	Temperature (˚C)	25
Fiber id (micron)	575	SWBr flowrate (L/min)	0.2
Fiber od (micron)	1025	SWBr pressure (bar)	0-20
Fiber length (cm)	15	WWRe flowrate (L/min)	0.2
Packing density	2.50%	WWRe pressure (bar)	0

Table 4.2 Summary of module parameters and operating conditions

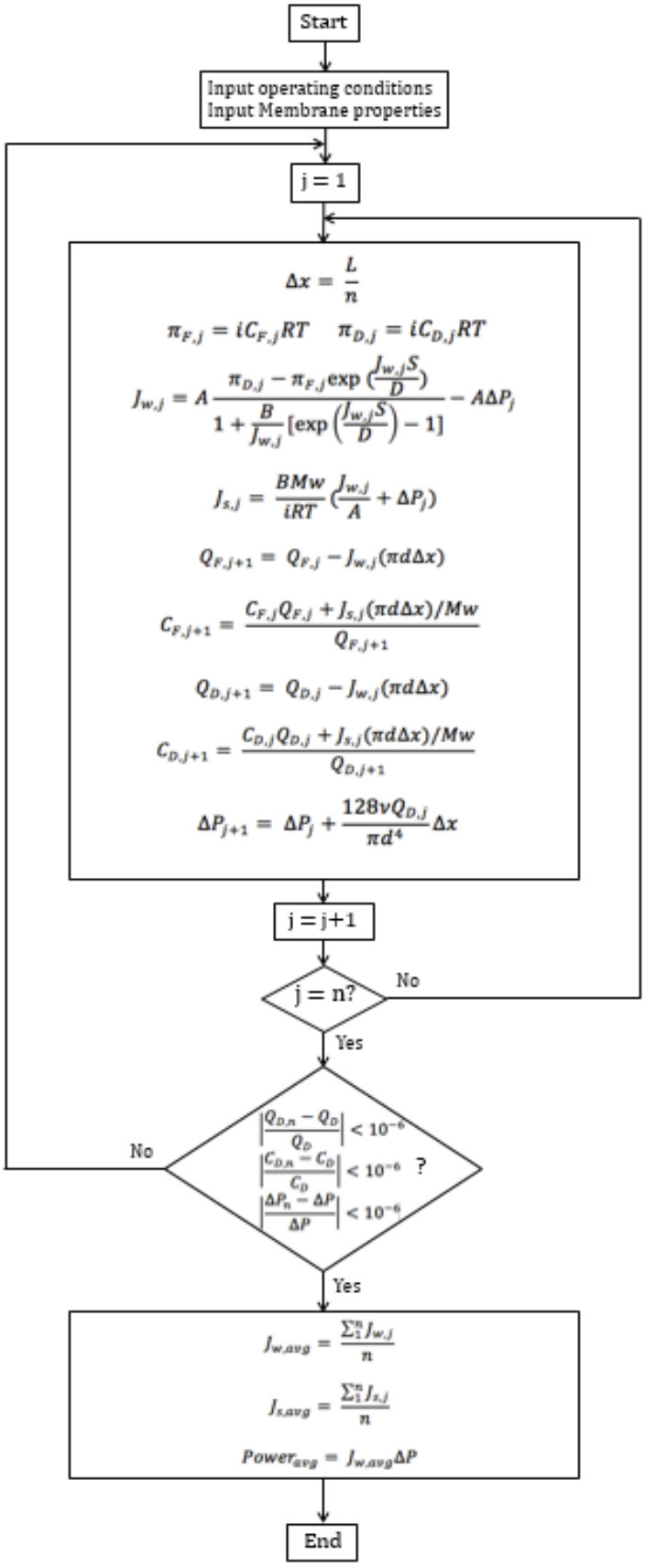

Figure 4.3 Computational flow diagram of simulation of the PRO process

4.4. Results and Discussion

4.4.1. Characterization of SWBr, WWRe and WWRe filtrates

As tabulated in Table 4.3, the osmolality values of the WWRe and the SWBr were 22±1 mmol and 1468±20 mmol, respectively. The equivalent NaCl concentrations were 0.011 M and 0.81 M, respectively, based on a standard concentration-osmolality calibration curve. Hence, 0.011 M and 0.81 M NaCl solutions were used as the artificial WWRe and the artificial SWBr in the following studies, respectively.

Solution ID	Osmolality (mmol)	pH	TOC (ppm)
SWBr	1468±20	7.30±0.02	66.1±3.8
WWBr	22±1	7.44±0.02	44.05±4.2

Table 4.3 Summary of osmolality, pH and TOC of seawater brine (SWBr) and wastewater brine (WWBr)

The TOC values in WWRe and SWBr were 44.05±4.1 ppm and 66.1±3.8 ppm, respectively. Since the TOC in the WWRe is relatively high, a severe fouling is expected when the WWRe flows through the porous surface of the PES substrate [15].

Commercial UF and NF membranes were used to pretreat the WWRe in order to mitigate fouling in the PRO process. After UF and NF, the TOC in WWRe was effectively reduced to 32.23 ppm and 22.59 ppm, respectively. Table 4.4 lists the major cations and anions in the original, UF and NF filtrated WWRe. The concentrations of calcium ion (72.70 ppm) and sulfate ion (253.54 ppm) were among the highest in the WWRe. Under the testing conditions, the saturation indexes (SI) of gypsum ($CaSO_4 \cdot 2H_2O$) was -1.39. Though gypsum was undersaturation in the WWRe, it might become supersaturated as water was

removed by the PRO membrane. Therefore, gypsum was suspected to be the main scalants in the PRO process [26].

Sample ID	TOC	Cl^-	Br^-	F^-	NO_3^-	PO_4^{3-}	SO_4^{2-}	Na^+	K^+	Ca^{2+}	Mg^{2+}	Fe^{2+}/Fe^{3+}	unit
Original WWBr	44.05	165.27	1.32	0.80	175.96	45.51	253.54	132.50	49.77	72.70	8.29	N.D.	ppm
WWBr UF Filtrate	32.23	161.04	1.31	0.66	171.62	34.77	248.87	128.50	49.57	68.61	7.95	N.D.	ppm
WWBr NF Filtrate	22.59	154.40	1.17	0.59	154.24	10.97	85.25	98.40	38.11	41.01	4.72	N.D.	ppm

Table 4.4 TOC and ion concentrations of original seawater brine (SWBr) and wastewater brine (WWBr) from the NEWater plant

4.4.2. The effects of Hydraulic Pressure Difference on PWP and Salt Permeability

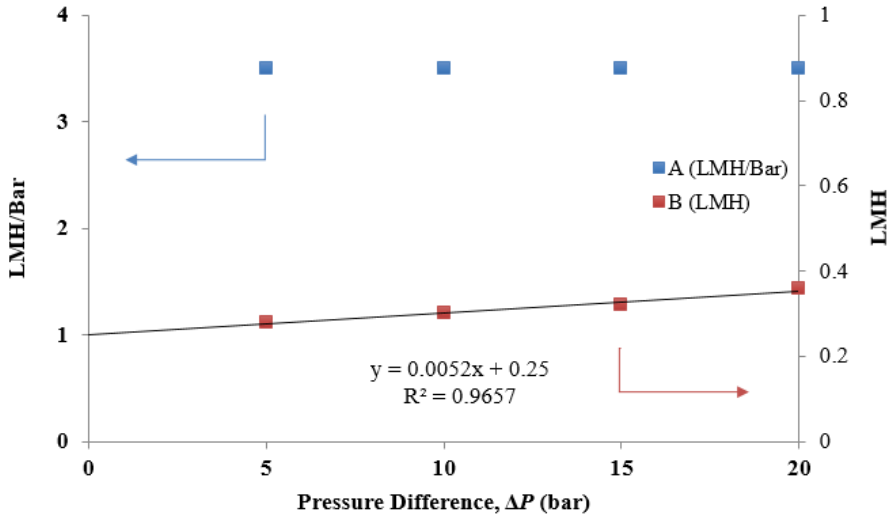

Figure 4.4 Pure water permeability, A, and salt permeability, B, of the stabilized TFC-PES hollow fiber membrane as a function of transmembrane pressure ΔP.

Pure water permeability, *A*, and salt permeability, *B*, of the stabilized TFC-PES membrane were tested from 5 bar to 20 bar at an increment of 5 bar. As summarized in Figure 4.4., the PWP was almost at a constant value of 3.5 LMH/bar throughout the pressure range, while the salt permeability increased monotonically from 0.28 LMH at 5 bar to 0.36 LMH at 20 bar. The increased salt permeability at high hydraulic pressures was due to the defects present on the polyamide layer [27, 28]. Since the amount of salts that transported

convectively through the membranes increased proportionally with hydraulic pressure [29-31], the salt permeability was observed to increase almost linearly with hydraulic pressure. The profile of *B* versus pressure is subsequently used in the PRO process simulation.

4.4.3. Power generation from SWBr and WWRe

Water flux and power density are the key performance indicators of a PRO process [32-34]. The reverse salt flux is also an important parameter. A high reverse salt flux will enhance the internal concentration polarization (ICP) in the porous substrates and compromise the PRO performance [27, 28, 35]. Figure 4.5 presents the performance of the PRO process using different combinations of draw and feed solutions. All data was collected after 30 min, when the water flux became stabilized as discussed in Section 4.6. The baseline was obtained using a 1 M NaCl solution as the draw solution and DI water as the feed solution. In the baseline condition, the power density reached 27.0 W/m^2 at 20 bar, which is the best ever reported in the literature. In conditions A and B, DI water was used as the feed solution, while the 0.81 M NaCl solution and the SWBr as draw solutions, respectively. In both cases, the water flux dropped from 64 LMH to 40 LMH when the transmembrane pressure increased from 0 to 20 bar. The water flux dropped faster at a higher transmembrane pressure due to a higher salt reverse flux and hence more enhanced ICP. The highest power densities achieved at 20 bar in condition A (21.3 W/M^2) and condition B (21.1 W/M^2) were very close, indicating that fouling of the SWBr on the selective skin was negligible, though the TOC was higher in the SWBr. This is because the SWBr

was facing the inner selective skin of the membrane and the water flux flowing across the membrane tended to wash off the foulants on the inner skin.

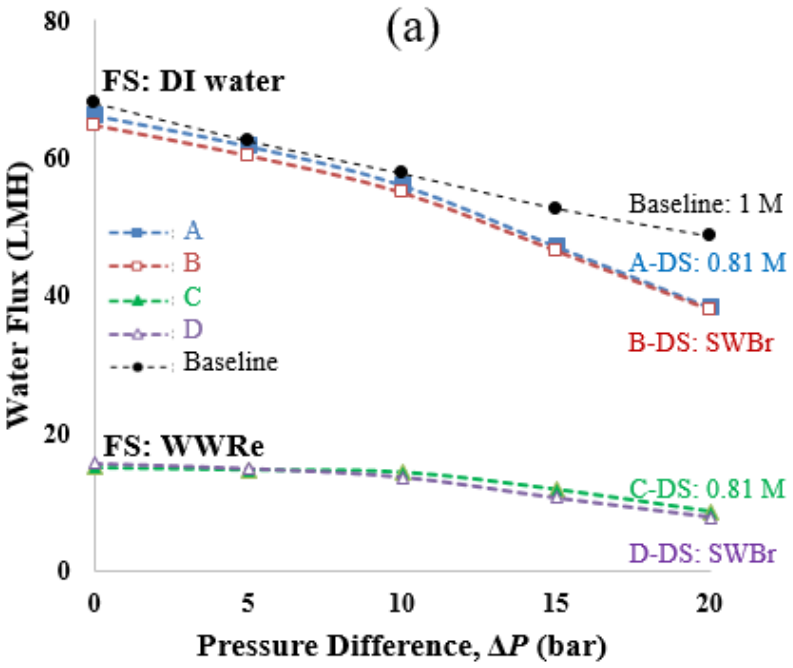

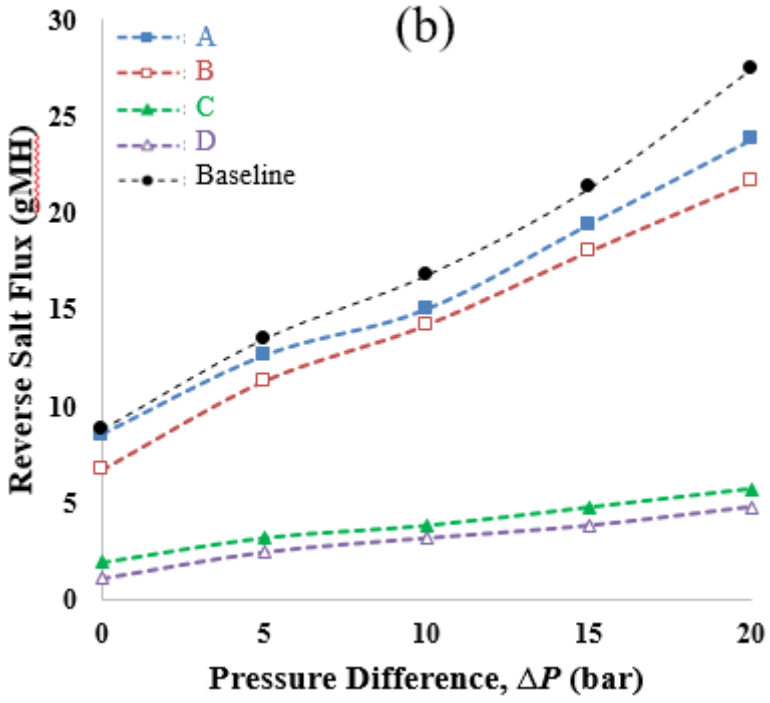

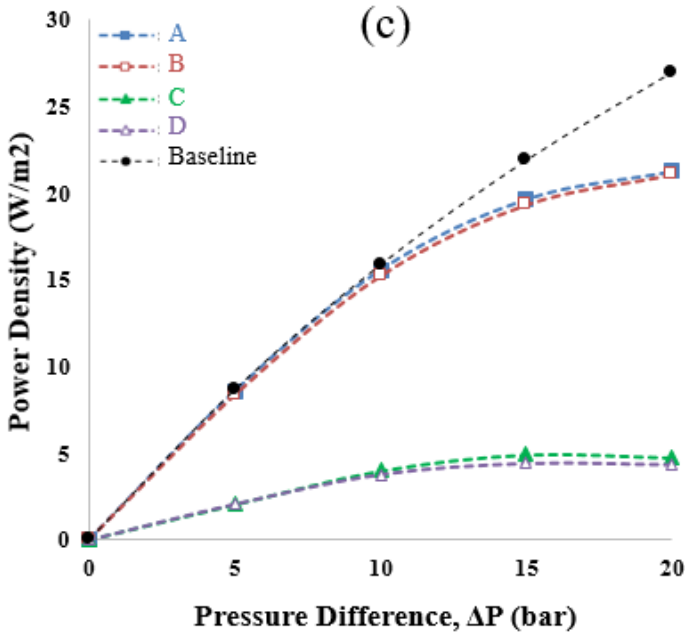

Figure 4.5 (a) water flux (b) reverse salt flux and (c) power density as functions of transmembrane pressure using Baseline: 1M NaCl solution as draw solution (DS) and DI water as feed solution (FS), A: 0.81M NaCl solution as DS and DI water as FS, B: SWBr as DS and DI water as FS, C: 0.81M NaCl solution as DS and WWRe brine as FS, D: SWBr as DS and WWRe as FS.

When DI water was replaced by the WWRe in conditions C and D, the water flux dropped by 75%-80%. The severe reduction in water flux was caused by the fouling of the WWRe on the porous substrates. Foulants were trapped into the porous structure of the membranes by the water flux across the membrane. Even though the driving force was higher at lower transmembrane pressures, the higher driving force was offset by the more server fouling induced by the higher initial water flux at lower transmembrane pressures.

Clearly, the fouling of the SWBr on the selective skin was negligible, while fouling of the WWRe on the porous substrates caused a 75%-80% reduction in water flux. The highest power density could only reach 4.55 W/m^2 at 20 bar when using WWRe as the feed solution. In order to mitigate fouling on the

porous substrates and boost the power density, UF and NF were used to pretreat the WWRe before the PRO tests.

4.4.4. Power generation from UF and NF treated SWBr and WWRe

Figure 4.6 (a) and (b) compares the water flux and power density of the PRO process using a 0.81 M NaCl solution as the draw solution and original, UF and NF treated WWRe as feed solutions. The membrane was conditioned with the respective feed solution for 30 min before the data were collected.

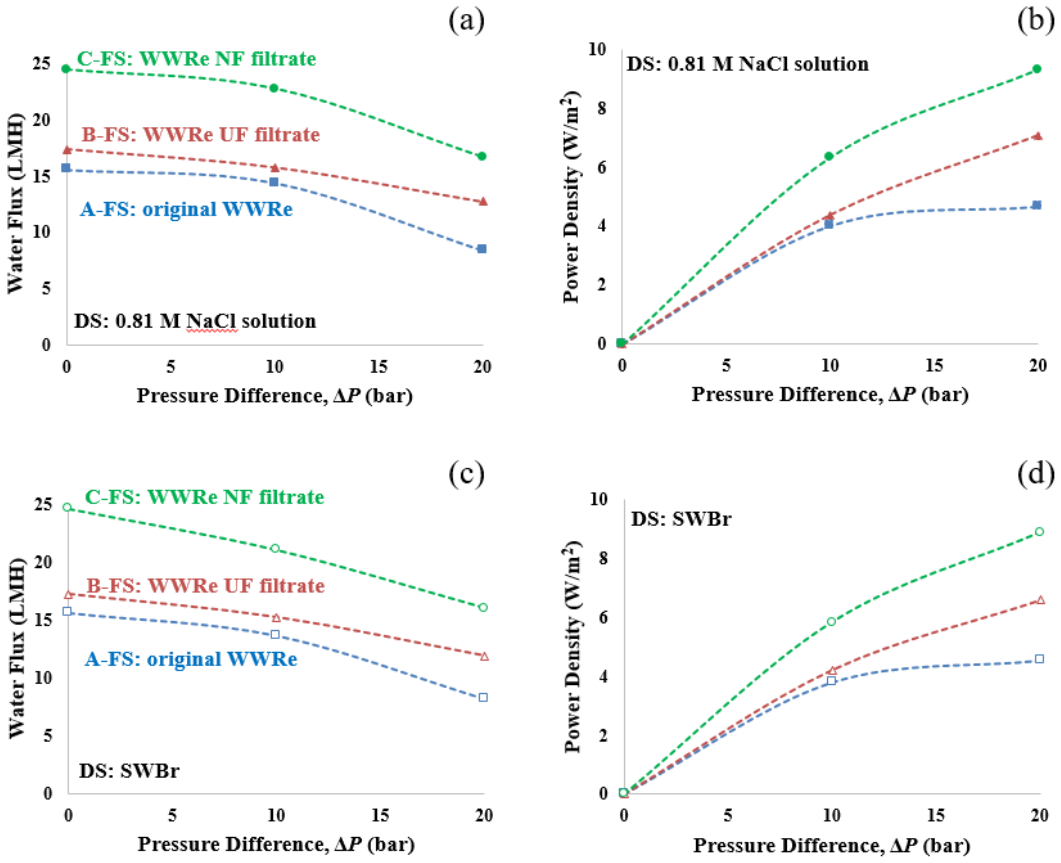

Figure 4.6 (a) Water flux and (b) power density as functions of transmembrane pressure using a 0.81M NaCl solution as the draw solution (DS) and A: original WWRe, B: WWRe UF filtrate and C: WWRe NF filtrate as feed solutions (FS), respectively.; (c) Water flux and (d) power density as functions of transmembrane pressure using SWBr as the DS and A: original WWRe, B: WWRe UF filtrate and C: WWRe NF filtrate as the FS, respectively.

After the UF pretreatment, the TOC of the WWRe was reduced from 44.05 ppm to 32.23 ppm without significant changes in ion concentrations. Only a marginal improvement was observed in the pressure range from 0 bar to 10 bar when the UF filtrate was used. Beyond 10 bar, the improvement became significant. Since there were negligible changes in ion concentrations, it was very likely that the improvement was resulted from the removal of organic foulants in UF. The NF treated WWRe further improved the PRO performance. This was due to the fact that the NF membrane not only effectively removed almost half of the TOC, but also reduced 66% and 43% of the sulfate and calcium ions, respectively. The performance enhancement may result from the reduced organic and gypsum fouling. However, even after the NF pretreatment, the highest power density achieved was only 9.31 W/m^2. It is over 50% less than that obtained from the artificial WWRe (i.e., 0.011 M NaCl solution).

The SWBr has a different composition from the 0.81 M NaCl solution because the former contains various metal cations. Thus, the reverse salt flux from SWBr can interact with the organic foulants in the feed solution and enhance fouling [36-38]. To rule out such possibilities, the above experiments were repeated using the SWBr as the draw solution. As shown in Figure 4.6 (c) and (d) and compared with Figure 4.6 (a) and (b), the difference in water flux was within 5%, confirming that the negative effects of the SWBr on the PRO membrane was minimal. The highest power density reached 6.6 W/m^2 and 8.9 W/m^2 when using SWBr as the draw solution, and UF and NF treated WWRe as feed solutions, respectively.

Although UF and NF pretreatments increased the power densities of the PRO process, they consumed energy. Thus a rough estimation was conducted to determine if a positive net energy density could be harvested under the following assumptions: 1) the transmembrane pressure of the UF and NF were maintained at 1 bar and 5 bar, respectively; 2) the PWP of the UF and NF remained constant at 83.3 LMH/bar and 4.32 LMH/bar, respectively; 3) 90% of the WWRe feed was recovered in the UF and NF processes; 4) 100% of the filtrate was utilized in the PRO process by recycling the filtrate. According to Table 4.5, positive energy outputs could be obtained in both cases. The net power densities of the PRO system with UF and NF pretreatment were 6.24 W/m^2 and 6.43 W/m^2, respectively. The power consumption was higher for the NF pretreatment because of the higher operating pressure, which somewhat offset the additional gain in power density after the NF pretreatment. Moreover, the NF pretreatment required a larger membrane area because of the lower PWP of the NF membrane.

Process	Power Density (W/m^2)	
	UF	NF
PRO	6.6	8.9
Pretreatment	-0.36	-2.47
Net	6.24	6.43

Table 4.5 Estimation of the net power density of the PRO process at 20 bar with UF or NF pretreatment.

4.4.5. Validation of the PRO Model

Using a 0.81 M NaCl solution as the draw solution, two PRO experiments and simulations were conducted by assuming the feed solution is either 0.011 M NaCl or DI water. Figure 4.7 shows the results. The differences between the

model prediction and experimental data in water flux, reverse salt flux and power density were within 11.4%, 13.2% and 4.9%, respectively. However, the water flux was higher at 0 bar in real cases, and dropped slightly faster. On the other hand, the reverse salt flux was lower at 0 bar in real cases, and increased slightly faster. The small difference in salt concentration between DI water and 0.011 M NaCl solutions resulted in a 33.5% reduction in water flux at 20 bar. The addition of 0.011M NaCl in the feed solution caused a reduction of 9.2% in the effective osmotic pressure difference across the selective layer and a drop of 33.5% in water flux due to enhanced ICP. At higher transmembrane pressures, the ICP induced by the increasing reverse salt flux in the case of using DI water as the feed solution became more severe, causing water flux to drop even faster. As a result, the difference in water flux between cases A and B diminished at higher transmembrane pressures.

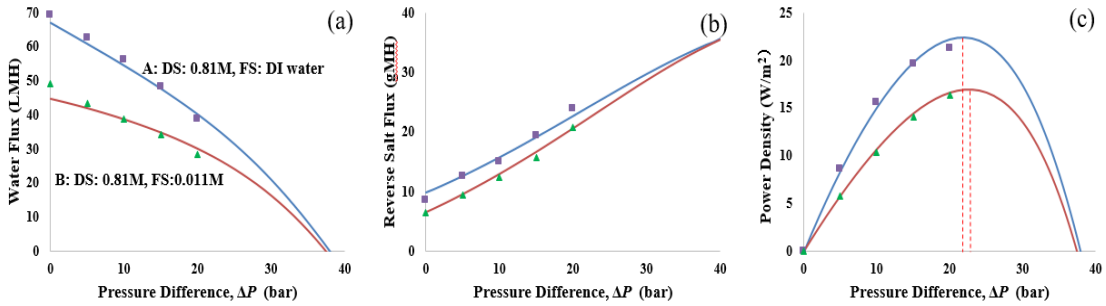

Figure 4.7 Comparisons of simulation and experiment results on a) water flux b) reverse salt flux c) power density of A: 0.81M NaCl solution as the draw solution (DS) and DI water as the feed solution (FS), B: 0.81M NaCl solution as DS and 0.011M NaCl solution as FS. The solid lines are the simulation results, and the scattered points are the experiment results.

As shown in Figure 4.7 (c), the profile of power density is not a perfect parabolic. The peak of power density was skewed toward the higher pressure range. In the ideal case, the power density should peak at one half of the osmotic pressure difference. However, because the effective driving force was compromised by

the hydraulic resistance, ICP and reverse salt flux, a higher transmembrane pressure is needed to achieve the maximum power density. According to the simulation results, the maximum power densities that can be achieved are 22.40 W/m^2 at 22 bar and 16.95 W/m^2 at 23 bar using DI water and 0.011 M NaCl as feed solutions, respectively.

4.4.6. Fouling of WWRe, WWRe UF filtrates and WWRe NF filtrates

In Figure 4.8 (a)-(c), water fluxes were recorded for the first 30 min of the PRO experiments using WWRe, UF and NF treated WWRe as feed solutions, respectively. The draw solution was a 0.81 M NaCl solution. In all the cases, the water flux dropped sharply in the first 5 min, slowed down gradually and continued to drop at a much slower rate over a long period. The water flux obtained using the WWRe NF filtrate was greater than that obtained using the WWRe UF filtrate, which was in turn greater than that obtained using the original WWRe.

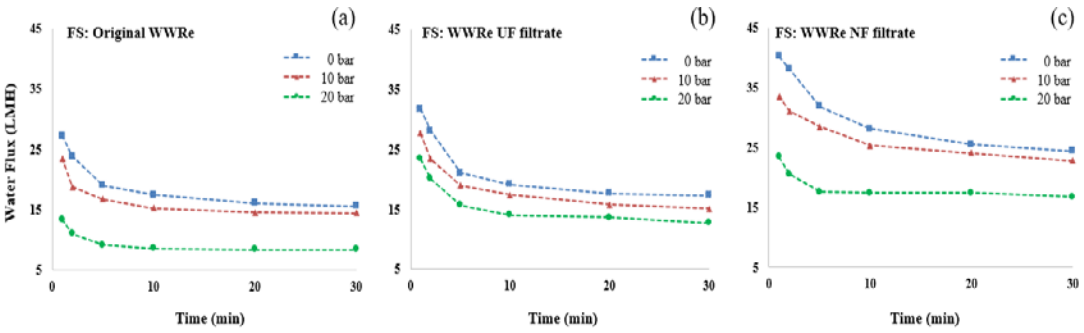

Figure 4.8 Water flux as a function of time using a 0.81 NaCl solution as the draw solution and (a) original WWRe (b) WWRe UF filtrate (c) WWRe NF filtrate as feed solutions at different pressures.

Fouling caused a reduction in water flux by decreasing PWP of the membrane and weakening the effective osmotic driving force. Finding how PWP was influenced by fouling is of great interest in this study. The aforementioned PRO

model was used to isolate the changes in transport properties of the PRO membrane from other factors. The PRO performance data were fitted into the PRO model (Figure 4.2) in order to calculate both *PWP* and *B* as functions of operation pressure and time through trial and error. As presented in Figure 4.9 (a)-(c), the *PWP* was improved by 17%, 6% and 61% at 0 bar, 10 bar and 20 bar, respectively, using the WWRe UF filtrate; and it was improved by 70%, 82% and 127% at 0 bar, 10 bar and 20 bar, respectively, using the WWRe NF filtrate.

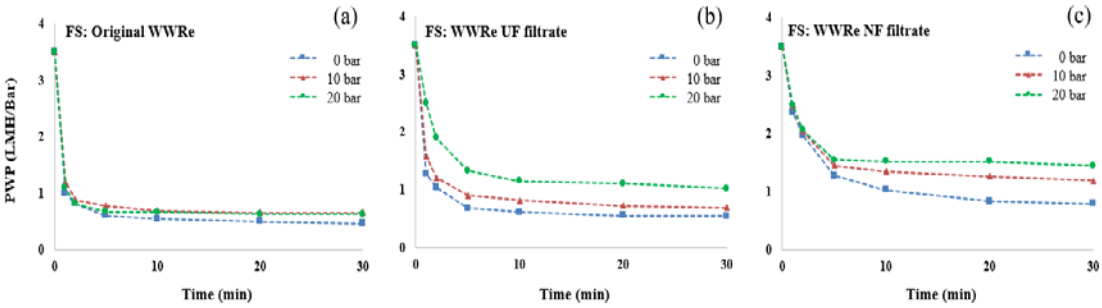

Figure 4.9 PWP as a function of time using (a) original WWRe (b) WWRe UF filtrate (c) WWRe NF filtrate as the feed solutions and 0.81 NaCl solution as the draw solution at different pressures.

When the original WWRe was used as the feed solution, the greatest drop in *PWP* was at 0 bar due to the high initial water flux, followed by at 20 bar and lastly at 10 bar. This was different from the cases when the UF filtrate and the NF filtrate were used as feed solutions, where the *PWP* reduction at 20 bar was smaller than that at 10 bar. One possible explanation is that fouling of the original WWRe was enhanced by the high reverse salt flux at 20 bar [37-39]. However, some foulants were effectively removed by the UF and NF, and therefore the fouling induced by the reverse salt flux became less severe when the UF filtrate and the NF filtrate were used. Even in the best case when the NF filtrate was used and tested at 20 bar, the PWP dropped to 1.45 LMH/bar, only 41% of that of a pristine membrane.

A resistance in series model coupled with the Darcy's law [40] can be used to relate the hydraulic resistance of the foulant to the *PWP* of the membrane by

$$PWP = \frac{1}{\mu}\left(\frac{1}{R_m + R_f}\right) \tag{19}$$

where R_m is the hydraulic resistance of the pristine membrane and R_f is the hydraulic resistance of the foulants. The changes of R_f with time is shown in Figure 4.10 (a)-(c). R_m was 1.14×10^{14} m^{-1}, calculated from the *PWP* of the pristine membrane. After the UF pretreatment of the WWRe, the R_f values were reduced by 14.5%, 5.7% and 37.9% at 0 bar, 10 bar and 20 bar, respectively; after NF pretreatment of the WWRe, the R_f values were reduced by 41.2%, 45.0% and 55.9% at 0 bar, 10 bar and 20 bar, respectively. In all cases, the R_f was the dominant hydraulic resistance and greatly compromised the performance of the PRO process.

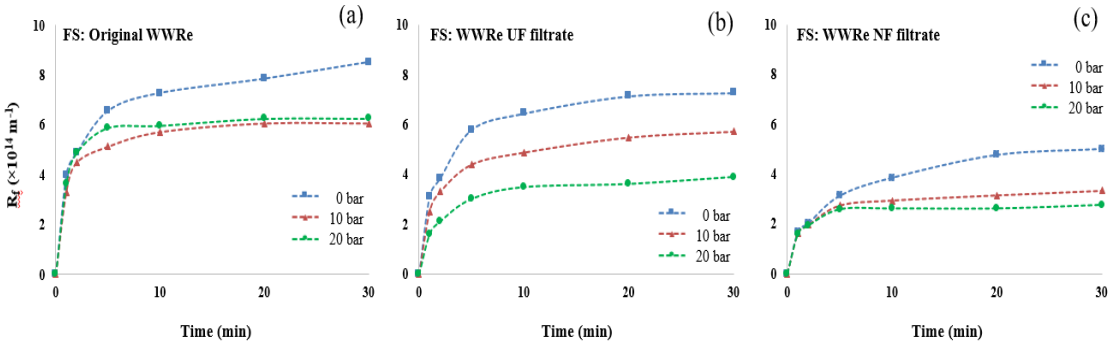

Figure 4.10 Rf as a function of time using (a) original WWRe (b) WWRe UF filtrate (c) WWRe NF filtrate as feed solutions and 0.81 NaCl solution as the draw solution at different pressures.

4.5. Conclusion and Implication

PRO is a promising process to harvest the osmotic energy. A high power density of 21 W/m^2 has been achieved using 0.81 M NaCl and DI water as feeds. However, the power density dropped to 4.55 W/m^2 when real SWBr and WWRe

were used. The fouling of the WWRe on the porous substrate of the TFC-PES membranes was identified as the main cause of this significant reduction in power density, while the negative effects of SWBr on the PRO performances were negligible. Both UF and NF processes were used to pretreat the WWRe, and the resultant power densities recovered to 6.6 W/m^2 and 8.9 W/m^2, respectively. Both were above the proposed power density of 5 W/m^2 set by Statkraft for the PRO process to be economical [5, 8, 9]. However, the additional cost of the pretreatment has to be studied before implementation.

As evidenced in this study, the hydraulic resistance of the foulants eventually became dominant in water transport across the membranes, despite of the high PWP of the membrane. Future researches should focus on the 1) development of innovative cleaning strategies for the PRO membrane[41, 42], 2) enhancement of the fouling resistance of the TFC membrane[43-46], while maintaining its good transport and mechanical properties, 3) development of anti-foulant [47, 48] and anti-scalant [49] that can be used for a wide range of feed solutions, 4) development of cost-effective pretreatment processes [16, 50]. A preferred anti-fouling strategy should effectively mitigate fouling without significantly increasing the operating cost or the footprint of the PRO process, which makes the development of innovative cleaning strategy and anti-fouling PRO membranes especially attractive.

References

[1] R. J. Aaberg, Osmotic power, Refocus, 4 (2003) 48-50.

[2] B. E. Logan, M. Elimelech, Membrane-based processes for sustainable power generation using water, Nature, 488 (2012) 313-319.

[3] Z. Jia, B. Wang, S. Song, Y. Fan, Blue energy: Current technologies for sustainable power generation from water salinity gradient, Renewable and Sustainable Energy Rev., 31 (2014) 91-100.

[4] T. S. Chung, X. Li, R.C. Ong, Q. Ge, H. Wang, G. Han, Emerging forward osmosis (FO) technologies and challenges ahead for clean water and clean energy applications, Curr. Opin. Chem. Eng., 1 (2012) 246-257.

[5] S. E. Skilhagen, J. E. Dugstad, R. J. Aaberg, Osmotic power — power production based on the osmotic pressure difference between waters with varying salt gradients, Desalination, 220 (2008) 476-482.

[6] S. Loeb, Production of energy from concentrated brines by pressure-retarded osmosis: I. Preliminary technical and economic correlations, J. Membr. Sci., 1 (1976) 49-63.

[7] S. Loeb, F. V. Hessen, D. Shahaf, Production of energy from concentrated brines by pressure-retarded osmosis: II. Experimental results and projected energy costs, J. Membr. Sci., 1 (1976) 249-269.

[8] K. Gerstandt, K.V. Peinemann, S.E. Skilhagen, T. Thorsen, T. Holt, Membrane processes in energy supply for an osmotic power plant, Desalination, 224 (2008) 64-70.

[9] T. Thorsen, T. Holt, The potential for power production from salinity gradients by pressure retarded osmosis, J. Membr. Sci., 335 (2009) 103-110.

[10] X. X. Song, Z.Y. Liu, D.D. Sun, Energy recovery from concentrated seawater brine by thin-film nanofiber composite pressure retarded osmosis

membranes with high power density, Energy & Environ. Sci., 6 (2013) 1199-1210.

[11] N. N. Bui, J.R. McCutcheon, Hydrophilic nanofibers as new supports for thin film composite membranes for engineered osmosis, Environ. Sci. Technol., 47 (2013) 1761-1769.

[12] I. L. Alsvik, M. B. Hägg, Pressure retarded osmosis and forward osmosis membranes: Materials and methods, Polymers, 5 (2013) 303-327.

[13] Y. K. Guan, The Singapore success story, Water & Waste. Int., 25 (2010) 27-28.

[14] K. N. Irvine, L. H. C. Chua, H. S. Eikass, The four national taps of Singapore: A holistic approach to water resources management from drainage to drinking water, J. Water Manag. Model., 2014.

[15] J. J. Qin, M. N. Wai, M. H. Oo, K. A. Kekre, H. Seah, Feasibility study for reclamation of a secondary treated sewage effluent mainly from industrial sources using a dual membrane process, Sep. Purif. Technol., 50 (2006) 380-387.

[16] K. Saito, M. Irie, S. Zaitsu, H. Sakai, H. Hayashi, A. Tanioka, Power generation with salinity gradient by pressure retarded osmosis using concentrated brine from SWRO system and treated sewage as pure water, Desalin. Water Treat., 41 (2012) 114-121.

[17] L.G. Palacin, F. Tadeo, C.d. Prada, K. Touati, Evaluation of the recovery of osmotic energy in desalination plants by using pressure retarded osmosis, Desalin. Water Treat., 51 (2013) 360-365.

[18] H. Seah, Biomimicry desalination Singapore takes a leaf out of nature's book, Water & Waste. Inte., 27 (2012) 41-42.

[19] A. Altaee, G. Zaragoza, A. Sharif, Pressure retarded osmosis for power generation and seawater desalination: Performance analysis, Desalination, 344 (2014) 108-115.

[20] J. L. Prante, J. A. Ruskowitz, A. E. Childress, A. Achilli, RO-PRO desalination: An integrated low-energy approach to seawater desalination, Applied Energy, 120 (2014) 104-114.

[21] T.S. Chung, S. Zhang, K.Y. Wang, J.C. Su, M.M. Ling, Forward osmosis processes: Yesterday, today and tomorrow, Desalination, 287 (2012) 78-81.

[22] A. Achilli, J. L. Prante, N. T. Hancock, E. B. Maxwell, A. E. Childress, Experimental results from RO-PRO: A next generation system for low-energy desalination, Environ. Sci. Technol., 48 (2014) 6437-6443.

[23] M. Darwish, A. H. Hassabou, B. Shomar, Using Seawater Reverse Osmosis (SWRO) desalting system for less environmental impacts in Qatar, Desalination, 309 (2013) 113-124.

[24] S. H. Yoon, S. Lee, I. T. Yeom, Experimental verification of pressure drop models in hollow fiber membrane, J. Membr. Sci., 310 (2008) 7-12.

[25] M.G. Marcovecchio, N.J. Scenna, P.A. Aguirre, Improvements of a hollow fiber reverse osmosis desalination model: Analysis of numerical results, Chem. Eng. Res. Des., 88 (2010) 789-802.

[26] M. Zhang, D. Hou, Q. She, C.Y. Tang, Gypsum scaling in pressure retarded osmosis: Experiments, mechanisms and implications, Water Res., 48 (2014) 387-395.

[27] S. Zhang, T.S. Chung, Minimizing the instant and accumulative effects of salt permeability to sustain ultrahigh osmotic power density, Environ. Sci. Technol., 47 (2013) 10085-10092.

[28] Q. She, X. Jin, C.Y. Tang, Osmotic power production from salinity gradient resource by pressure retarded osmosis: Effects of operating conditions and reverse solute diffusion, J. Membr. Sci., 401-402 (2012) 262-273.

[29] R.B. Bird, W.E. Stewart, E.N. Lightfoot, Transport Phenomena, 2nd ed Wiley & Sons, Inc., 2002.

[30] A. K. Ghosh, B.H. Jeong, X. F. Huang, E. M. V. Hoek, Impacts of reaction and curing conditions on polyamide composite reverse osmosis membrane properties, J. Membr. Sci., 311 (2008) 34-45.

[31] Y.H. La, R. Sooriyakumaran, D.C. Miller, M. Fujiwara, Y. Terui, K. Yamanaka, B.D. McCloskey, B.D. Freeman, R.D. Allen, Novel thin film composite membrane containing ionizable hydrophobes: ph dependent reverse osmosis behavior and improved chlorine resistance, J. Mater. Chemi., 20 (2010) 4615-4620.

[32] G. Han, S. Zhang, X. Li, T.-S. Chung, High performance thin film composite pressure retarded osmosis (PRO) membranes for renewable salinity-gradient energy generation, J. Membr. Sci., 440 (2013) 108-121.

[23] S. Zhang, P. Sukitpaneenit, T. S. Chung, Design of robust hollow fiber membranes with high power density for osmotic energy production, Chem. Engin. J., 241 (2014) 457-465.

[34] N.Y. Yip, A. Tiraferri, W.A. Phillip, J.D. Schiffman, L.A. Hoover, Y.C. Kim, M. Elimelech, Thin-film composite pressure retarded osmosis membranes for sustainable power generation from salinity gradients, Environ. Sci. Technol., 45 (2011) 4360-4369.

[35] A. Achilli, T. Y. Cath, A. E. Childress, Power generation with pressure retarded osmosis: An experimental and theoretical investigation, J. Membr. Sci., 343 (2009) 42-52.

[36] S.C. Chen, X.Z. Fu, T.-S. Chung, Fouling behaviors of polybenzimidazole (PBI)–polyhedral oligomeric silsesquioxane (POSS)/polyacrylonitrile (PAN) hollow fiber membranes for engineering osmosis processes, Desalination, 335 (2014) 17-26.

[37] Q. She, Y.K.W. Wong, S. Zhao, C.Y. Tang, Organic fouling in pressure retarded osmosis: Experiments, mechanisms and implications, J. Membr. Sci., 428 (2013) 181-189.

[38] M.M. Motsa, B.B. Mamba, A. D'Haese, E.M.V. Hoek, A.R.D. Verliefde, Organic fouling in forward osmosis membranes: The role of feed solution chemistry and membrane structural properties, J. Membr. Sci., 460 (2014) 99-109.

[39] W.R. Thelin, E. Sivertsen, T. Holt, G. Brekke, Natural organic matter fouling in pressure retarded osmosis, J. Membr. Sci., 438 (2013) 46-56.

[40] G. Bolton, D. Lacasse, R. Kuriyel, Combined models of membrane fouling: Development and application to microfiltration and ultrafiltration of biological fluids, J. Membr. Sci., 277 (2006) 75-84.

[41] N.Y. Yip, M. Elimelech, Influence of natural organic matter fouling and osmotic backwash on pressure retarded osmosis energy production from natural salinity gradients, Environ. Sci. Technol., 47 (2013) 12607-12616.

[42] B.X. Mi, M. Elimelech, Gypsum scaling and cleaning in forward osmosis: measurements and mechanisms, Environ. Sci. Technol., 44 (2010) 2022-2028.

[43] X. Li, T. Cai, T.S. Chung, Anti-fouling behavior of hyperbranched polyglycerol-grafted poly(ether sulfone) hollow fiber membranes for osmotic power generation, Environ. Sci. Technol., 48 (2014) 9898-9907.

[44] P.H. Duong, T.S. Chung, S. Wei, L. Irish, Highly permeable double-skinned forward osmosis membranes for anti-fouling in the emulsified oil-water separation process, Environ. Sci. Technol., 48 (2014) 4537-4545.

[45] P.H.H. Duong, T. S. Chung, Application of thin film composite membranes with forward osmosis technology for the separation of emulsified oil–water, J. Membr. Sci., 452 (2014) 117-126.

[46] W. Fang, R. Wang, S. Chou, L. Setiawan, A.G. Fane, Composite forward osmosis hollow fiber membranes: Integration of RO- and NF-like selective layers to enhance membrane properties of anti-scaling and anti-internal concentration polarization, J. Membr. Sci., 394-395 (2012) 140-150.

[47] S.R. Pandey, V. Jegatheesan, K. Baskaran, L. Shu, Fouling in reverse osmosis (RO) membrane in water recovery from secondary effluent: a review, Rev. Environ. Sci. Bio/Technol., 11 (2012) 125-145.

[48] R.Y. Ning, T.L. Troyer, R.S. Tominello, Chemical control of colloidal fouling of reverse osmosis systems, Desalination, 172 (2005) 1-6.

[49] A. Antony, J.H. Low, S. Gray, A.E. Childress, P. Le-Clech, G. Leslie, Scale formation and control in high pressure membrane water treatment systems: A review, J. Membr. Sci., 383 (2011) 1-16.

[50] N. Sato, R. Xie, T. Yoneda, Y. Xing, A. Noro, K. Robinson, R. Villalobos, Water Quality Improvement by Combined UF, RO, and Ozone/Hydrogen Peroxide System (HiPOx) in the Water Reclamation Process, Ozone: Sci. Eng., 36 (2014) 153-165.

Chapter 5: Energy recovery by pressure retarded osmosis (PRO) in SWRO-PRO integrated processes

5.1. Introduction

The seawater reverse osmosis and pressure retarded osmosis (SWRO-PRO) integrated process has received increasing attention recently [1-7]. In the Japan Megaton Water Project, a PRO system where a maximum power density of 13.3 W/m^2 at a hydraulic pressure difference of approximately 27 bar was developed using the SWRO brine as the draw solution and freshwater as the feed [6, 8]. In this prototyped plant, hydro-turbines were used to harvest the osmotic energy. In 2014, Sarp et al. [5] and Prante et al. [4] independently proposed two modeled SWRO-PRO processes, where the high-pressure diluted seawater brine from PRO was used to pressurize the seawater feed to SWRO through a PX. However, most of the SWRO-PRO processes are conceptual and detailed process designs are missing in the literatures. Moreover, systematic SWRO-PRO models are needed for the integrated process design and optimization.

In this study, detailed configurations of two novel SWRO-PRO integrated processes in terms of the positions and functions of each PX and HP were specified. The closed-loop SWRO-PRO may significantly reduce the seawater pretreatment cost and recover more osmotic energy from the brine, while the open-loop SWRO-PRO may offer greater flexibility for process design. Moreover, mathematical models that describe both the transport phenomena on a module level and the energy flow on a system level are developed to evaluate the performances of the SWRO-PRO processes. These two models are closely related by the flowrate and the pressure of the seawater/brine stream can be used

to optimize the entire SWRO-PRO system. These models will provide useful guidelines for process design and optimization.

5.2. Theory

5.2.1. Process descriptions

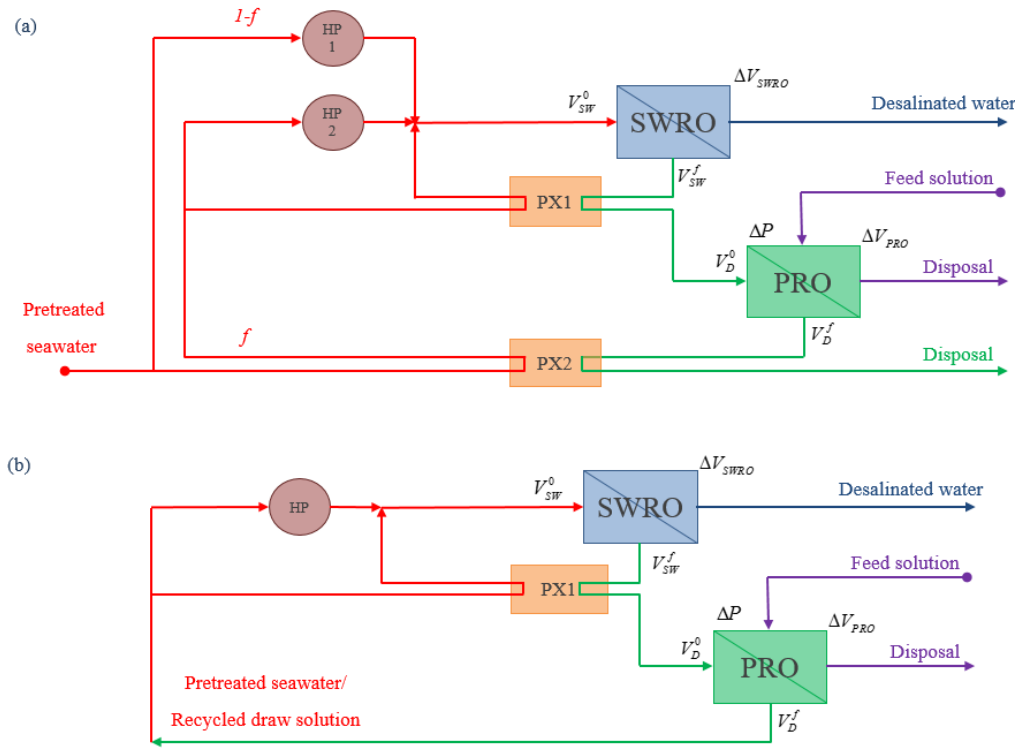

Figure 5.1 Schematic drawings of the integrated SWRO-PRO processes (a) $\Delta V_{PRO} < \Delta V_{SWRO}$ (b) $\Delta V_{PRO} = \Delta V_{SWRO}$.

Figure 5.1 (a) presents a general process of the integrated SWRO-PRO. Since it usually takes a huge membrane area to transport the same amount of water in PRO as in SWRO, the permeate volume in PRO is usually less than that in SWRO (i.e., $\Delta V_{PRO} < \Delta V_{SWRO}$) in the actual application. Therefore, the pretreated seawater under this condition is split into two streams before PX2. The fraction of pretreated seawater pressurized by PX2 is assumed to be *f*, and then the fraction of the pretreated seawater directly pressurized to the operating pressure

of SWRO by HP1 will be (*1-f*). In PX2, the pretreated seawater is pressurized to a medium-high pressure by the diluted draw solution from PRO. Subsequently, the effluent from PX2 is split into two streams before PX1: one is pressurized by PX1 using the high-pressure brine from SWRO and the other is pressurized by a high-pressure pump HP2 to the operating pressure of the SWRO system. All three feed streams are then combined and enter the SWRO system, where pure water is produced. The high-pressure brine from the SWRO passes part of its energy to seawater via PX1, and its pressure is reduced to a medium-high value. The medium-high pressure brine acts as the draw solution in the PRO system. In the PRO system, the concentrated brine gets diluted. As water permeates through the PRO membrane, the chemical potential is converted to the hydraulic pressure of the draw solution. Therefore, the draw solution is able to maintain its medium-high pressure at an increased volumetric flowrate. The diluted draw solution is then utilized in PX2 to pressurize the pretreated seawater. When $\Delta V_{PRO}<\Delta V_{SWRO}$, the diluted draw solution from PRO has a salinity that is higher than the pretreated seawater and it is not economical to recycle it as the feed solution to SWRO, because this will require a higher energy input to achieve the same recovery in SWRO and also result in salt accumulation in the seawater feed. Hence, the diluted draw solution is discharged after pressure exchanging with the pretreated seawater feed. It is worth mentioning that the PX does not have an efficiency of 100% and therefore a boost pump is always needed to make up the pressure loss, which is not shown in the process flow diagrams.

In the special case of f = 1, the general SWRO-PRO process can be simplified as presented in Figure 5.1 (b). In this process, the permeate volume in PRO is the same as that in SWRO, i.e. $\Delta V_{PRO}=\Delta V_{SWRO}$ and $V^{0}_{SW}= V^{f}_{D}$. Therefore, the diluted draw solution from PRO can be directly used as the feed solution to SWRO. This process has several additional advantages: (1) recycling the draw solution as the feed to SWRO can tremendously cut down the pretreatment cost of SWRO, (2) it eliminates the need of addition HP1 and PX2 as in Figure 5.1 (a), (3) there is no pressure lost due to the less than 100% efficiency of PX2. As presented, the pretreated seawater or the diluted draw solution with a medium-high pressure splits into two streams before PX1: one is pressurized by PX1 using the high-pressure brine from the SWRO system and the other is pressurized by a high-pressure pump (HP) to the operating pressure of the SWRO system. The two streams are then combined, enter the SWRO system and go through the same cycle as the process in Figure 5.1 (a). Though the recycled draw solution can be any type of draw solution indeed [9, 10], pretreatment seawater is preferred because it requires less modification of the existing and heavily-optimized SWRO system.

5.2.2. Material balance

In both processes, the seawater or its concentrated brine runs through the entire system. The recovery of SWRO and dilution factor of PRO can be conveniently defined as follows to facilitate further investigations of the processes. The recovery of the SWRO system, *Rec*, is defined as the flowrate ratio of the permeate water over the total seawater feed.

$$\text{Rec} = \frac{V_{SW}^{0} - V_{SW}^{f}}{V_{SW}^{0}} = \frac{\Delta V_{SWRO}}{V_{SW}^{0}} \tag{5.1}$$

where V_{SW}^{0} is the flowrate at which the feed seawater enters the SWRO system, V_{SW}^{f} is the flowrate at which the seawater brine exits the SWRO system and ΔV_{SWRO} is the flowrate of the permeate from the SWRO membrane.

The dilutive factor of the draw solution in the PRO system, *DF*, is defined as follows.

$$DF = \frac{V_{D}^{0}}{V_{D}^{f}} = 1 - \frac{\Delta V_{PRO}}{V_{D}^{f}} \tag{5.2}$$

where V_{D}^{0} is the flowrate at which the draw solution (i.e., the concentrated seawater brine) enters the PRO system. Numerically, V_{D}^{0} is equal to V_{SW}^{f}. V_{D}^{f} is the flowrate at which the diluted draw solution exits the PRO system and ΔV_{PRO} is the flowrate at which water permeates through the PRO membrane. The DF indicates the fraction of the concentrated brine in the diluted brine after PRO. A DF approaching 0% indicates the draw solution is infinitely diluted, while a DF approaching 100% indicates the draw solution is not diluted.

As previously defined, *f* is the fraction of the total seawater feed V^{0}_{SW} that is pressurized by PX2. It is essential to keep the flowrates of the diluted draw solution and the feed seawater entering PX2 equal in order to maximize the efficiency of PX1 [11]. Therefore, the flowrate of the diluted draw solution is also a fraction of the total seawater feed.

$$f = \frac{V_{D}^{f}}{V_{SW}^{0}} \leq 1 \tag{5.3}$$

The following two equations can be obtained from eqn. 5.1 and 5.2 by carrying out mass balance over the entire system.

$$\Delta V_{PRO} = \frac{\text{Rec} + f - 1}{\text{Rec}} \Delta V_{SWRO} \tag{5.4}$$

$$DF = \frac{1 - \text{Rec}}{f} \tag{5.5}$$

5.2.3. PRO modelling

In a PRO system, the amount of energy can be harvested is proportional to the mixing volume. Therefore, dilution of the draw solution is inevitable. On one hand, more energy can be harvested as dilution goes on; and on the other hand, dilution causes reductions in the effective driving force and therefore reduction in the average power density. These two effects result in an increased demand of membrane areas in order to achieve a higher dilution of the draw solution. Eventually, the total amount of energy can be harvested and the average power density of a PRO system will be limited by the membrane areas available [12].

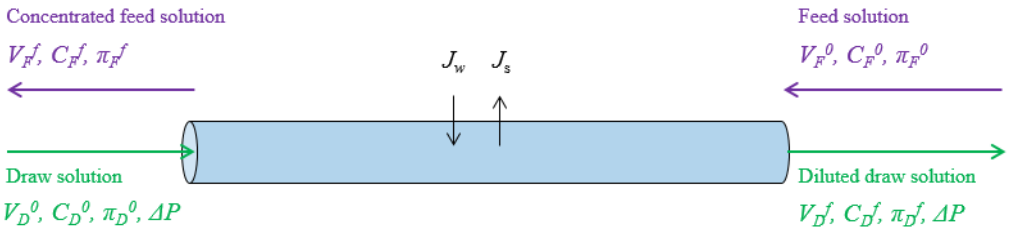

Figure 5.2 Schematic drawing of the PRO process in a single hollow fiber.

As shown in Figure 5.2, the feed and draw solutions flow counter-currently in the hollow fiber module. The draw solution is on the lumen side while the feed

solution is on the shell side of the module. The flow direction of the draw solution is arbitrarily chosen as the positive direction.

During the design of a PRO system, it is important to find out the membrane areas required to achieve a certain dilution of the draw solution or recovery of the feed solution and the corresponding optimum operating conditions. The dilutive factor of the draw solution, DF, and the recovery of the feed solution, REC_{PRO}, are the two sides of the same coin and can be interconverted through the following equation.

$$REC_{PRO} = \frac{V_D^0}{V_F^0}\left(\frac{1}{DF} - 1\right) \tag{5.6}$$

Since seawater and its brine runs through the entire SWRO-PRO process, the analyses will be more systematic by carrying out material balance of the seawater/brine streams. A one dimensional mass transfer model can be developed as following.

$$d\left(\rho_D V_D\right) = \rho_W J_W dA_m \tag{5.7}$$

$$d\left(\rho_F V_F\right) = \rho_W J_W dA_m \tag{5.8}$$

$$d\left(C_D V_D\right) = -J_S dA_m \tag{5.9}$$

$$d\left(C_F V_F\right) = -J_S dA_m \tag{5.10}$$

where ρ_D, ρ_F and ρ_W are the densities of the draw solution, feed solution and pure water respectively. ρ_W are used in the right sides of the eqn. 5.7-5.10 because it is the pure water rather than the feed solution that passes through the PRO membrane. ρ_D and ρ_F vary as the concentrations of the draw solution and feed solution change. Since both the feed solution and the draw solution are

diluted aqueous solutions, ρ_D and ρ_F can be estimated from the following equations.

$$\rho_D = \rho_W + C_D \tag{5.11}$$

$$\rho_F = \rho_W + C_F \tag{5.12}$$

Up to a salt concentration of 400 g/L, which is far beyond the salt concentration of the brine from conventional SWRO, the above equations can accurately predict the densities with less than 5% deviation from the correlations provided by Sharqawy et al. [13]. It is worth noting that the units of C_D and C_F are g/L in all the equations.

Eqn. 5.7-5.10 can be rearranged as functions of dV_D as shown in Appendix A and integrated with the following boundary conditions to analyze the performance of the PRO hollow fibers as dilution occurs. At the entrance of the draw solution where no dilution occurs (i.e., $V_D = V_D^0$), we have $A_m(V_D^0) = 0$ and $C_D(V_D^0) = C_D^0$. At the exit of the draw solution where the draw solution is diluted (i.e., $V_D = V_D^f = \frac{V_D^0}{DF}$), we have $V_F(V_D^f) = V_F^0$ and $C_F(V_D^f) = C_F^0$. The integration is carried out in this special way to evaluate the membrane area needed, the total amount of energy harvested and the average power density obtained at a certain dilution of the draw solution.

The average water flux of the hollow fiber module, $\bar{J}_w$, can be defined as following.

$$\bar{J}_w = \frac{V_D^f - V_D^0}{A_m} = \left(\frac{1}{DF} - 1\right)\frac{V_D^0}{A_m} \tag{5.13}$$

The pressure ratio, PR, is defined as the ratio of the hydraulic pressure difference over the maximum osmotic pressure difference between the draw and feed solutions in the PRO system.

$$PR = \frac{\Delta P}{\Delta \pi_{\max}} \tag{5.14}$$

where $\Delta \pi_{\max}$ is the maximum osmotic pressure difference between the draw and feed solutions at their respective inlets. If freshwater or solution of very low salinity is used as the feed solution, $\Delta \pi_{\max}$ can be estimated as following.

$$\Delta \pi_{\max} = \pi_D^0 - \pi_F^0 \approx \pi_D^0 = \frac{\pi_{sw}}{1 - \mathrm{Rec}} \tag{5.15}$$

where π_{sw} is the osmotic pressure of the seawater feed to the SWRO system. $\frac{\pi_{sw}}{1-\mathrm{Rec}}$ is the osmotic pressure of the draw solution (i.e., the concentration brine), which is also the minimum pressure that has to be overcome to achieve a recovery of *Rec* in SWRO.

The average power density of the module, $\overline{PD}$, at a constant ΔP is defined as following.

$$\overline{PD} = \overline{J}_w \Delta P \tag{5.16}$$

The residence time of the draw solution in the hollow fiber module, *t*, is defined as the ratio of the volume enclosed by the hollow fibers over the flowrate of the draw solution.

$$t = \frac{A_m d_i}{4 V_D^0} \tag{5.17}$$

5.2.4. Energy consumption of the SWRO-PRO process

The specific energy consumption of a stand-alone SWRO, SEC_{SWRO}, depends on the recovery ratio. A minimum hydraulic pressure equal to the osmotic pressure of the concentrated brine has to be applied in SWRO to achieve a desired recovery. In reality the operating pressure is often 10-20% higher than this minimum value to compensate the pressure loss and enhance the SWRO water flux [14]. The specific energy consumption (SEC) to produce 1 m^3 of freshwater in the absence of an ERD is given by the following equation [15, 16].

$$SEC_{SWRO} = \frac{\pi_{SW}}{\eta_P Rec(1-Rec)} \tag{5.18}$$

where η_P is the efficiency of the HP. The SEC_{SWRO} has been significantly reduced due to the invention of ERD. The specific energy consumption of SWRO in the presence of a single ERD, SEC_{SWRO}^{ERD}, can be calculated from the equation below [15, 16].

$$SEC_{SWRO}^{ERD} = \frac{[1-\eta_E(1-Rec)]\pi_{SW}}{\eta_P Rec(1-Rec)} \tag{5.19}$$

where η_E is the efficiency of the ERD. However, this equation cannot be directly applied to the integrated SWRO-PRO processes.

In the SWRO-PRO processes, more energy can be further recovered in the PRO system. Specific energy recovery is defined as the amount of energy that can be recovered from the brine for every m^3 of freshwater produced in SWRO. If a process as shown in Figure 5.1 (a) is employed, eqn. 5.3-5.5 and 5.13-5.16 can be combined as follows.

$$SER_{PRO,a} = \frac{A_m \overline{PD}}{V_D^0} \frac{(1-\text{Rec})}{\text{Rec}} = \frac{PR(\text{Rec} + f - 1)}{\text{Rec}(1-\text{Rec})} \pi_{SW} \quad (5.20)$$

The factor of $\frac{(1-\text{Rec})}{\text{Rec}}$ in eqn. 5.20 is to convert the energy production of the PRO system from per m^3 of the concentration brine basis to per m^3 of desalinated water basis as used in eqn. 5.19.

It should be noted that not only the permeate flow from the PRO system but also the draw solution is used for energy recover in PX2. Thus, the amount of energy recovered in PX2 is as follows.

$$SER_{PX\,2,a} = \frac{fPR}{\text{Rec}(1-\text{Rec})} \pi_{SW} \eta_{E,2} \quad (5.21)$$

The amount of energy recovered in PX1 can be calculated from the following equation.

$$SER_{PX\,1,a} = \frac{(1-PR)}{\text{Rec}} \pi_{SW} \eta_{E,1} \quad (5.22)$$

The specific energy consumption for the integrated SWRO-PRO process in Figure 5.1 (a), SEC_a, is the difference between the energy consumed in the SWRO and those recovered in PX1 and PX2.

$$\begin{aligned} SEC_a \eta_P &= SEC_{SWRO} \eta_P - SER_{PX\,1,a} - SER_{PX\,2,a} \\ &= \frac{[1-(1-\text{Rec})(1-PR)\eta_{E,1} - fPR\eta_{E,2}]\pi_{SW}}{\eta_P \text{Rec}(1-\text{Rec})} \end{aligned} \quad (5.23)$$

Applying the same analysis for the process Figure 5.1 (b), SEC_b, can be calculated from eqn. 5.23 by setting *f=1*. Since the diluted draw solution is recycled to the SWRO instead of being used for pressure exchanging in PX2, eqn. 5.24 can be obtained by further setting $\eta_{E,2}$=100% in eqn. 5.23.

$$SEC_b = \frac{(1-PR)[1-(1-\mathrm{Rec})\eta_{E,1}]\pi_{SW}}{\eta_P \mathrm{Rec}(1-\mathrm{Rec})} \quad (5.24)$$

As shown in eqn. 5.23 and 5.24, SEC of SWRO-PRO is a solely function of PR for given Rec and *f*. Therefore, finding the optimum PR is of vital importance to determine the specific energy consumption of a SWRO-PRO system. The SECs of different SWRO-involved processes are summarized in Figure 5.3.

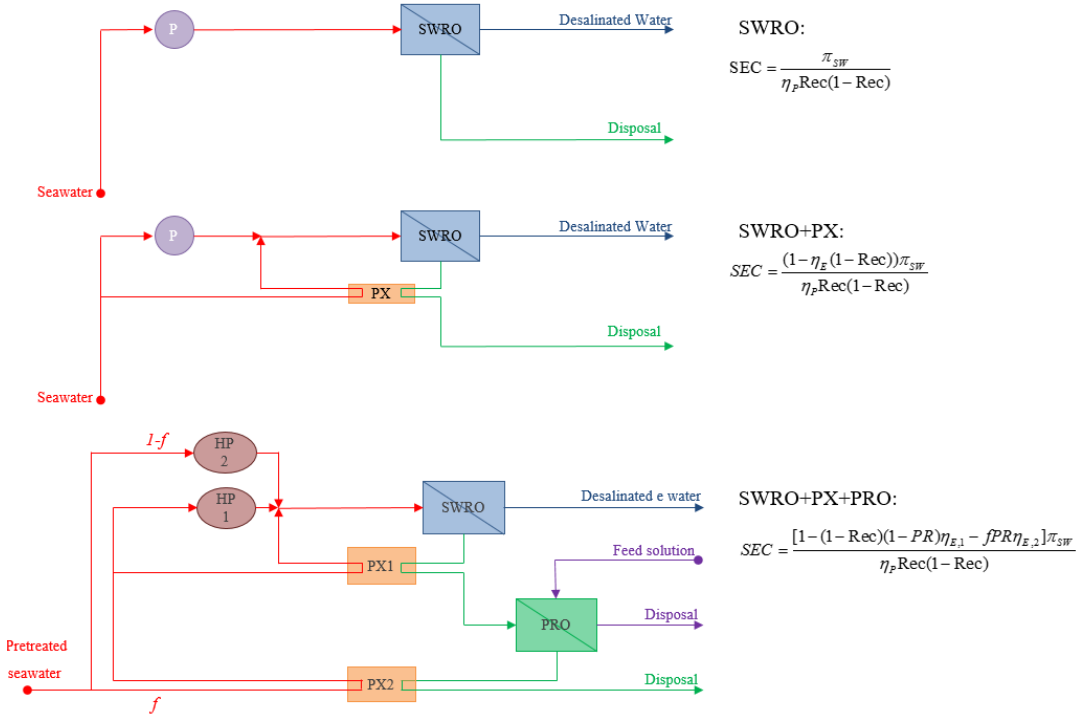

Figure 5.3 Summary of the specific energy consumptions (SECs) on per m^3 of desalinated water basis in various SWRO-involved systems.

5.3. Results and Discussion

5.3.1. Simulation inputs

The simulations in this study are based on the state-of-the-art PES-TFC hollow fiber membranes developed in our previous work, where a power density of 27 W/m^2 at 20 bar has been obtained in lab-scale tests using 1M NaCl solution as the draw solution and deionized water as the feed solution [17, 18]. The characteristics of the membranes and the hypothetical module parameters are

summarized in Table 5.1. The membranes in the modules are assumed to have the same characterizations, which in reality may vary.

Two scenarios are investigated in this study. In the first scenario, the recovery of the SWRO is 25%, which is a typical recovery of a one-stage SWRO system. In the second scenario, the recovery of the SWRO is 50%, which is a typical recovery of a multi-stage SWRO system. In each scenario, two types of feed solutions – freshwater (0 M) and wastewater (0.01 M) – are used in PRO. Wastewater, such as the typical secondary effluent from a wastewater plant or even the reject from a wastewater reverse osmosis plant, can be effectively used as the feed solution for PRO, due to its low TDS and low TOC. In both the cases, the salt concentration of the seawater is 35 g/L and the temperature of the solutions is 25℃.

Membrane Characterizations		Module Parameters	
A (LMH/bar)	3.5	Diameter (cm)	25.4
B (LMH)	0.3	Packing Density (%)	33
S (micron)	450	Number of hollow fibers	20000
Outer diameter (micron)	1025	Total draw flowrate (L/min)	20 - 200
Inner diameter (micron)	575	Total feed flowrate (L/min)	eqn. (5.25)

Table 5.1 Summary of membrane characterizations and module parameters

Specifically, the results presented here are based on the total flowrate of the draw solution in the range of 20-200 L/min in each module. In a PRO process, it is advisable that the maximum recovery of the low salinity source should not exceed 80% in order not to aggravate fouling [19]. Therefore, the flowrate of

the feed solution used in the simulations can be calculated from eqn. 5.6 as following.

$$V_F^0 = \frac{V_D^0}{80\%}\left(\frac{1}{DF} - 1\right) \tag{5.25}$$

5.3.2. Average power density of the PRO modules in the SWRO-PRO process

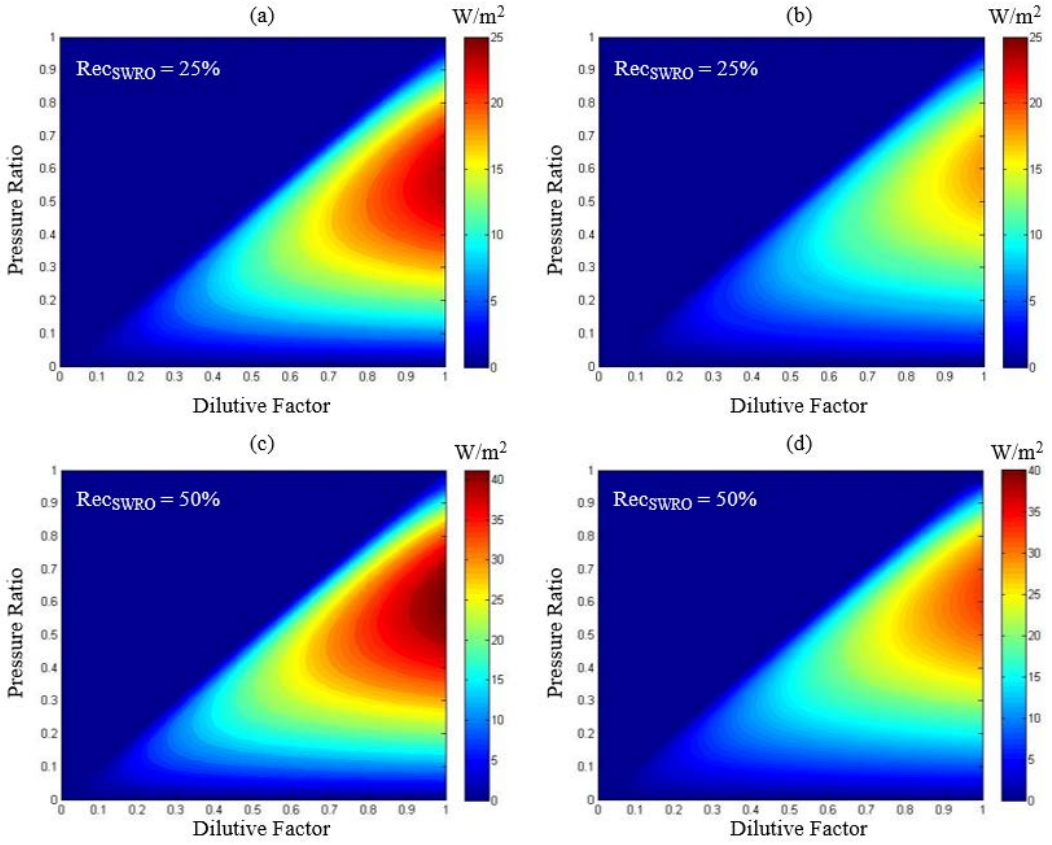

Figure 5.4 Average power density as functions of pressure ratio and dilutive factor
(a) Rec_{SWRO} = 25%, C_D^0 = 0.8 M, C_F^0 = 0 M,
(b) Rec_{SWRO} = 25%, C_D^0 = 0.8 M, C_F^0 = 0.01 M,
(c) Rec_{SWRO} = 50%, C_D^0 = 1.2 M, C_F^0 = 0 M,
(d) Rec_{SWRO} = 50%, C_D^0 = 1.2 M, C_F^0 = 0.01 M.

The average power densities of the module at different conditions are presented in Figure 5.4 (a)-(d). In all of the four cases, the average power densities are functions of both the pressure ratio and the dilutive factor. Since the dilutive factor is only defined for the PRO system, the figures can be used extensively

for any process that involves a PRO system with the same feed and draw solutions.

The diagonal line in each figure presents the operating condition that the hydraulic pressure difference equals the osmotic pressure difference at the inlet of the draw solution, above which the water flux and power density become negative. Therefore, it is not practical to operate the PRO system beyond this line, and the average power density is set to 0 by default. At a given dilutive factor, the average power density is a bell-shaped function of the pressure ratio. The average power density is maximized at the optimal pressure ratio. Either over-pressurizing or under-pressurizing from the optimal point will result in a reduced average power density. At a given pressure ratio, the average power density increases with the dilutive factor and reaches a maximum when there is minimal dilution (i.e., DF → 1).

In Figure 5.4 (a) and (b), the recovery of the SWRO system is 25% and therefore the concentration of the draw solution entering the PRO system is 0.8 M. The average power density of the PRO system at a given dilutive factor and pressure ratio is always smaller when wastewater containing 0.01 M NaCl is used due to the enhanced ICP with increasing salt concentration in the feed solution [20-22]. The maximum average power densities appear as $DF \rightarrow 1$ (i.e., minimal dilution of the draw solution). The maximum average power densities are 23.8 W/m^2 and 18.0 W/m^2, respectively, when freshwater and wastewater are used as the feed. In Figure 5.4 (c) and (d), the recovery of the SWRO system is 50% and therefore the concentration of the draw solution entering the PRO system is 1.2

M, and the maximum average power densities is boosted to 42.0 W/m^2 and 32.9 W/m^2, respectively, when freshwater and wastewater are used as the feed.

Ideally, the maximum power density should increase quadratically with the concentration of the draw solution. However, the results show that when the bulk concentration of the draw solution is increased to 150%, the maximum average power density is increased to 176% instead of 225% when freshwater is used as the feed solution. This can be attributed to ICP – the main factor that compromises the PRO performance [20, 21], which becomes more severe due to the increased reverse salt flux at the high draw solution concentrations [17, 20-22]. This results in a less than ideal increase in the maximum power density.

5.3.3. Optimal operating pressure of PRO

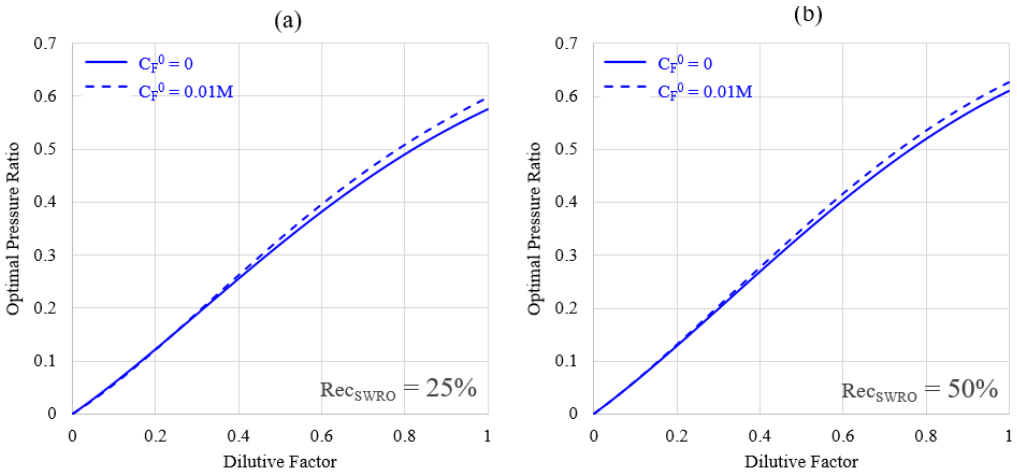

Figure 5.5 The optimal pressure ratio as a function of the dilutive factor
(a) Rec_{SWRO} = 25%, C_D^0 = 0.8 M, C_F^0 = 0 or 0.01 M
(b) Rec_{SWRO} = 50%, C_D^0 = 1.2 M, C_F^0 = 0 or 0.01 M

The operating lines of the PRO systems, presented in Figure 5.5 (a) and (b), are obtained by connecting the points of maximum average power densities at different dilutive factors in Figure 5.4 (a-d). In general, the optimal pressure

ratio is higher at a higher draw solution concentration. This is because the ICP effect is more enhanced due to the increased reverse salt flux at a higher draw solution concentration. At 25% recovery, the optimal pressure ratios at $DF \rightarrow 1$ are 0.58 and 0.60, respectively, when freshwater and wastewater are used. When the draw solution concentration increases from 0.8 M to 1.2 M, the optimal pressure ratios at $DF \rightarrow 1$ are increased to 0.60 and 0.63, respectively. As dilution occurs (decreasing DF), the driving force – the osmotic pressure difference – decreases and the corresponding optimal pressure ratio decreases as well.

5.3.4. Shortest resident time and the minimum membrane area required

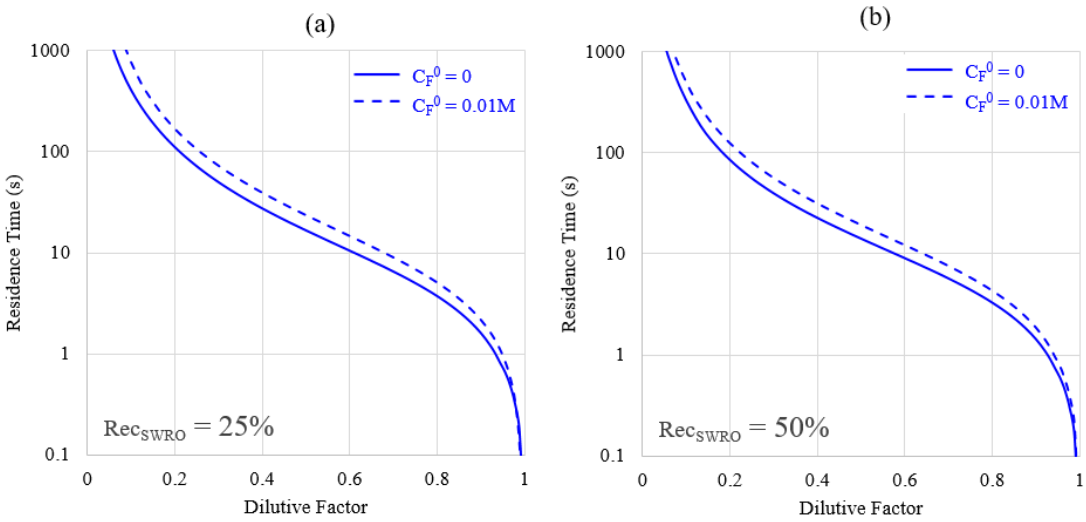

Figure 5.6 Shortest resident time of the draw solution inside the module as a function of the dilutive factor.
(a) Rec_{SWRO} = 25%, C_D^0 = 0.8 M, C_F^0 = 0 or 0.01 M
(b) Rec_{SWRO} = 50%, C_D^0 = 1.2 M, C_F^0 = 0 or 0.01 M

Therefore, the required membrane area can be minimized if the PRO is operated at the optimal pressure ratio along the operating line where the average power density of the module is maximized. The normalized membrane area in terms of residence time (eqn. 5.17) is presented in Figure 5.6 (a) and (b). In both cases,

the residence time increases more steeply when the dilutive factor approaches 0 or 100%. Therefore, it would be preferred to operate the PRO system with a dilutive factor in the range of 30% to 80% to enhance the stability of the system.

The amount of energy that can be harvested from per m^3 of draw solution in the PRO system at a given dilutive factor and pressure ratio is fixed by the following equation.

$$\frac{W_{PRO}}{V_D^0} = \frac{PR}{DF}\frac{\pi_{sw}}{1-\mathrm{Rec}} \tag{5.26}$$

The minimum membrane area required can be affected by both the concentrations of the feed solution and the draw solution. On one hand, the minimal membrane areas are reduced by 15% on average due to the increased water fluxes when the draw solution concentration is increased from 0.8 M to 1.2 M. On the other hand, the effect of increasing the salt concentration in the feed solution can be more significant: when the feed solution concentration increases from 0 M to 0.01 M, the minimal membrane area required is increased by more than 50% on average in both cases.

5.3.5. Comparisons of SECs in various SWRO-involved systems

The specific energy consumption on a basis of per m^3 of desalinated water for various processes at 25% SWRO recovery and 50% SWRO recovery are summarized in Figure 5.7 (a) and (b), respectively. According to eqn. 5.4, the following equation has to be satisfied so that the SWRO-PRO process is physically possible.

$$\frac{f}{1-\mathrm{Rec}} > 1 \tag{5.27}$$

The value of $\frac{f}{1-\text{Rec}}$ indicates the ratio of flowrates of the draw solution exiting and entering the PRO system. A value of $\frac{f}{1-\text{Rec}}$ larger than unity indicates a positive ΔV_{PRO}. A larger f indicates that more water is drawn by the PRO system, and more energy can be recovered in PX2. Therefore, the SEC is smaller at a larger f.

As shown in Figure 5.7 (a), at 25% recovery, it takes 5.51 kWh to produce 1 m^3 of desalinated water. A PX can effectively reduce the SEC by 67.5% to 1.79 kWh/m^3. Currently, the PX is the dominant technology for energy recovery in a SWRO plant [11, 23]. By diluting the concentrated brine (the draw solution) to the seawater level, the PRO is able to further decrease the SEC to 1.08 kWh/m^3 at f = 100%.

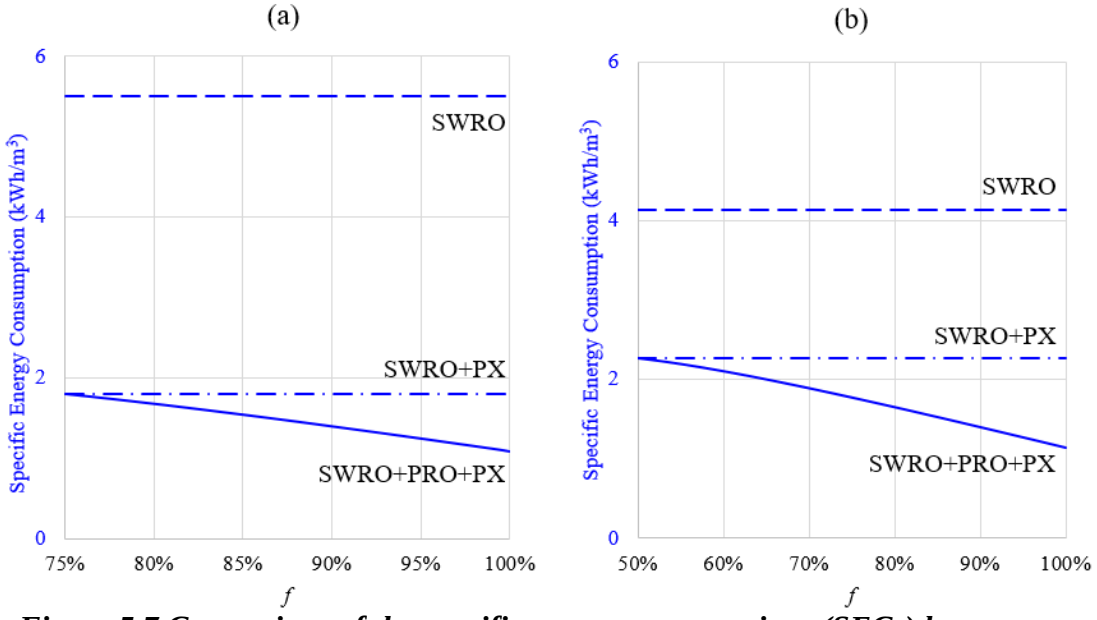

Figure 5.7 Comparison of the specific energy consumptions (SECs) between SWRO, SWRO+PX and SWRO+PRO+PX. While the SECs of SWRO and SWRO+PX are independent of f, the SEC of SWRO+PRO+PX can be further reduced because more energy can be recovered in PRO at a higher f. The values are calculated with η_P=80% and η_E=90%. (a) Rec_{SWRO} = 25% (b) Rec_{SWRO} = 50%.

As shown in Figure 5.7 (b), at 50% recovery, the SEC of the SWRO plant without a PX is 4.13 kWh/m^3, which is lower that of the 25% recovery plant. This is because even though it takes a lower pressure to achieve the 25% recovery, the energy used to pressurize the remaining 75% brine is wasted without a PX. If the energy in the brine is recovered by a PX, the SEC of a 50% recovery SWRO becomes 2.27 kWh/m^3, 26.8% higher than that of the 25% recovery SWRO with a PX. When PRO is used for energy recovery, the SEC of the SWRO-PRO process further drops to 1.14 kWh/m^3 at f = 100%.

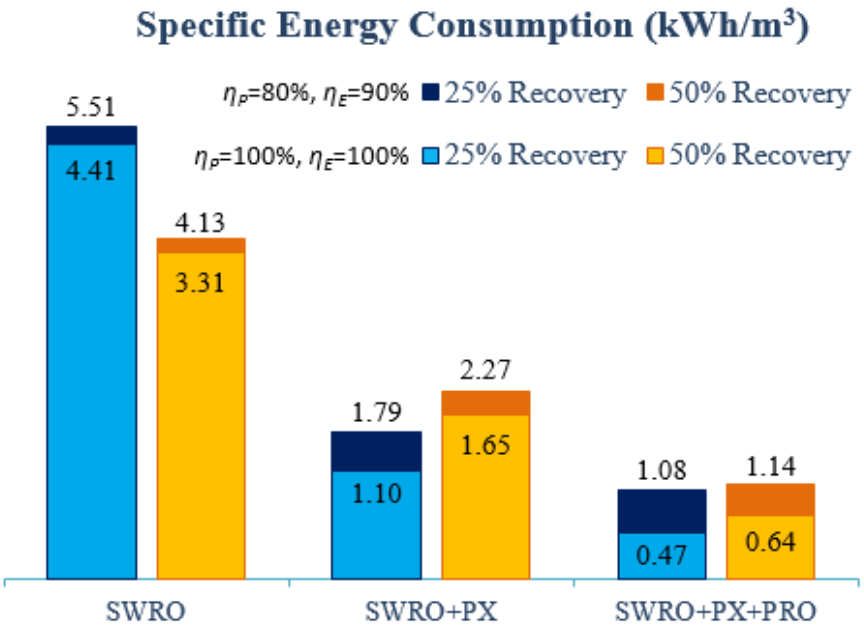

Figure 5.8 Comparison of the minimum specific energy consumptions of the SWRO, SWRO+PX, SWRO+PX+PRO processes with different efficiencies of the HP and PX

Figure 5.8 summarizes the minimal SECs of various SWRO-involved processes with different efficiencies of the HP and the PX. As shown, the SECs are increased due to the when the efficiencies of PX and HP are reduced. Interestingly, the smaller the recovery of SWRO, the larger the increase in SECs due to the reduced efficiencies. This is because there is more energy carried by the concentrated brine at a smaller recovery. As more energy can be recovered

by incorporating PX and PRO, low efficiency will cause more energy losses. This is also why the energy loss due to the reduced efficiencies in SWRO+PX+PRO is larger than that in SWRO+PX, which in turn is larger than that in SWRO.

5.3.6. SER and SEC of SWRO-PRO integrated processes

The relative amounts of specific energy recovery (SER) and specific energy consumption (SEC) in an ideal process (i.e., η_P = 100%, η_E = 100%) are investigated and the results are presented in Figure 5.9 (a). The y-axis is the flowrate of the brine/seawater streams normalized by the flowrate of the pretreated seawater feed, and the x-axis is the pressure of the brine/seawater streams normalized by the operating pressure of SWRO. Therefore, the area enclosed by x = y = 100% represents the total energy required for the desalination step (eqn. 5.18). Area 1 represents the SER by PX1 (eqn. 5.22), and area 2 represents the SER by PX2 (eqn. 5.21). Figure 5.9 (a) also exposes the limitations of energy recovery by PRO in the SWRO-PRO integrated process. Firstly, the concentration brine has enough energy to pressurize the feed seawater to the operating pressure of SWRO, but its flowrate cannot match that of the feed seawater because a fraction of Rec of the feed seawater is recovered as freshwater in SWRO. Secondly, the flowrate of the diluted brine is always less than or equal to the flowrate of the feed seawater, and it does not have the adequate energy to pressurize the feed seawater directly to the operating pressure of SWRO because the operating pressure of PRO is only a fraction of PR of the operating pressure of SWRO. Therefore, areas 3 and 4 represents the dead loss of energy that cannot be recovered, which is the specific energy

consumption of the process. Area 3 is indeed the energy loss due to inadequate dilution of the draw solution in PRO, which can be completely eliminated by increasing f to 1 as in Figure 5.1 (b). Area 4 is the energy loss due to the operation of the SWRO-PRO system. It cannot be eliminated as long as freshwater is produced. The additional energy that can be recovered by PRO (eqn. 5.21) in the SWRO+PX+PRO process is presented in area 5 in Figure 5.9 (b), which is only a fraction of Rec of the energy recovered by PX1 (area 2). Area 6 in Figure 5.9 (b) represents the energy recovered in the SWRO+PX process. As shown, area 6 is the sum of area 1 and the upper portion of area 2. This is because in the SWRO+PX process, all the energy carried by the high pressure brine is used for energy recovery, and therefore the pressure of the brine can be reduced to 0. However, in the SWRO+PX+PRO process, the brine exiting PX1 still has a medium high pressure as required by the PRO system.

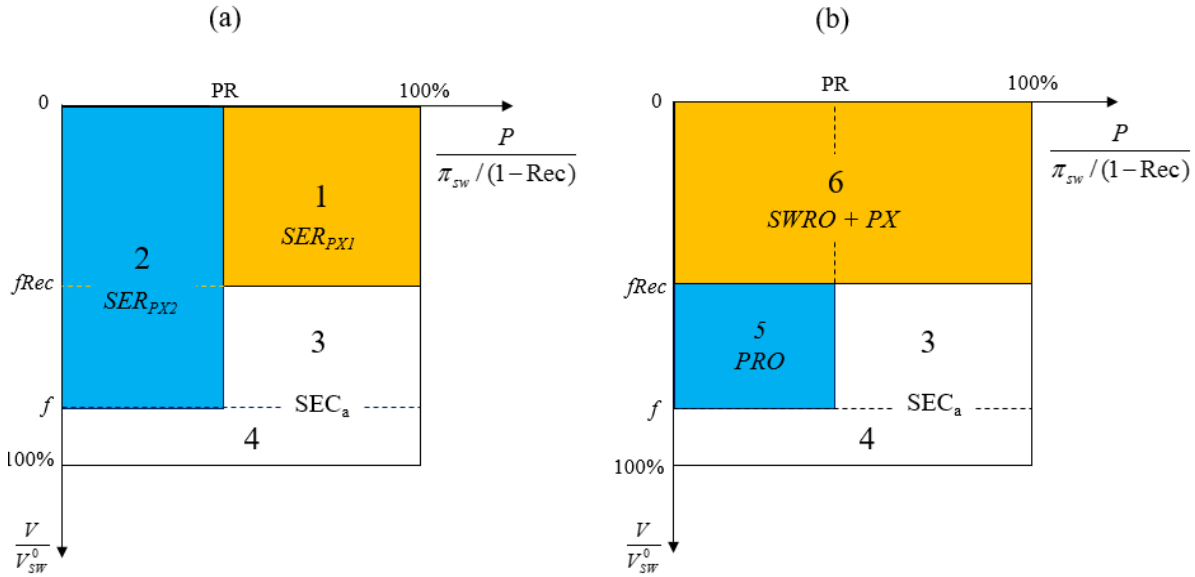

Figure 5.9 (a) The specific energy recovery (SER) by PX1 and PX2 and specific energy consumption (SEC) in a SWRO+PX+PRO process as fractions of the total energy required for desalination. Area 1: SER by PX1, Area 2: SER by PX2, Area 3+Area 4: SEC

(b) The additional SER by PRO compared to the conventional SWRO+PX process as fractions of the total energy required for desalination, Area 5: additional SER by PRO, Area 6: SER by the conventional SWRO+PX process.

Incorporating a PRO system into the existing SWRO-PX plant will lead to an energy saving of 0.71 – 1.13 kWh/m^3. It is projected that 36 million m^3/day of desalinated water will be produced by SWRO by 2016 [24]. Therefore, it is estimated that 25.6 – 40.7 million kWh/day can be saved globally.

5.4. Conclusion

In this study, detailed designs of novel SWRO-PRO processes are presented, with the option to form a closed-loop process that can substantially cut down the pretreatment costs of the seawater. The SECs of various SWRO-involved processes are investigated. It shows that the SEC of the SWRO-PRO integrated process is the lowest among all the cases. When the SWRO is operated at 25% and 50% recovery and the brines are diluted to the seawater level, the SECs to produce 1 m^3 of desalinated water can be reduced to 1.08 kWh and 1.14 kWh, respectively. It is evidenced from the SWRO-PRO model that finding the optimal operating pressure of the PRO system is of vital importance to maximize the average power density of the PRO system and minimize the SEC of the SWRO-PRO integrated process. While the integration of SWRO and PRO is possible, development of new PRO membranes that can sustain the optimal operating pressure of the PRO system and maintain a high water flux is needed.

Nomenclature and units

A: pure water permeability (PWP) [$m^3/(m^2 s Pa)$]

A_m: membrane area [m^2]

B: salt permeability [$m^3/(m^2s)$]

C: concentration [g/m^3]

D: diffusivity [m^2/s]

d_i: inner diameter [m]

f: fraction

i: Van't Hoff factor

J_s: reverse salt flux [$g/(m^2s)$]

J_w: water flux [$m^3/(m^2s)$]

k: mass transfer coefficient [$m^3/(m^2s)$]

P: pressure [Pa]

R: universal gas constant [J/(moleK)]

S: structure parameter [m]

t: residence time [s]

T: temperature [K]

V: flowrate [m^3/s]

W: work [J]

Greek Symbols

ε: porosity

η: efficicency

τ: tortuosity

λ: wall thickness [m]

π: osmotic pressure [Pa]

Abbreviations

DF: dilutive factor

PD: power density

PR: pressure ratio

Re: Reynold number

Rec: recovery

Sc: Schmidt number

Sh: Sherwood number

SEC: specific energy consumption [J/ m^3]

SER: specific energy recovery [J/ m^3]

Subscripts

a: process in Figure 1 (a)

b: process in Figure 1 (b)

E: energy recovery device

D: draw solution

F: feed solution

P: pump

PRO: pressure retarded osmosis

PX1: pressure exchanger 1

PX2: pressure exchanger 2

SW: seawater

SWRO: seawater reverse osmosis

Superscripts

0: initial state

f: final state

PRO: with pressure retarded osmosis

ERD: with energy recovery device

Appendices

Appendix A

Eqn. 5.7-5.10 can be rearranged as functions of dV_D as follows.

$$dA_m = \frac{\rho_W}{\rho_W J_W + J_S} dV_D \tag{5.28}$$

$$dV_F = dV_D \tag{5.29}$$

$$dC_D = -\left(\frac{J_S \rho_W}{V_D(\rho_W J_W + J_S)} + \frac{C_D}{V_D}\right) dV_D \tag{5.30}$$

$$dC_F = -\left(\frac{J_S \rho_W}{V_F(\rho_W J_W + J_S)} + \frac{C_F}{V_F}\right) dV_D \tag{5.31}$$

Appendix B

The osmotic pressure of the feed seawater is π_{sw}. After a recovery of *Rec*, the osmotic pressure of the concentrated brine becomes $\frac{\pi_{sw}}{1-\mathrm{Rec}}$, which is also the minimum operating pressure required to achieve such a recovery in SWRO and therefore the hydraulic pressure of the concentrated brine. The total energy required for desalination is as follows.

$$W_{SWRO} = V_{sw}^0 \frac{\pi_{SW}}{1-\mathrm{Rec}} \tag{5.32}$$

The following equation can be derived by normalizing eqn. 5.32 by the flowrate of the desalinated water.

$$SEC_{SWRO} = \frac{W_{SWRO}}{\mathrm{Rec} V_{sw}^0} = \frac{\pi_{SW}}{\mathrm{Rec}(1-\mathrm{Rec})} \tag{5.33}$$

For the process in Figure 5.1 (a), the hydraulic pressure of the concentrated brine is reduced to $PR\frac{\pi_{sw}}{1-\mathrm{Rec}}$ in PX2. Therefore the total energy recovery by PX2 is as follows.

$$W_{PX\,2a} = V_{sw}^{f}\Delta P_{PX\,2}\eta_E = [(1-\mathrm{Rec})V_{SW}^{o}][(1-PR)\frac{\pi_{SW}}{1-\mathrm{Rec}}]\eta_{E,2} \tag{5.34}$$

The following equation can be derived by normalizing eqn. 5.34 by the flowrate of the desalinated water.

$$SER_{PX\,2,a} = \frac{W_{PX\,2}}{\mathrm{Re\,c}V_{SW}^{0}} = \frac{(1-PR)}{\mathrm{Rec}}\pi_{SW}\eta_{E,2} \tag{5.35}$$

After PRO, the flowrate of the diluted brine increases from V_{sw}^{f} to fV_{SW}^{0} and the pressure is maintained at $PR\frac{\pi_{sw}}{1-\mathrm{Rec}}$. In PX1, the pressure of the diluted brine is reduced to 0. Therefore, the total energy recovery by PX1 is as follows.

$$W_{PX1,a} = fV_{sw}^{0}\Delta P_{PX1}\eta_E = fV_{sw}^{0}[\frac{PR}{(1-\mathrm{Rec})}\pi_{SW} - 0]\eta_{E,1} \tag{5.36}$$

The following equation can be derived by normalizing eqn. 5.36 by the flowrate of the desalinated water.

$$SER_{PX1,a} = \frac{W_{PX1,a}}{\mathrm{Rec}V_{SW}^{o}} = \frac{fPR}{\mathrm{Rec}(1-\mathrm{Rec})}\pi_{SW}\eta_{E,1} \tag{5.37}$$

By energy conservation, pumping (NEC_a) is needed to provide the energy, in additional to those recovered in PX1 and PX2, for desalination in SWRO.

$$SEC_{SWRO}\eta_P = SEC_a\eta_P + SER_{PX1,a} + SER_{PX\,2} \tag{5.38}$$

Substituting the expressions of SEC_{SWRO}, SER_{PX1} and $SER_{PX\,2}$ into eqn. 5.36 and rearranging them yields the following equation.

$$SEC_a \eta_P = SEC_{SWRO} \eta_P - SER_{PX1,a} - SER_{PX2,a}$$
$$= \frac{[1-(1-\text{Rec})(1-PR)\eta_{E,1} - fPR\eta_{E,2}]\pi_{SW}}{\eta_P \text{Rec}(1-\text{Rec})} \quad (5.39)$$

For the process in Figure 5.1 (b), the same amount of energy is recovered in PX2. However, the flowrate of the diluted brine only increases to fV_{SW}^0 in the PRO system. Therefore, the SER of PX1 and NEC_b are as follows.

$$SEC_b = \frac{(1-PR)[1-(1-\text{Rec})\eta_{E,1}]\pi_{SW}}{\eta_P \text{Rec}(1-\text{Rec})} \quad (5.40)$$

References

[1] Kim J, Lee J, Kim JH. Overview of pressure-retarded osmosis (PRO) process and hybrid application to sea water reverse osmosis process. Desalin. Water Treat. 2012;43:193-200.

[2] Kim J, Park M, Snyder SA, Kim JH. Reverse osmosis (RO) and pressure retarded osmosis (PRO) hybrid processes: model-based scenario study. Desalination. 2013;322:121-30.

[3] Achilli A, Prante JL, Hancock NT, Maxwell EB, Childress AE. Experimental results from RO-PRO: a next generation system for low-energy desalination. Environ. Sci. Technol. 2014;48:6437-43.

[4] Prante JL, Ruskowitz JA, Childress AE, Achilli A. RO-PRO desalination: An integrated low-energy approach to seawater desalination. Applied Energy. 2014;120:104-14.

[5] Sarper S, In-Ho Y, Yong Gyun P. Membrane based desalination apparatus with osmotic energy recovery and membrane based desalination method with osmotic energy recovery. US2014/0238938A1, GS Engineer & Construction Corp 2014.

[6] Saito K, Irie M, Zaitsu S, Sakai H, Hayashi H, Tanioka A. Power generation with salinity gradient by pressure retarded osmosis using concentrated brine from SWRO system and treated sewage as pure water. Desalin. Water Treat. 2012;41:114-21.

[7] Sharqawy MH, Zubair SM, Lienhard JH. Second law analysis of reverse osmosis desalination plants: an alternative design using pressure retarded osmosis. Energy. 2011;36:6617-26.

[8] Tanioka A. Energy recovery by pressure retarded osmosis using concentrated brine from SWRO and treated waste water. http://www.megatonwater.com/2014.

[9] Han G, Ge Q, Chung T-S. Conceptual demonstration of novel closed-loop pressure retarded osmosis process for sustainable osmotic energy generation. Applied Energy. 2014;132:383-93.

[10] Efraty A. Pressure retarded osmosis in closed circuit: a new technology for clean power generation without need of energy recovery. Desalin. Water Treat. 2013;51:7420-30.

[11] Hauge LJ. The pressure exchanger – a key to substantial lower desalination cost. Desalination. 1995;102:219-23.

[12] Banchik LD, Sharqawy MH, Lienhard JH. Limits of power production due to finite membrane area in pressure retarded osmosis. J. Membr. Sci. 2014;468:81-9.

[13] Sharqawy MH, Lienhard JH, Zubair SM. Thermophysical properties of seawater: a review of existing correlations and data. Desalin. Water Treat. 2012;16:354-80.

[14] Elimelech M, Phillip WA. The future of seawater desalination: energy, technology and the environment. Science. 2011;333:712-17.

[15] Zhu A, Christofides PD, Cohen Y. Minimization of energy consumption for a two-pass membrane desalination: Effect of energy recovery, membrane rejection and retentate recycling. J. Membr. Sci. 2009;339:126-37.

[16] Zhu A, Christofides PD, Cohen Y. Effect of thermodynamic restriction on energy cost optimization of RO membrane water desalinition. Ind. Eng. Chem. Res. 2009:6010-21.

[17] Wan CF, Chung TS. Osmotic power generation by pressure retarded osmosis using seawater brine as the draw solution and wastewater brine as the feed. J. Membr. Sci. 2015;479:148-158

[18] Zhang S, Sukitpaneenit P, Chung T-S. Design of robust hollow fiber membranes with high power density for osmotic energy production. Chem. Eng. J. 2014;241:457-65.

[19] Thorsen T, Holt T. The potential for power production from salinity gradients by pressure retarded osmosis. J. Membr. Sci. 2009;335:103-10.

[20] Achilli A, Cath TY, Childress AE. Power generation with pressure retarded osmosis: an experimental and theoretical investigation. J. Membr. Sci. 2009;343:42-52.

[21] She Q, Jin X, Tang CY. Osmotic power production from salinity gradient resource by pressure retarded osmosis: Effects of operating conditions and reverse solute diffusion. J. Membr. Sci. 2012;401-402:262-73.

[22] Zhang S, Chung TS. Minimizing the instant and accumulative effects of salt permeability to sustain ultrahigh osmotic power density. Environ. Sci. Technol. 2013;47:10085-92.

[23] Migliorini G, Luzzo E. Seawater reverse osmosis plant using the pressure exchanger for energy recovery: a calculation model. Desalination. 2004;165:289-98.

[24] GWI. Desalination market 2010. Global Water Intelligence 2010.

Chapter 6: Maximize the operating profit of a SWRO-PRO integrated process for optimal water production and energy recovery

6.1. Introduction

In our previous study, we calculated that the SECs of SWRO-PRO are 1.08 kWh/(m^3 of desalinated water) and 1.14 kWh/(m^3 of desalinated water) for 25% and 50% recovery, respectively [1]. However, the optimal operating condition of the SWRO-PRO process might be different from the conventional SWRO without PRO, because the system dynamics of the SWRO-PRO process is different from that of the conventional SWRO process. A SWRO recovery of 25% or 50% may no longer be the optimal recovery in a SWRO-PRO process. Therefore, in this work, we will continue to investigate the system dynamics of SWRO-PRO and develop a strategy to optimize it. Moreover, the SWRO-PRO process can mitigate the negative environmental impacts of the SWRO brine disposal by diluting the brine to the same salinity of seawater in PRO [2-4]. While most of the previous modelling works focused on the local mass transfer [5, 6], there are limited studies that investigated the PRO performance under dilution along the membrane modules [1, 7-12]. Investigation of dilution effects often requires integration of mass transport equations [1, 7-12]. Xiao et al. and Sivertsen et al. have developed full models to describe the inherit concentration polarization and dilution effects in hollow fiber modules [25, 26].

In this study, based on reasonable assumptions and simplifications, an analytical model that can be easily implemented without complicated integrations has been developed. Not only can it predict the PRO performance with a high

accuracy but also perform as a handy tool for the process design and optimization. With this model, we will present a holistic view of the SWRO-PRO process by introducing the operating profit, namely, the profit generated for every m^3 of seawater entering the process, to facilitate the optimization of the SWRO-PRO process in its entirety.

6.2. Theory

6.2.1. Process description

Figure 6.1 (a) and 1 (b) present the process flow diagrams of a SWRO and a SWRO-PRO processes, respectively. In the SWRO process, seawater is directly pressurized by a high pressure pump and sent to the SWRO unit. The brine from the SWRO unit then goes through an energy recovery device (ERD) to recover the energy carried by the high pressure brine, which can be used to compensate the energy consumption of the high pressure pump. In the SWRO-PRO process, the brine after ERD 1 can be used as the draw solution in the PRO unit and subsequently the osmotic energy can be harvested in ERD 2 to further compensate the energy consumption of the high pressure pump. The ERD can be any device that recovers the energy from a high pressure stream, but a pressure exchanger (PX) is preferred because of its ease to operate and high efficiency [13]. The feed solution to the PRO can be fresh surface water or treated wastewater with a low salinity. The SWRO should be strategically located near such a low salinity water source in order to reduce the piping and pumping costs and potentially to recover more osmotic energies from the concentrated brine if more feed solutions are readily available. Although the detailed process design in terms of pipelines and energy integration can be

different [1, 14, 15], Figure 6.1 (b) presents a universal process flow that can be modified to more specific designs.

The recovery of the SWRO unit, *R*, is defined as the flowrate ratio of the SWRO permeate over the seawater feed.

$$R = \frac{\Delta V_{SWRO}}{V_{SW}} \tag{6.1}$$

Where V_{SW} is the flowrate of seawater feed entering the SWRO unit and ΔV_{SWRO} is the flowrate of the SWRO permeate.

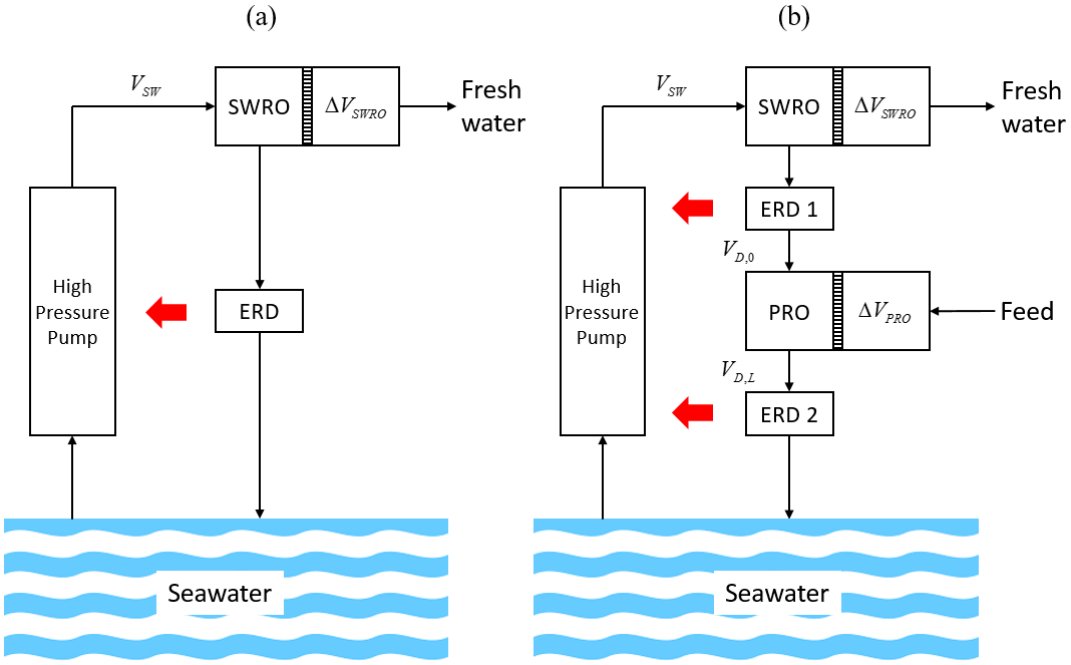

Figure 6.1 Schematic drawings of (a) a SWRO process (b) a SWRO-PRO process.

The dilution factor of the draw solution exiting the PRO unit, DF_L, is defined as the percentage of the original draw solution in the diluted draw solution.

$$DF_L = \frac{V_{D,0}}{V_{D,L}} = 1 - \frac{\Delta V_{PRO}}{V_{D,L}} \tag{6.2}$$

where $V_{D,0}$ is the flowrate of the draw solution feed (i.e., concentrated seawater brine) to the PRO unit, $V_{D,L}$ is the flowrate of the diluted draw solution exiting the PRO unit and ΔV_{PRO} is the flowrate of the PRO permeate. A DF_L approaching 0% indicates the draw solution is getting infinitely diluted and a DF_L aproaching100% indicates the draw solution is not getting diluted.

It is most desirable to dilute the SWRO brine to the same salinity as seawater in the PRO unit before discharge in order to minimize the negative impact on the marine ecosystem and recover more osmotic energies. This is also important if a PX is used as ERD 2 in order to minimize mixing and maximize the efficiency of the PX [16]. Therefore, the following equation needs to be satisfied.

$$\Delta V_{PRO} = \Delta V_{SWRO} \tag{6.3}$$

Under this condition, Eqn. 6.2 can be written as follows.

$$DF_L = 1 - R \tag{6.4}$$

6.2.2. Power generation by PRO

For an ideal semi-permeable membrane, the water permeation flux is proportional to the pure water permeability (PWP), A, and the driving force, which is the difference between the osmotic pressure difference $\Delta\pi$ and the hydraulic pressure difference ΔP.

$$J_w^{ideal} = A(\Delta\pi - \Delta P) \tag{6.5}$$

The actual water flux of a PRO membrane is, however, lower than that of the ideal case, due to the effects of internal concentration polarization (ICP), external concentration polarization (ECP) and the reverse salt flux (J_s). An

actual/ideal flux ratio, θ, can be used to correct the difference between the actual and ideal water fluxes [17]. θ can be considered as a constant with satisfactory accuracy over a wide range of operating hydraulic pressure differences across the PRO membrane [17].

$$J_w = \theta J_w^{ideal} \tag{6.6}$$

The power density, *PD*, of a PRO membrane is the product of hydraulic pressure difference, ΔP, and water permeation flux, J_w.

$$PD = J_w \Delta P \tag{6.7}$$

Combining the above equations yields an equation of *PD* as a quadratic function of ΔP.

$$PD = \theta A(\Delta\pi - \Delta P)\Delta P \tag{6.8}$$

Eqn. 6.8 has a maximum value of $1/4\theta A\Delta\pi^2$ when the optimum hydraulic pressure difference equals to one half of the osmotic pressure difference.

6.2.3. PRO model

As shown in Figure 6.2, the draw solution and the feed solution go counter-currently in the hollow fiber module. The draw solution is on the lumen side of the module while the feed solution is on the shell side of the module. The flow direction of the draw solution is arbitrarily chosen as the positive direction. For a differential area of the PRO membrane, the volume of water leaves the feed solution equals to that enters the draw solution.

$$dV_{PRO} = A(\Delta\pi - \Delta P)dM \tag{6.9}$$

where *dM* is the differential membrane area.

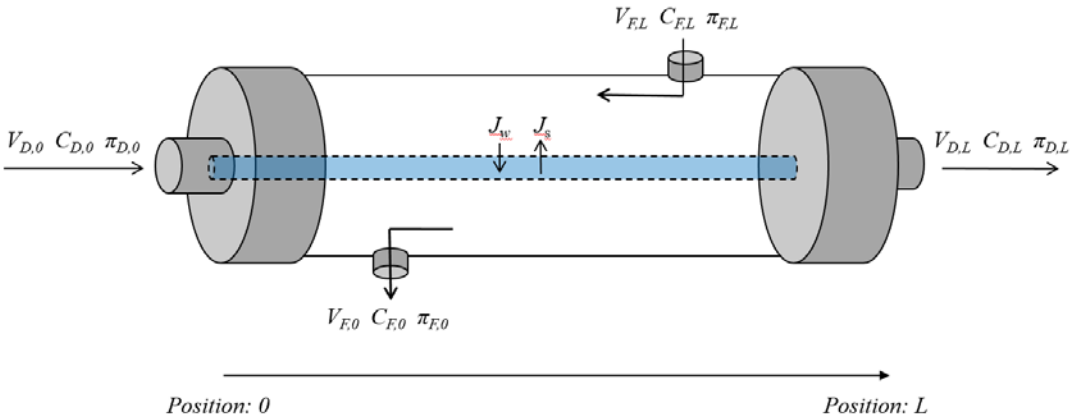

Figure 6.2 Schematic drawing of the PRO process in a single piece of hollow fiber.

By the modifications and simplifications presented in the Appendix, the following equations can be obtained.

$$\int \frac{d(\Delta\pi - \Delta P)}{(\Delta\pi - \Delta P)} = \theta A \frac{\Delta\pi_L - \Delta\pi_0}{\Delta V_{PRO}} M \tag{6.10}$$

$$\overline{J_w} = \frac{\Delta V_{PRO}}{M} = \theta A \frac{(\Delta\pi_L - \Delta P) - (\Delta\pi_0 - \Delta P)}{\ln(\Delta\pi_L - \Delta P) - \ln(\Delta\pi_0 - \Delta P)} = \theta A (\Delta\pi - \Delta P)_{LM} \tag{6.11}$$

where $\overline{J_w}$ is the average water flux of the hollow fiber module, $(\Delta\pi - \Delta P)_{LM}$ is the log-mean driving force difference, $\Delta\pi_0$ and $\Delta\pi_L$ are the osmotic pressure differences between the draw solution and the feed solution at the inlet and outlet of the PRO module, respectively.

The following dimensionless numbers – local dilutive factor (DF), local concentrative factor (CF), initial flowrate ratio (FR), initial concentration ratio (CR) and operating pressure ratio (PR) – are defined to facilitate the analyses.

$$DF = \frac{C_D}{C_{D,0}} \tag{6.12}$$

$$CF = \frac{C_F}{C_{F,0}} \tag{6.13}$$

$$FR = \frac{V_{F,0}}{V_{D,0}} \tag{6.14}$$

$$CR = \frac{C_{F,0}}{C_{D,0}} \tag{6.15}$$

$$PR = \frac{\Delta P}{\pi_{D,0}} \tag{6.16}$$

where *DF* is the local dilution factor of the draw solution, *CF* is the local concentration factor of the feed solution, *FR* and *CR* are the initial flowrate ratio and the initial concentration ratio between the feed solution and the draw solution, respectively, and *PR* is the pressure ratio of the operating pressure of PRO over the osmotic pressure of the concentrated brine from SWRO.

The normalized water flux, φ, is defined as follows.

$$\varphi = \frac{\overline{J_w}}{\theta A \pi_{D,0}} \tag{6.17}$$

The average power density of the module can be calculated from the average water flux.

$$\overline{PD} = \overline{J_w} \Delta P \tag{6.18}$$

Similarly, the normalized average power density, ω, is the product of the normalized water flux and pressure ratio.

$$\omega = \frac{\overline{PD}}{\theta A \pi_{D,0}^{\ 2}} = \varphi PR \tag{6.19}$$

The optimal operating pressure ratio can be found by solving the following equation.

$$\frac{d(\varphi PR)}{dPR} = 0 \tag{6.20}$$

As shown, φ and ω are only functions of the operation parameters. They are independent of the membrane properties. Therefore, the conclusion can be extended to a wide range of PRO membranes. It should be noted that Eqn. 6.17-6.20 can also be applied to the case where the draw solution and feed solution go concurrently in the PRO hollow fiber modules.

6.2.4. Energy consumption of SWRO

The specific energy consumption (SEC) of a stand-alone SWRO, is limited by its recovery. For a perfect semi-permeable membrane, the minimum specific energy consumption on per m^3 of seawater feed basis in the presence of a RED, SEC_{SWRO}, can be calculated from the equation below [18, 19]:

$$SEC_{SWRO} = \frac{1-\eta_E(1-R)}{\eta_p(1-R)}\pi_{SW} \tag{6.21}$$

where π_{SW} is the osmotic pressure of the seawater, η_P is the efficiency of the high pressure pump and η_E is the efficiency of the ERD.

In the SWRO-PRO process, more energy can be recovered from the high-pressure brine by incorporating the PRO system as follows [1, 14]:

$$SEC_{SWRO-PRO} = \frac{1-\eta_E(1-R+PR\cdot R)}{\eta_p(1-R)}\pi_{SW} \tag{6.22}$$

As shown in Eqn. 6.22, the SEC of a SWRO-PRO process is a function of recovery of the SWRO system and operating pressure ratio of the PRO system. One may reach the conclusion that $SEC_{SWRO-PRO}$ can be minimized if PR is unity. However, a PR of unity indicates no driving force for PRO and hence the water flux and power density are 0. The optimal value of PR are restricted by the

dynamics of the SWRO-PRO system as described in session 6.2.2. Hence, Eqn. 6.17-20 and 22 imply the trade-off between the specific energy consumption of the SWRO-PRO system and the power density of the PRO unit: a reduction of $SEC_{SWRO-PRO}$ requires a smaller R and a larger PR, which inevitably compromises water production and the power density of the PRO unit.

6.2.5. Operating profit of a SWRO-PRO system

The operating profit of SWRO-PRO, OP ($/m^3 of seawater), can be defined as the profit generated for every m^3 of seawater that enters the SWRO-PRO system.

$$OP = \alpha R - \beta SEC \tag{6.23}$$

where α is the water price ($/m^3 of freshwater), β is the electricity price ($/J).

The prices of water and electricity can be used as the weighting factors to determine the optimal operating condition of the SWRO-PRO system. Noticing that the unit of water price is in $/m^3 while the electricity price is in $/J, the following factors are defined to compare the two prices on the same basis.

$$\gamma = \frac{\beta \pi_{sw}}{\alpha} \tag{6.24}$$

where $\beta \pi_{sw}$ is the modified price of electricity ($/m^3 of seawater, 1 J/Pa = 1 m^3) and γ is the price ratio. Therefore, the dimensionless operating profit, ρ, can be expressed as follows.

$$\rho = \frac{OP}{\alpha} = (R - \gamma SEC) \tag{6.25}$$

The operating profit of a conventional SWRO process can be calculated from the following equation.

$$\rho_{SWRO} = R - \frac{\gamma[1-\eta_E(1-R)]}{\eta_P(1-R)} \tag{6.26}$$

In an ideal case where the high pressure pump and the pressure exchanger are 100% efficient, Eqn. 6.26 can be reduced to the following equation.

$$\rho_{SWRO} = R - \frac{\gamma R}{1-R} \tag{6.27}$$

If $\gamma < 1$, the above equation has the maximal value at the optimal recovery.

$$\rho_{SWRO,\max} = (1-\sqrt{\gamma})^2 \tag{6.28}$$

$$R_{SWRO,opt} = 1-\sqrt{\gamma} \tag{6.29}$$

Similarly, in the SWRO-PRO process, the operating profit can be calculated from the following equation.

$$\rho_{SWRO-PRO} = R - \frac{\gamma[1-\eta_E(1-R+PR\cdot R)]}{\eta_P(1-R)} \tag{6.30}$$

If the high pressure pump and the pressure exchanger are 100% efficient, Eqn. 6.30 can be reduced to the following equation.

$$\rho_{SWRO-PRO} = R - \frac{\gamma(R-PR\cdot R)}{1-R} \tag{6.31}$$

For a fixed value of *PR*, the above equation has a maximal value at the optimal recovery.

$$\rho_{SWRO-PRO,\max} = (1-\sqrt{\gamma(1-PR)})^2 \tag{6.32}$$

$$R_{SWRO-PRO,opt} = 1-\sqrt{\gamma(1-PR)} \tag{6.33}$$

By comparing Eqn. 6.32 and 6.33 with Eqn. 6.28 and 6.29, the advantages of the SWRO-PRO process over the conventional SWRO process are that SWRO-PRO can (1) be operated at a higher recovery and (2) achieve a higher operating profit for every m^3 of seawater entering the system.

6.2.6. Optimization of the SWRO-PRO process

The strategy to optimize the SWRO-PRO process is (1) to maximize the operating profit of SWRO-PRO and (2) simultaneously to maintain the highest possible power density of PRO at the respective recovery of SWRO. Mathematically, this means finding the maximal value of Eqn. 6.30 subjecting to the relationship between *R* and *PR* as described by Eqn. 6.19 and 6.20.

6.3. Results and Discussion

6.3.1. Model validation

6.3.1.1. Prediction of PRO water flux

Figure 6.3 compares the experimental water flux of the TFC-PES hollow fiber [15] with water fluxes calculated from different models including the ideal model (Eqn. 6.5), the modified model with θ (Eqn. 6.6) and a full model considering ICP, ECP and J_s effects [1, 6] under the following conditions: $C_{D,0}$ = 1000 mole/m^3, $C_{F,L}$ = 0 mole/m^3 and T = 298K. The TFC-PES membrane was developed in our previous studies and its properties are presented in Table 5.1 [20]. As shown, the ideal model tends to overestimate the water flux by a factor over 150%. The actual/ideal flux ratio can be determined by linear fitting the experimental data with the modified model (Eqn. 6.6). In this case, θ is determined to be 0.45 with a R^2 of 0.994 between the experimental data and the modified model. A similar value was also reported by Efraty [17, 21] against other published experimental data sets with high accuracy [5, 6, 22].

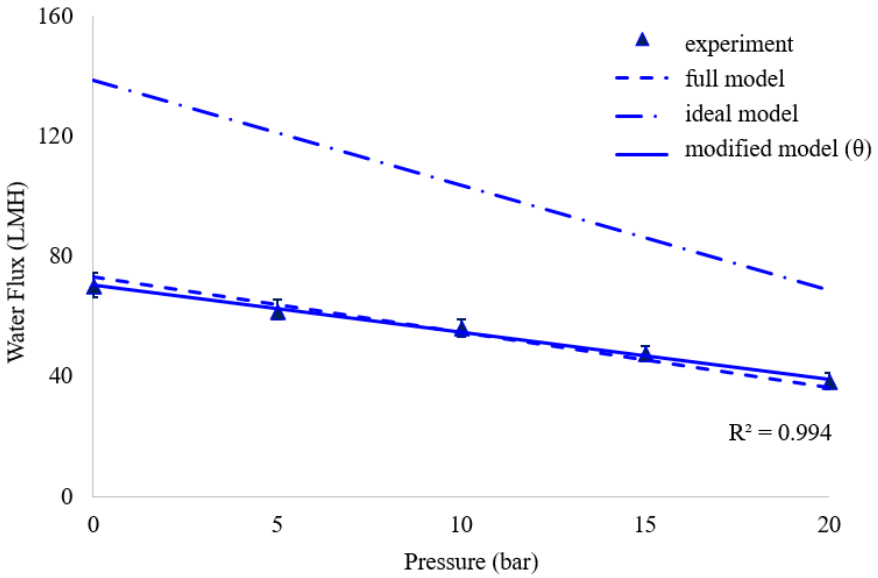

Figure 6.3 A comparison between the experimental water flux and water fluxes predicted by different models.

6.3.1.2. Prediction of PRO membrane area

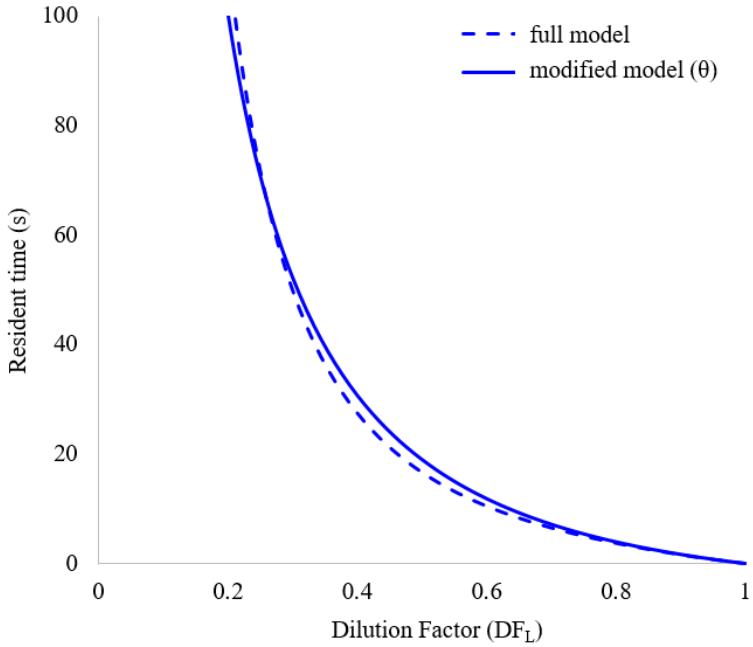

Figure 6.4 A comparison of the draw solution resident time predicted by the full model and the modified model.

Eqn. 6.11 is validated in terms of its accuracy to predict the membrane areas needed to achieve a certain dilution. The total membrane area, A_m, is an important parameter for the design of membrane processes. However, A_m

increases with the capacity of the PRO unit (i.e., higher draw solution and feed solution flowrates). Therefore, it is more practical to examine the resident time of the draw solution in the module, which can be calculated from Eqn. 6.11 as follows:

$$t = \frac{Md_i}{4V_{D,0}} = (1 - DF_L)\frac{d_i}{4\overline{J_w}} \tag{6.34}$$

where t is the residence time of the draw solution and di is the inner diameter of the hollow fiber. Figure 6.4 shows a comparison of the residence time predicted by the full model [1, 6] and the modified model with θ. The deviation of the modified model from the full model is within 14%. This deviation is the accumulated deviation throughout the hollow fiber module. Because the membrane area required increases exponentially as dilution occurs, it is recommended to keep the dilution factor above 20%.

6.3.2. Optimal operating pressure and pressure ratio

The power density normalized by the osmotic pressure of the draw solution (Eqn. 6.19) as a function of pressure ratio and dilution factor in the PRO unit is presented in Figure 6.5. The vertical axis of the figure is divided by (*1-CR*) to eliminate the effect of the feed concentration. At a given dilution factor, the normalized power density is a bell-shaped function of the pressure ratio. In general, the maximal normalized power density and the optimal pressure ratio decrease as dilution occurs. Only at DF_L approaches 1 when no dilution happens, the optimal modified pressure ratio (i.e., PR/(1-CR)) approaches 0.5 and the maximal normalized power density approaches 0.25, corresponding to the optimal operating pressure of $1/2\Delta\pi$ and the maximum power density of

$1/4\theta A\Delta\pi^2$. As dilution happens, the osmotic pressure of the draw solution decreases and the maximum power density drops as well. At DF_L=0.5, the optimal modified pressure ratio is 0.32 and the maximal normalized power density drops to $0.12\theta A\Delta\pi^2$. This indicates that the maximal power density of a PRO unit under 50% dilution is less than 50% of the maximal power density when no dilution occurs. The modified pressure ratio and the maximal power density keep dropping and approach 0 as the dilution factor approaches 0 under infinite dilution. The optimal operating curve of a PRO unit is obtained by connecting the peak power density at each dilution factor in Figure 6.5.

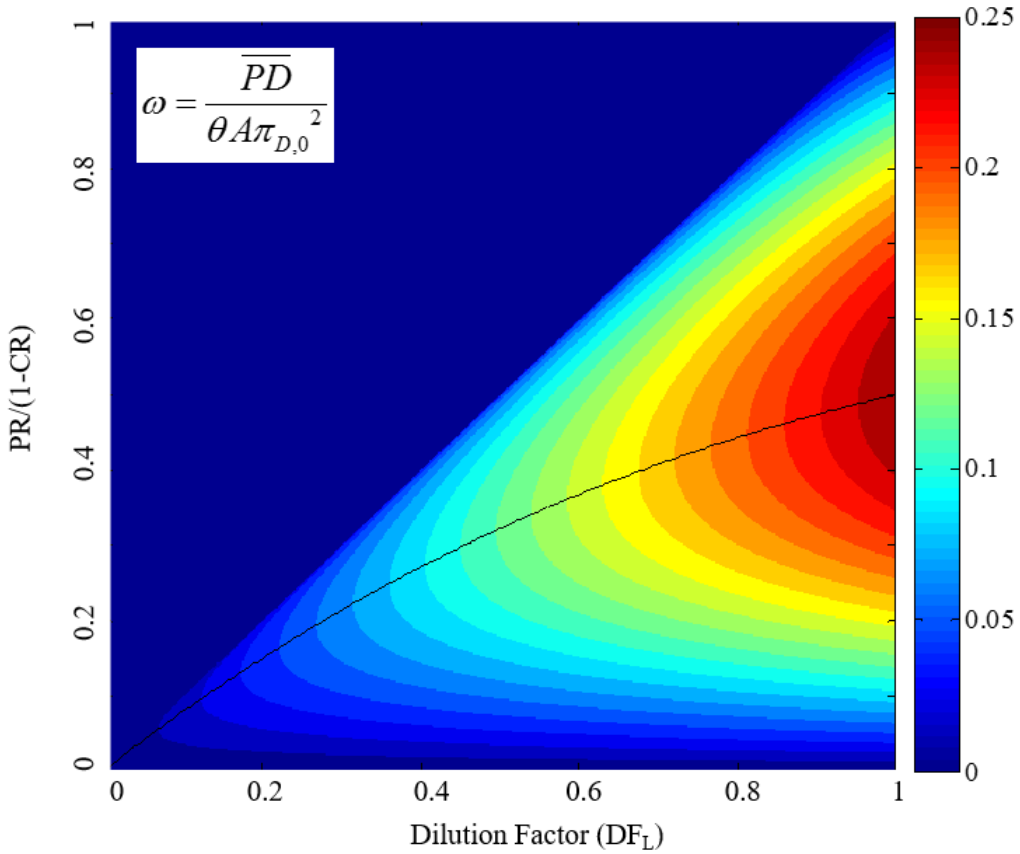

Figure 6.5 Normalized power density by the osmotic pressure of the draw solution (ω) as a function of dilution factor and normalized pressure ratio in a PRO unit for a given πD,0. The solid line is the optimal operating pressure ratio as a function of the dilution factor of the PRO unit.

Figure 6.5 shows how the normalized power density by the osmotic pressure of the draw solution (ω) changes with dilution for a given draw solution concentration in the PRO unit. However, in the SWRO-PRO system, the draw solution concentration (i.e., the concentrated brine) entering the PRO unit varies with the recovery of the SWRO unit. The initial osmotic pressure of the draw solution, $\pi_{D,0}$, increases with the recovery of SWRO as follows.

$$\pi_{D,0} = \frac{\pi_{SW}}{1-R} \tag{6.35}$$

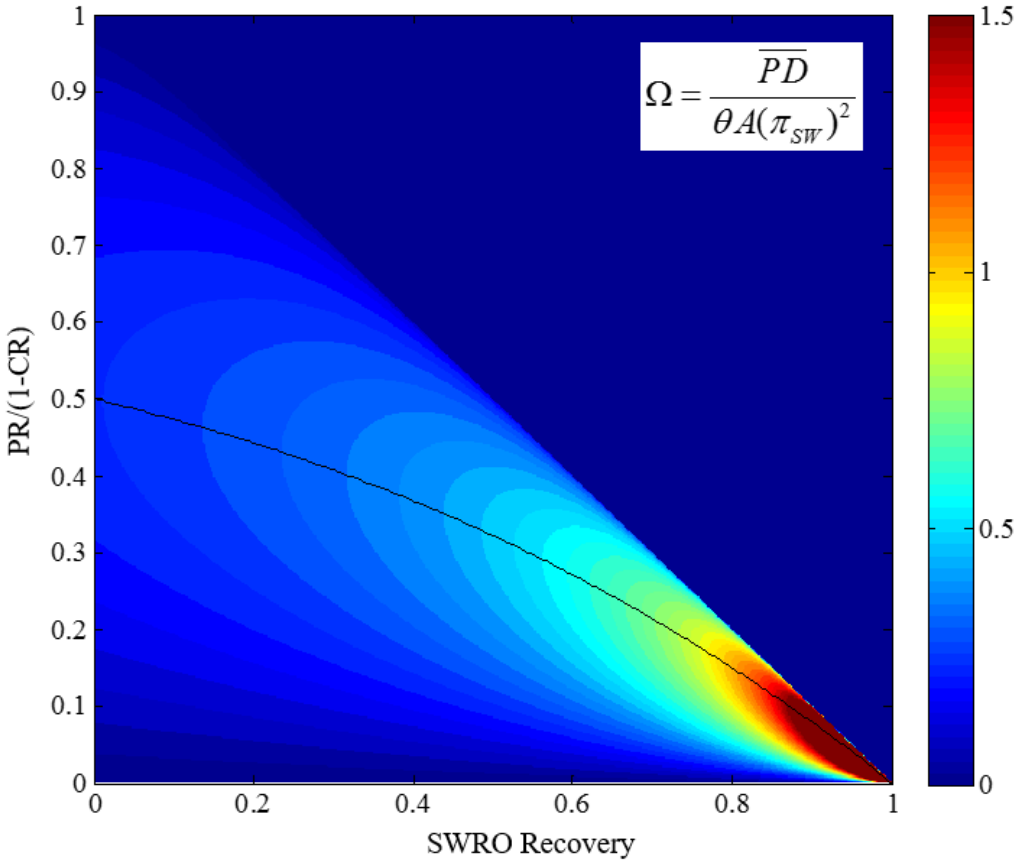

Figure 6.6 Normalized power density by the osmotic pressure of sea water (Ω) as a function of recovery of the SWRO unit and the normalized pressure ratio of the PRO unit in the SWRO-PRO process. The solid line is the optimal operating pressure ratio as a function

Therefore, the maximal amount of energy that can be harvested in PRO also increases with the recovery of SWRO. In order to compare the power densities on the same basis of π_{SW}, the power densities are then normalized by the osmotic

pressure of seawater instead of the osmotic pressure of the concentrated brine as follows.

$$\Omega = \frac{\overline{PD}}{\theta A(\pi_{SW})^2} = \frac{\omega}{(1-R)^2} \tag{6.36}$$

Ω is the normalized power density by the osmotic pressure of seawater. As shown in Figure 6.6, the maximal power density that can be recovered is smaller when the recovery is lower due to the low concentration of the brine. The maximal value of Ω at the respective recovery increases gradually from 0.25 to 0.5 when the recovery increases from 0 to 0.5, and increases more rapidly as the recovery approaches 1. The optimal operating curve of the PRO unit in a SWRO-PRO is obtained by connecting the peak power density at each SWRO recovery in Figure 6.6.

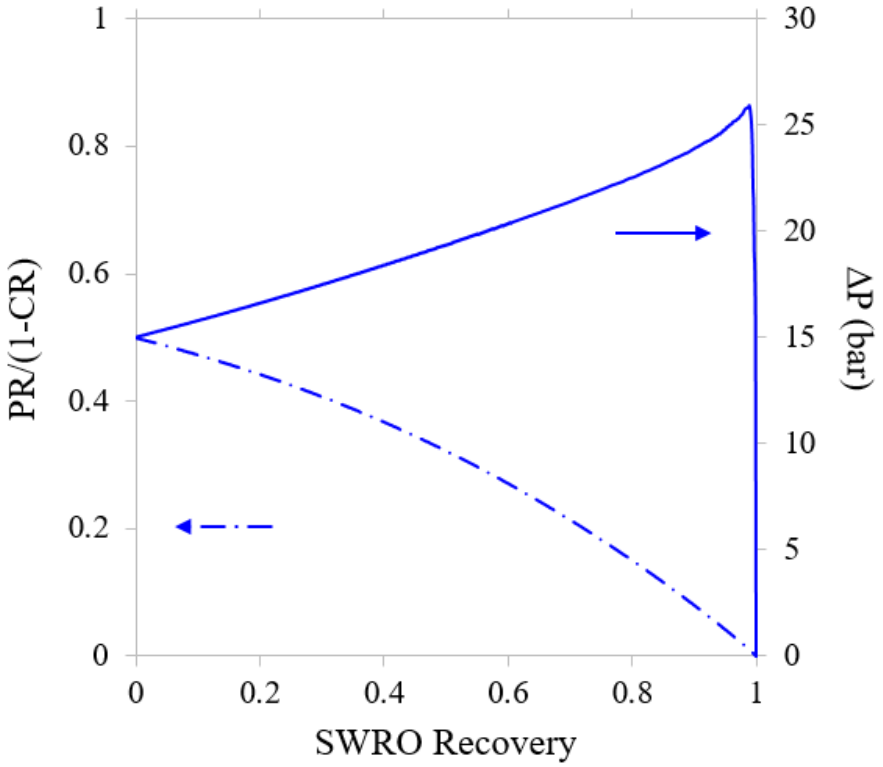

Figure 6.7 Optimal operating pressure and normalized pressure ratio of PRO as a function of SWRO recovery, calculated with π_{SW}=30 bar.

Since the absolute operating pressure in PRO is the product of the pressure ratio and the osmotic pressure of the draw solution, the absolute operating pressure of PRO increases with the osmotic pressure of the draw solution but decreases with the pressure ratio at increasing recovery. Figure 6.7 presents the optimal modified pressure ratio and the absolute pressure in PRO calculated using π_{SW} = 30 bar with an equivalent NaCl concentration of 600 mole/m^3 and freshwater as feeds. While the modified pressure ratio monotonically decreases from 0.5 to 0, the absolute pressure increases gradually from 15 to 26 bar when recovery increases from 0 to 99% and then drops abruptly as recovery approaches 1 and the modified pressure ratio approaches 0. However, it should be noted that it is not practical to operate SWRO at recoveries approaching 100%. At a recovery of 50%, the absolute operating pressure is approximately 20 bar. The maximal value of the absolute operating pressure of PRO is approximately 26 bar. Therefore, PRO membranes that can withstand a pressure of 26 bar will be strong enough for the proposed SWRO-PRO process.

6.3.3. Optimization of SWRO-PRO

The price ratio between electricity and water reflects their relative demands. A smaller electricity-to-water price ratio implies that more energy can be consumed to produce water while maintaining the SWRO-PRO process profitable. On the contrary, a larger ratio implies that electricity is scarcer than water and the SWRO-PRO process may no longer be profitable if it consumes too much energy. While the water price influences the total profit of the SWRO-PRO process, it is only the electricity-to-water price ratio that determines the optimal operating condition of the process according to Eqn. 6.31. The

electricity price, water price and their ratios in different countries are listed in Table 6.1. As shown, the price ratio ranges from 0.01 to 0.5 in most countries. Interestingly, Jamaica and Denmark have similar electricity prices, but their water prices are 12 times different. This will significantly impact the optimal operating condition of SWRO-PRO.

Country	Water Price, (α, USD/m^3)	Elec. Price (β, USD/kWh)	Mod. Elec. Price ($\beta\pi_{sw}$, USD/m^3)	Price Ratio ($\gamma=\beta\pi_{sw}/\alpha$)
Jamaica	0.76	0.45	0.375	0.489
Singapore	0.94	0.21	0.173	0.185
US	1.30	0.17	0.140	0.108
Dubai	2.64	0.06	0.049	0.019
Denmark	9.21	0.40	0.33	0.036

Table 6.1 Summary of water and electricity prices in different countries

The normalized operating profits obtained are presented in Figure 6.8. The maximal normalized operating profit is unity at the price ratio of 0. This means electricity is free and therefore the SWRO can operate at a recovery of 100% and still make a good profit. As the price ratio increases, the optimal recovery decreases and at some point the operating profit becomes 0 or even negative because electricity cost surpasses the profit of producing desalinated water. Eventually, as price ratio continues to increase, the operating profit will become negative at all recoveries. In the price ratio range between 0.01 and 0.5, the optimal recovery is between 0.38 and 0.9. The optimal operating curve of the

SWRO unit is obtained by connecting the maximal operating profit at each price ratio in Figure 6.8.

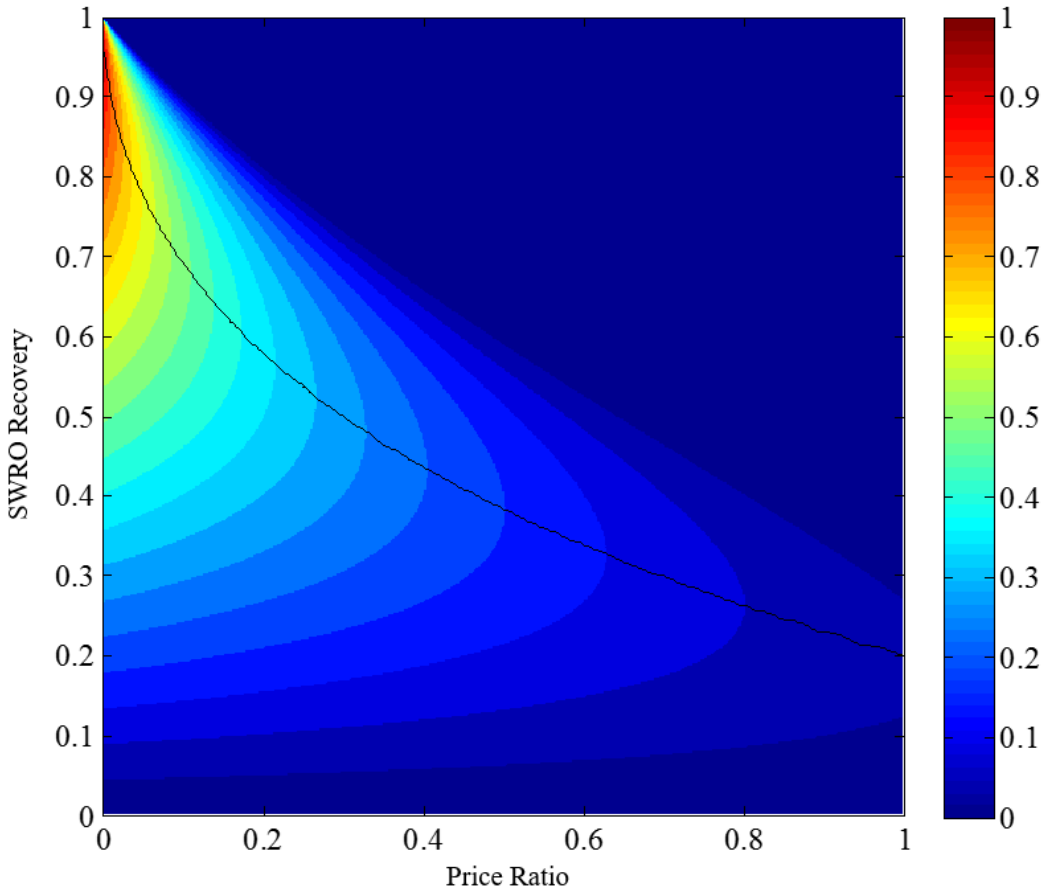

Figure 6.8 Normalized operating profit (ρ) as a function of price ratio and SWRO recovery of SWRO-PRO. The solid line is the optimal recovery of SWRO-PRO as a function of the electricity-water price ratio.

6.3.4. Normalized operating profit and specific energy consumption

The maximal normalized operating profits of the conventional SWRO process and the SWRO-PRO process are shown in Figure 6.9. Since the price ratio in most countries are smaller than 0.2, SWRO-PRO can harvest additional operating profits up to 22%. At a price ratio of 0.5, more than 100% of additional operating profit can be achieved.

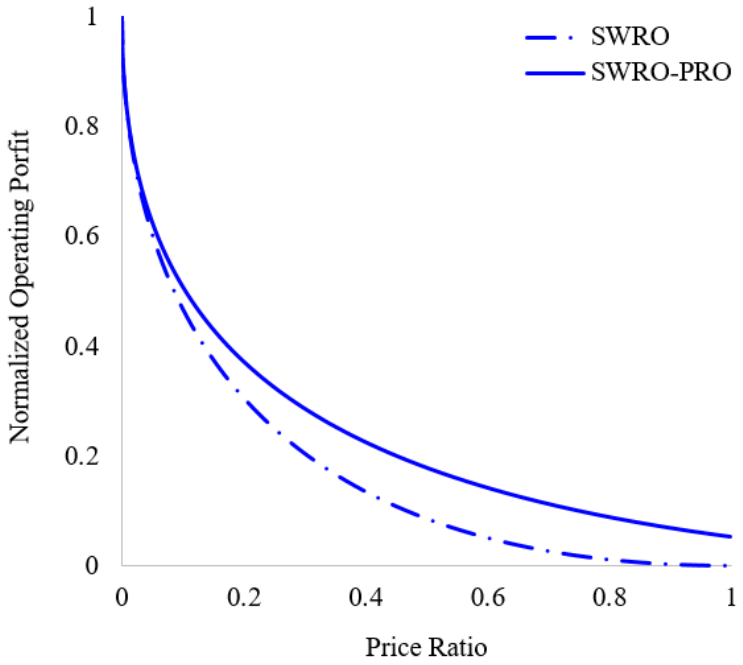

Figure 6.9 A comparison of the maximal normalized operating profits (ρmax) of SWRO and SWRO-PRO at different price ratios, calculated with η_P = 90% and η_E = 95%.

Another important parameter of desalination is the specific energy consumption to generate 1 m^3 of desalinated water. Eqn. 6.37 and 6.38 can be obtained by dividing Eqn. 6.21 and 6.22 by R to convert the basis from per m^3 of seawater to per m^3 of desalinated water.

$$SEC'_{SWRO} = \frac{1-\eta_E(1-R)}{\eta_p R(1-R)}\pi_{SW} \tag{37}$$

$$SEC'_{SWRO-PRO} = \frac{1-\eta_E(1-R+PR\cdot R)}{\eta_p R(1-R)}\pi_{SW} \tag{38}$$

Figure 6.10 presents the specific energy consumptions to generate 1 m^3 of desalinated water by SWRO and SWRO-PRO. Though there is a minimum value between 10% and 20% recovery in both cases, this would be the optimal recovery only if the electricity-to-water price ratio is equal to 1 as shown in Figure 6.8. In other words, the efforts to minimize the SEC of SWRO is based on the assumption that the price of water produced is equally to the cost of

electricity. However, in most of the countries, the electricity-to-water price ratio is much smaller than 1 and hence operating the system at a higher recovery is indeed favored to increase the operating profits. Therefore, maximizing the operating profit of SWRO can be a better strategy than minimizing SEC to optimize a SWRO-PRO process. As shown, the SWRO-PRO system is able to reduce the specific energy consumption by up to 35%.

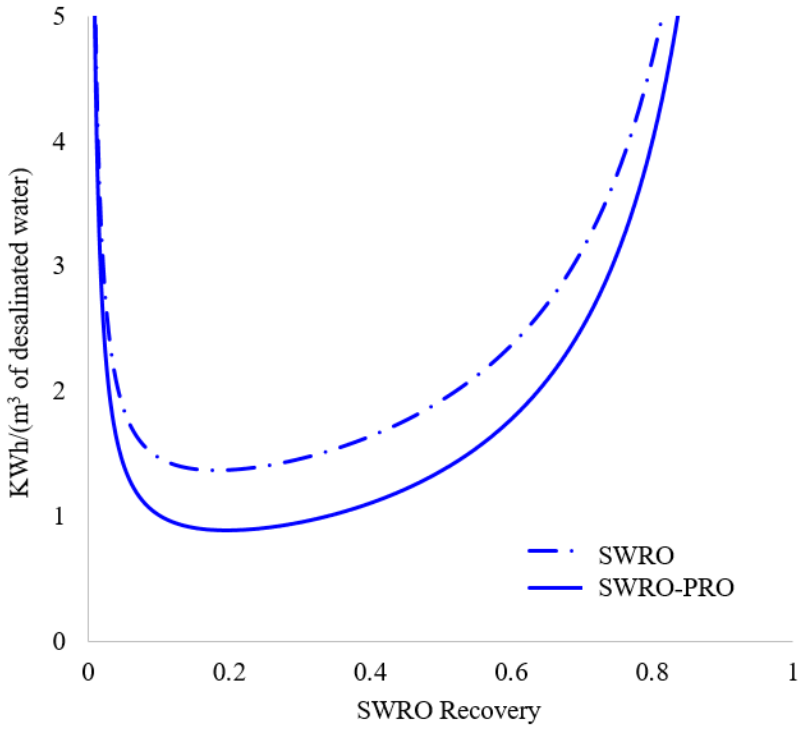

Figure 6.10 A comparison of specific energy consumptions to generate 1 m^3 of desalinated water between SWRO and SWRO-PRO, calculated with π_{sw}= 30 bar, η_P = 90% and η_E = 95%.

6.4. Conclusion

The operating profit, the uttermost objective, of a SWRO-PRO process has been investigated in this study. Maximization of the operating profit of SWRO can be a better approach than minimization of SEC in order to optimize SWRO-PRO, since it takes into account of the relative demands of water and energy. The SWRO-PRO process can be optimized by finding the optimal recovery that

maximizes the operating profit and the optimal pressure ratio that maximizes the power density at the respective recovery. The model shows that while the prices of water and electricity determine the operating profit of the system, only their ratio determines the optimal operating condition. As evidenced from the analyses, integration of SWRO with PRO will push the recovery above 50%, reduce the specific energy consumption by up to 35% and increase the operating profit by up to 100%. Development of membranes that can withstand a hydraulic pressure difference of 26 bar and have a good water permeability are needed for the proposed SWRO-PRO system. While integration of PRO with SWRO will reduce the specific energy of desalination and increase the operating profit, such integration requires additional capital investment in membranes, pumps and energy recovery devices. Detailed techno-economic and life cycle analyses are needed in the future to investigate in terms of capital expense (CAPEX) and operating expense (OPEX) in order to fully assess the feasibility of SWRO-PRO.

Nomenclatures

A: pure water permeability [$m^3/(m^2sPa)$]

B: salt permeability [$m^3/(m^2s)$]

C: concentration [$mole/m^3$]

d_i: inner diameter [m]

i: Van't Hoff factor

J_w: water flux [$m^3/(m^2s)$]

M: membrane area [m^2]

P: pressure [Pa]

R: Recovery

T: temperature [K]

V: flowrate [m^3/s]

Greek Symbols

α: price of water [\$/m^3 of freshwater]

β: price of electricity [\$/J]

φ: normalized water flux

γ: price ratio

η: efficiency

π: osmotic pressure [Pa]

θ: actual/ideal flux ratio

ρ: normalized operating profit

ω: normalized power density by the osmotic pressure of the brine

Ω: normalized power density by the osmotic pressure of seawater

Abbreviations

CF: concentrative factor of feed

DF: dilutive factor of draw

FR: feed/draw flowrate ratio

OP: operating profit

PD: power density

PR: pressure ratio

SEC: specific energy consumption per m^3 of seawater [J/ m^3]

Subscripts

D: draw solution

E: energy recovery device

F: feed solution

P: High pressure pump

SW: seawater

SWRO: conventional SWRO process

SWRO-PRO: SWRO-PRO process

0: at the draw solution entrance of the module

L: at the draw solution exit of the module

Superscripts

ideal: under ideal conditions

SEC': specific energy consumption per m^3 of desalinated water [J/ m^3]

Appendix

The dilution factor of the draw solution in the PRO unit, *DF*, is defined as the percentage of the original draw solution in the diluted draw solution or the ratio of the draw solution over its initial concentration. Similarly, the concentration factor of the feed solution in the PRO unit, *CF*, is defined as the ratio of the feed solution concentration over its initial value. One of the important characters of PRO membranes is the low salt permeability and $J_s/J_w << 1$ [20, 22-24].Therefore, the following equations can be derived from Eqn. 6.12 and 6.13.

$$DF = \frac{C_D}{C_{D,0}} = \frac{V_{D,0}}{V_D} \quad \text{(a1)}$$

$$CF = \frac{C_F}{C_{F,0}} = \frac{V_{F,0}}{V_F} \quad \text{(a2)}$$

Eqn a3 and a4 can be obtained by differentiating the above two equations

$$dDF = d(\frac{V_{D,0}}{V_D}) = (-\frac{V_{D,0}}{V_D^2})dV_{PRO} = (-\frac{DF^2}{V_{D,0}})dV_{PRO} \quad \text{(a3)}$$

$$dCF = d(\frac{V_{F,0}}{V_F}) = (-\frac{V_{F,0}}{V_F^2})dV_{PRO} = (-\frac{CF^2}{V_{F,0}})dV_{PRO} \quad \text{(a4)}$$

The pressure drops of the feed and draw solutions should be minimized during operation of the PRO module. When the osmotic pressure difference between the draw and feed solutions changes significantly, $d\Delta P$ becomes much smaller than $d\Delta\pi$.

$$d(\Delta\pi - \Delta P) = d(\Delta\pi) = d(\pi_D - \pi_F) \quad \text{(a5)}$$

$$d(\Delta\pi - \Delta P) = d(\pi_{D,0}DF - \pi_{F,L}CF) \quad \text{(a6)}$$

Eqn. a6 can be expanded with substitution of Eqn. a2-a3.

$$d(\Delta\pi - \Delta P) = -(\frac{\pi_{D,0}DF^2}{V_{D,0}} - \frac{\pi_{F,L}CF^2}{V_{F,0}})\theta A(\Delta\pi - \Delta P)dM \quad \text{(a7)}$$

where $\pi_{D,0}$ and $\pi_{F,L}$ are the osmotic pressures of the draw and feed solutions entering the PRO process, respectively. Rearranging the above equation and integrating both sides yield the following equation.

$$\int \frac{d(\Delta\pi - \Delta P)}{(\Delta\pi - \Delta P)} = -\int (\frac{\pi_{D,0}DF^2}{V_{D,0}} - \frac{\pi_{F,L}CF^2}{V_{F,0}})\theta A dM \quad \text{(a8)}$$

Noticing that *DF* and *CF* are the only two variables on the right side of Eqn. a8, the following estimations can be applied to simplify the integration. The deviation between this estimation and the exact solution, as we calculated, is less than 10%.

$$DF^2 = DF_0 DF_L \quad \text{(a9)}$$

$$CF^2 = CF_0 CF_L \quad \text{(a10)}$$

Based on the material balance between the draw and feed solutions, the following equation can be obtained from Eqn. 12-14.

$$\frac{1}{CF_0} = 1 - \frac{1}{FR}\left(\frac{1}{DF_L} - 1\right) \tag{a11}$$

Combining Eqn.a8-a11 and integrating from $A_m = 0$ yields the following equations.

$$\int \frac{d(\Delta\pi - \Delta P)}{(\Delta\pi - \Delta P)} = \theta A \frac{\Delta\pi_L - \Delta\pi_0}{\Delta V_{PRO}} dM \tag{a12}$$

$$\overline{J_w} = \frac{\Delta V_{PRO}}{M} = \theta A \frac{(\Delta\pi_L - \Delta P) - (\Delta\pi_0 - \Delta P)}{\ln(\Delta\pi_L - \Delta P) - \ln(\Delta\pi_0 - \Delta P)} = \theta A (\Delta\pi - \Delta P)_{LM} \tag{a13}$$

References:

[1] C.F. Wan, T.S. Chung, Energy recovery by pressure retarded osmosis (PRO) in SWRO-PRO integrated processes, Applied Energy 162 (2016) 687-698.

[2] T.S. Chung, L. Luo, C.F. Wan, Y. Cui, G. Amy, What is next for forward osmosis (FO) and pressure retarded osmosis (PRO), Separation and Purification Technology (2015), in-press for publication

[3] G. Han, S. Zhang, X. Li, T.S. Chung, Progress in pressure retarded osmosis (PRO) membranes for osmotic power generation, Progress in Polymer Science 51 (2015) 1-27.

[4] T.S. Chung, S. Zhang, K.Y. Wang, J.C. Su, M.M. Ling, Forward osmosis processes: yesterday, today and tomorrow, Desalination 287 (2012) 78-81.

[5] A. Achilli, T.Y. Cath, A.E. Childress, Power generation with pressure retarded osmosis: An experimental and theoretical investigation, Journal of Membrane Science 343 (2009) 42-52.

[6] N.Y. Yip, A. Tiraferri, W.A. Phillip, J.D. Schiffman, L.A. Hoover, Y.C. Kim, M. Elimelech, Thin-film composite pressure retarded osmosis membranes for sustainable power generation from salinity gradients, Environmental Science & Technology 45 (2011) 4360-4369.

[7] A.P. Straub, S. Lin, M. Elimelech, Module-scale analysis of pressure retarded osmosis: performance limitations and implications for full-scale operation, Environmental Science & Technology 48 (2014) 12435-12444.

[8] B.J. Feinberg, G.Z. Ramon, E.M.V. Hoek, Scale-up characteristics of membrane-based salinity-gradient power production, Journal of Membrane Science 476 (2015) 311-320.

[9] L.D. Banchik, M.H. Sharqawy, J.H. Lienhard, Limits of power production due to finite membrane area in pressure retarded osmosis, Journal of Membrane Science 468 (2014) 81-89.

[10] S. Zhang, T.S. Chung, Osmotic power production from seawater brine by hollow fiber membrane modules net power output and optimum operating conditions, AIChE Journal (2015)

[11] D. Xiao, W. Li, S. Chou, R. Wang, C.Y. Tang, A modeling investigation on optimizing the design of forward osmosis hollow fiber modules, Journal of Membrane Science 392-393 (2012) 76-87.

[12] E. Sivertsen, T. Holt, W. Thelin, G. Brekke, Pressure retarded osmosis efficiency for different hollow fibre membrane module flow configurations, Desalination 312 (2013) 107-123.

[13] L.J. Hauge, The pressure exchanger - a key to substantial lower desalination cost, Desalination 102 (1995) 219-223.

[14] J.L. Prante, J.A. Ruskowitz, A.E. Childress, A. Achilli, RO-PRO desalination: An integrated low-energy approach to seawater desalination, Applied Energy 120 (2014) 104-114.

[15] M.H. Sharqawy, S.M. Zubair, J.H. Lienhard, Second law analysis of reverse osmosis desalination plants: an alternative design using pressure retarded osmosis, Energy 36 (2011) 6617-6626.

[16] G. Migliorini, E. Luzzo, Seawater reverse osmosis plant using the pressure exchanger for energy recovery: a calculation model, Desalination 165 (2004) 289-298.

[17] A. Efraty, Pressure retarded osmosis in closed circuit: a new technology for clean power generation without need of energy recovery, Desalination and Water Treatment 51 (2013) 7420-7430.

[18] A. Zhu, P.D. Christofides, Y. Cohen, Minimization of energy consumption for a two-pass membrane desalination: effect of energy recovery, membrane rejection and retentate recycling, Journal of Membrane Science 339 (2009) 126-137.

[19] A. Zhu, P.D. Christofides, Y. Cohen, Effect of thermodynamic restriction on energy cost optimization of RO membrane water desalinition, Industrial & Engineering Chemistry Research (2009) 6010-6021.

[20] S. Zhang, P. Sukitpaneenit, T.S. Chung, Design of robust hollow fiber membranes with high power density for osmotic energy production, Chemical Engineering Journal 241 (2014) 457-465.

[21] A. Efraty, Closed circuit PRO series no 2: performance projections for PRO membranes based on actual/ideal flux ratio of forward osmosis, Desalination and Water Treatment (2015) 1-11.

[22] G. Han, T.S. Chung, Robust and high performance pressure retarded osmosis hollow fiber membranes for osmotic power generation, AIChE Journal 60 (2014) 1107-1119.

[23] C.F. Wan, T.S. Chung, Osmotic power generation by pressure retarded osmosis using seawater brine as the draw solution and wastewater brine as the feed, Journal of Membrane Science 479 (2015) 148-158.

[24] K.L. Hickenbottom, J. Vanneste, M. Elimelech, T.Y. Cath, Assessing the current state of commercially available membranes and spacers for energy production with pressure retarded osmosis, Desalination (2015), in-press for publication.

Chapter 7: Design and fabrication of inner-selective thin-film composite (TFC) hollow fiber modules for pressure retarded osmosis (PRO)

7.1. Introduction

In our previous studies, we developed a robust inner-selective TFC polyethersulfone (PES) hollow fiber membrane that exhibited a power density above 25 W/m^2 using 1M NaCl solution and DI water as the feed pair at 20 bar [1, 2]. This membrane must be assembled into useful forms, i.e., modules, in order to modularize installation and operation and fully access the feasibility of PRO [3-5]. Therefore, module engineering plays an important role to optimize membrane performance for PRO in terms of increasing the membrane area per module, optimizing the flow pattern and enhancing the mechanical properties of the modules [3, 6]. However, techniques to fabricate hollow fiber modules have always been kept as trade secrets. Up to date, there are limited literatures on fabrication of scalable hollow fiber modules [7-10]. In most studies, interfacial polymerization was conducted on mini-modules comprising 3-10 pieces of hollow fiber membranes instead of scalable modules [4, 5].

In this work, we investigated the science and engineering to fabricate TFC hollow fiber module by assembling hollow fibers into a semi-pilot-scale module and subsequently conducting interfacial polymerization to form thin-film layers on the inner surfaces of the hollow fibers. These knowledge and skills are important to fabricate TFC hollow fiber modules for PRO, reverse osmosis, nanofiltration and other applications, bridging the gaps between membrane fabrication and module fabrication.

7.2. Fabrication of TFC-PES hollow fiber modules

7.2.1. Fabrication of TFC-PES hollow fiber modules

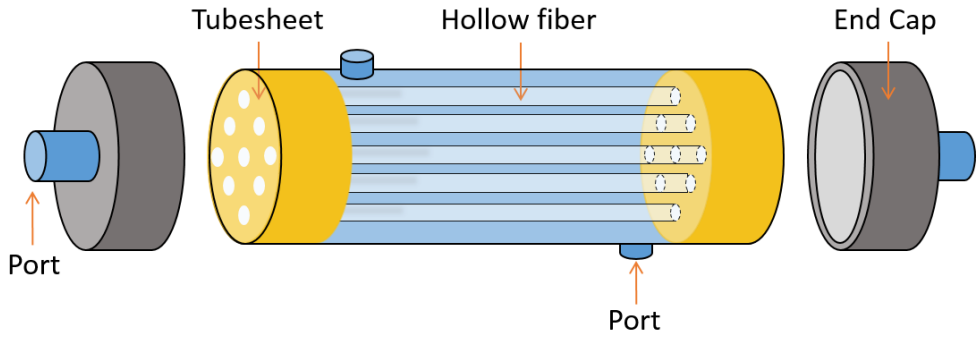

Figure 7.1 Schematic drawing of a PRO hollow fiber module

Figure 7.1 presents a general configuration of the inner-selective PRO hollow fiber module with the draw solution flowing along the lumen side and the feed solution flowing along the shell side. The housing has two ports for the introduction and exit of the feed solution, respectively. The draw solution enters the port from one end cap, flows though the fiber lumens and exits from the other end cap. Tubesheets are formed at the two ends of the housing with openings to the lumens of the hollow fiber membranes. The tubesheets work as physical barriers to separate the feed solution from the draw solution and prevent mixing. Therefore, the only path for the feed solution to meet the draw solution is by passing through the walls of the hollow fiber membranes.

7.2.2. Fabrication of PES hollow fiber modules

The step-by-step fabrication of a hollow fiber module is presented in Figure 7.2. The PES hollow fiber substrates after the glycerol post-treatment were collected into a bundle. The amount of hollow fibers in each bundle was calculated to meet the target packing density, which was defined as the volumetric fraction of the modules occupied by the hollow fibers.

$$n = \frac{\phi D^2}{d^2} \tag{7.1}$$

where n is the total number of hollow fibers in the module, ϕ is the packing density, D is the inner diameter of the module housing and d is the outer diameter of the hollow fiber.

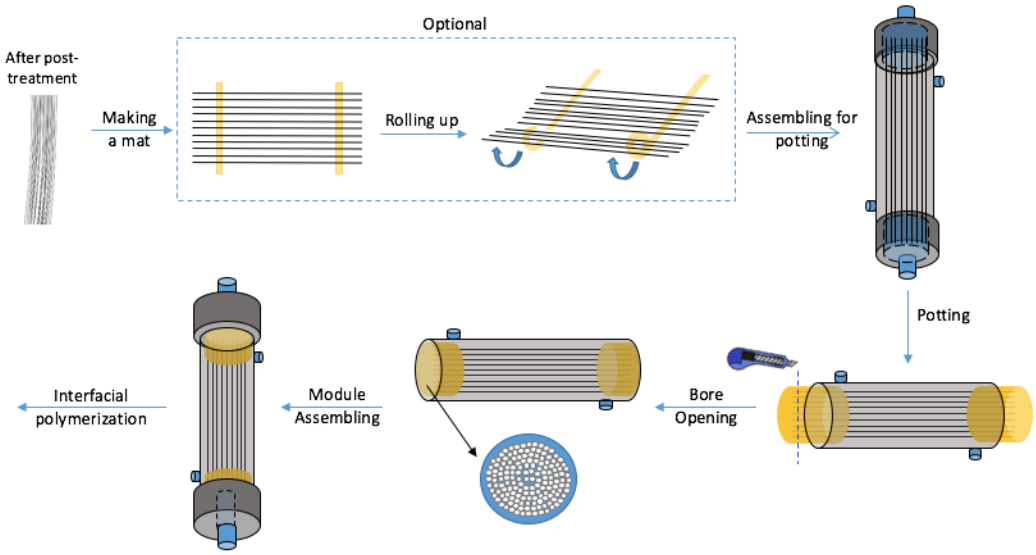

Figure 7.2 Schematic drawings of the procedures to fabricate hollow fiber modules

Hollow fiber modules with 30% and 50% packing densities were prepared. The simplest way to prepare the hollow fiber bundle is to collect the hollow fibers and arrange them in parallel randomly to form a bundle. However, when the packing density is low, the hollow fiber may not distribute uniformly and fill up the housing [11]. To overcome these shortcomings, structured hollow fiber bundles were prepared by laying down the hollow fibers in parallel at a uniform spacing to form a hollow fiber mat and then rolling up the mat to form a structured bundle [12, 13]. This method is relatively complicated but yields a more uniformly packed bundle even at a low packing density. At a high packing density, the hollow fibers can support each other and distribute more uniformly in a random packing bundle [11].

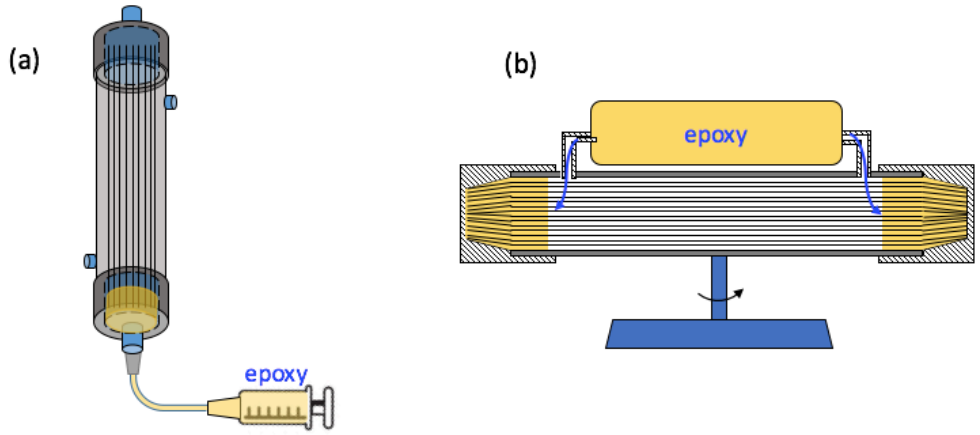

Figure 7.3 Formation of tubesheet by (a) gravitational potting (b) centrifugal potting

The bundle was then cut into a desired length and inserted to the module housing. The lumens of the hollow fibers were temporarily sealed with glue or cement to prevent intrusions of epoxy during formation of the tubesheet. Formation of the tubesheet was conducted by potting the hollow fibers into a mold filled with epoxy. Two potting techniques were widely used; namely, gravitationally potting [14] and centrifugal potting [15]. In gravitationally potting as shown in Figure 7.3 (a), the module was held vertically and the epoxy was introduced from the bottom of the mold. The epoxy gradually settled down and penetrated to the space between hollow fibers under the gravitational force. To produce a tubesheet with high packing density, centrifugal potting was used to ensure that the space between hollow fibers was filled up with epoxy. During centrifugal potting, the module and the epoxy container were fixed horizontally along the central axis of the centrifuge machine as shown in Figure 7.3 (b). Two flow channels connect the epoxy container and the two molds. Under the centrifugal force, the epoxy was sent to fill up the molds and form the tubesheets. However, centrifugal potting is electricity-consuming and its productivity is limited by the capacity of the centrifuge machine. After the epoxy was solidified, the molds

were removed and the additional epoxy was cut off to re-expose the lumens of the hollow fibers.

7.2.3. Interfacial polymerization on the inner surface of hollow fiber modules

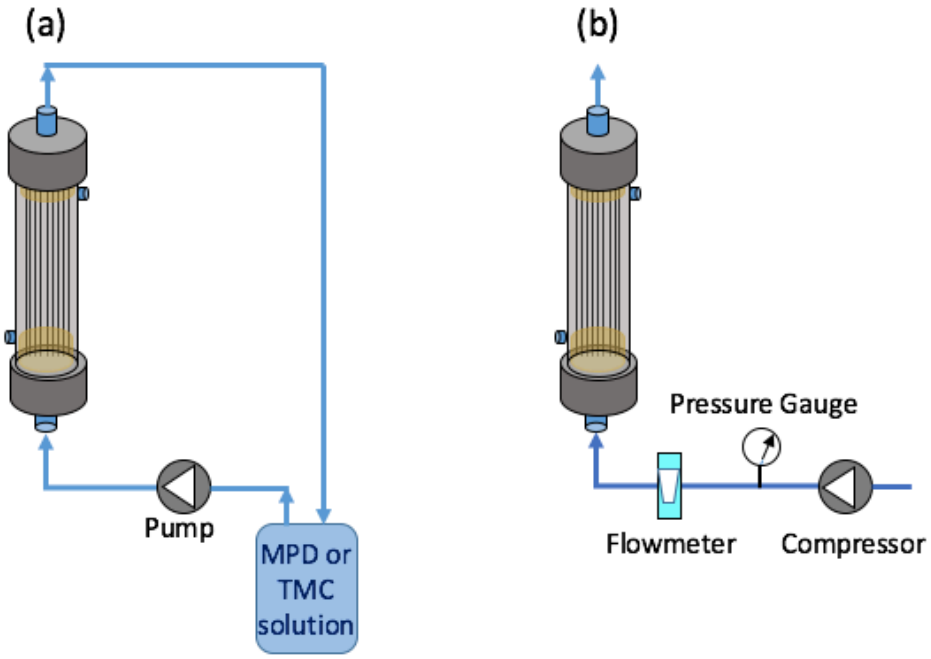

Figure 7.4 Procedures for interfacial polymerization of hollow fiber modules: (a) circulation of MPD and TMC solutions and (b) purging

Interfacial polymerization was carried out on the inner surface of each hollow fiber to form a polyamide selective layer. First, the MPD solution was circulated in the lumen at a flowrate of 0.5 ml/min per hollow fiber for a certain duration using the setup sketched in Figure 7.4 (a). A duration of 3 min was employed to fabricate coupons of hollow fibers [1, 16], but the duration was increased to 5 min and 7 min to ensure all the hollow fibers were effectively rinsed with the MPD solution. The excessive MPD solution was then removed by purging it out with compressed nitrogen for 5 min using the setup sketched in Figure 4 (b). Secondly, the TMC solution was circulated in the lumens at a flowrate of 0.5

ml/min per hollow fiber for a certain duration, ranging from 5 min as fabrication of 3 pieces of TFC-PES hollow fibers to 7 min and 9 min, to ensure polyamide layers were successfully formed on the hollow fiber membranes. The excessive TMC solution was then removed by purging it with compressed nitrogen for 2 min.

7.2.4. Detection and repair of hollow fiber membranes

7.2.4.1. Detection of broken TFC-PES hollow fibers

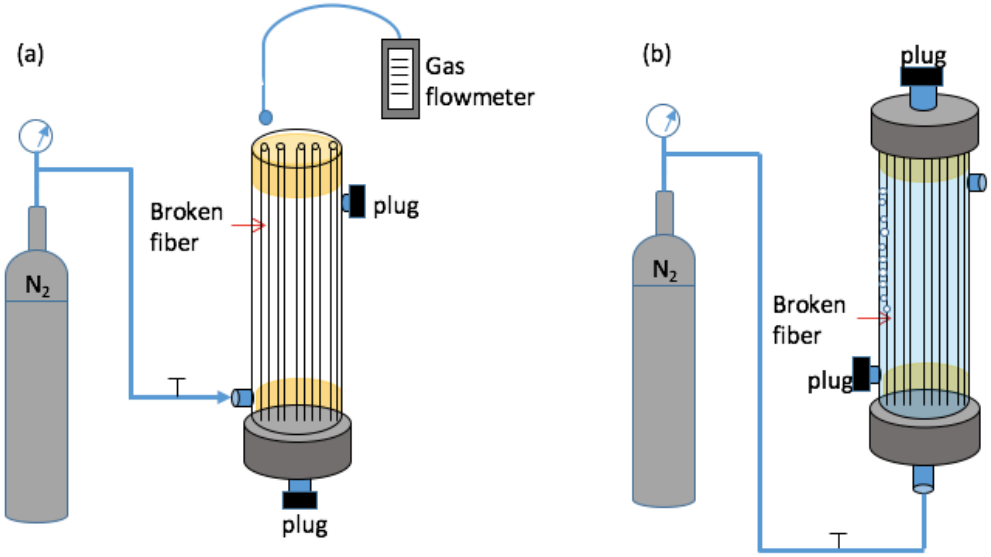

Figure 7.5 (a) A leakage test on the tubesheet to identify the broken fiber and (b) A leakage test on the hollow fiber bundle to identify the spot of leakage

The hollow fibers could be damaged during handling and high pressure testing. Such broken fibers must be identified and plugged to restore the performance of the modules. In Figure 7.5 (a), the module housing was pressurized with compressed nitrogen at 10 bar. One end cap was plugged and the other remained open. If there were any gas leakages from the shell to the lumens, they should be detected by a gas detector at the open end of the module. By moving the gas detector across the tubesheet, the broken fibers could be located.

In order to further identify the most vulnerable portion of the hollow fibers along the axis, bubbling tests were carried out by filling the housing with water and compressing the hollow fibers from inside out with nitrogen. As shown in Figure 7.5 (b), at the spot of leakage, continuous bubbling was observed.

2.4.2. Repair of hollow fiber modules

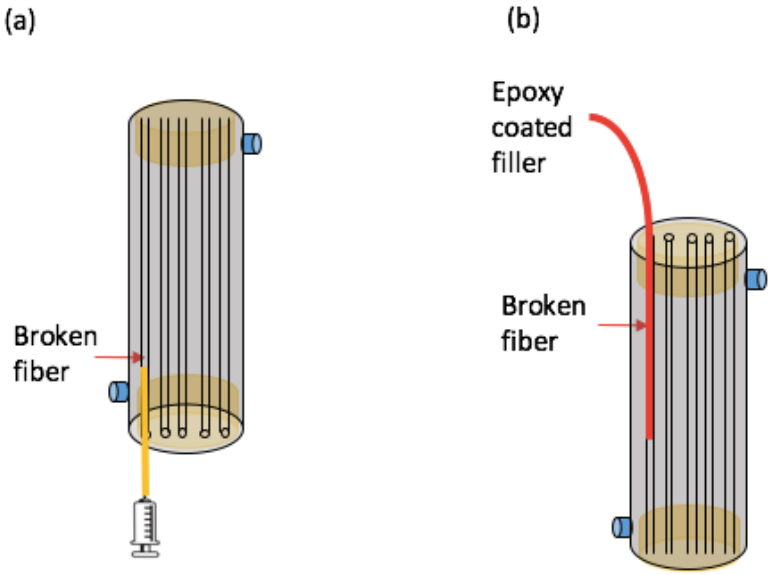

Figure 7.6 Repair of hollow fiber modules by (a) injection of epoxy and (b) insertion of epoxy coated fillers

The broken fibers were subsequently repaired after identification. Epoxy was partially solidified before injection to prevent the epoxy from flowing out. As shown in Figure 7.6 (a), a syringe pump was used to push the viscous epoxy through a small nozzle into the fibers. Another method to plug the broken fibers is by insertion of a filler, as shown in Figure 7.6 (b). The epoxy-coated filler had to be inserted at least 3 cm into the broken hollow fiber to prevent leakages and provide adequate mechanical supports against the pressure difference across the tubesheet. The epoxy was then fully solidified before tests. During

repair, it was important to apply the epoxy only to the leakage area without plugging other fibers in order to minimize the loss of effective areas.

7.3. Results and discussion

7.3.1. Structured and random packing of hollow fibers

At a packing density of 30% with 180 pieces of hollow fibers, the hollow fibers cannot disperse uniformly in the housing if they are randomly collected into a bundle. As shown in Figure 7.7 9 (a), the hollow fibers are densely packed in the central and right areas. However, there is a gap between the bundle and the housing on the left side, which will cause channeling and bypassing in the shell. Bypassing will reduce the flow going into the bundle, worsen the concentration polarization and compromise the PRO performance [17-20]. These issues can be overcome by arranging the fibers in an orderly structure as presented in Figure 7.7 9 (b). The diameter of the bundle can be controlled by changing the spacing between the hollow fibers [12, 13] to fill up the housing and therefore minimize bypassing. Another way to improve the uniformity of packing is to increase the packing density of the hollow fiber bundle [11, 21]. At an increased packing density of 50% with 300 pieces of hollow fibers, hollow fibers will effectively fill up the housing and leave a little room for fibers to move around. Though some area may have a denser packing and some area may have a looser packing, the total uniformity of the bundle is significantly improved when comparing Figure 7.7 (c) to Figure 7.7 (a). However, a higher packing density may introduce more dead zones in the shell that may enhance concentration polarization and also make the module more prone to fouling [6, 22]. The optimal packing density of the TFC-PES hollow fiber modules for PRO will be

investigated under different flow and fouling conditions in the future [23-25]. In this study, hollow fiber modules with 30% structured packing and 50% random packing were chosen for further investigations

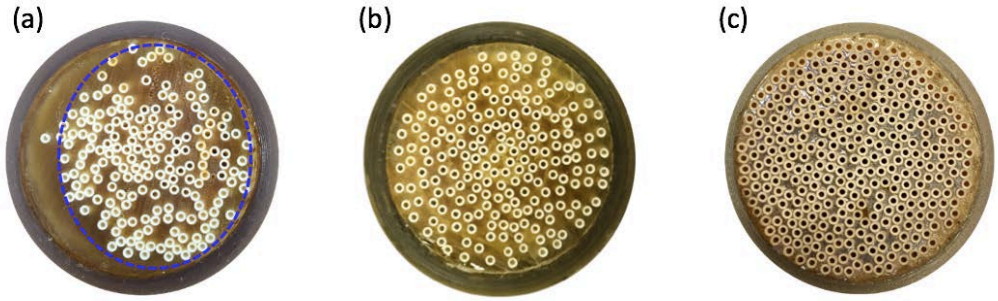

Figure 7.7 Cross sections of (a) a tubesheet of 30% random packing, (b) a tubesheet of 30% structured packing and (c) a tubesheet of 50% random packing

7.3.2. Effects of MPD and TMC circulation durations on interfacial polymerization

MPD Time (min)	A (LMH/bar)	B (LMH)
3	2.5	0.9
5	2.3	0.6
7	1.9	0.4

Table 7.1 Pure water permeability (A) and salt permeability (B) at different MPD solution circulation times

To maximize the module performance, the effects of MPD and TMC circulation durations during interfacial polymerization on the permeability properties of the polyamide layer were studied. The MPD solution was circulated through the module lumen for 3 min, 5 min or 7 min while the circulation time of the TMC solution was maintained at 5 min. Table 7.1 summarizes the A and B values of the resultant modules from each experimental condition. Both A and B values decrease with an increase in MPD circulation duration because MPD may

penetrate deeper into the substrate at a longer circulation time, possibly leading to a thicker polyamide layer [26, 27].

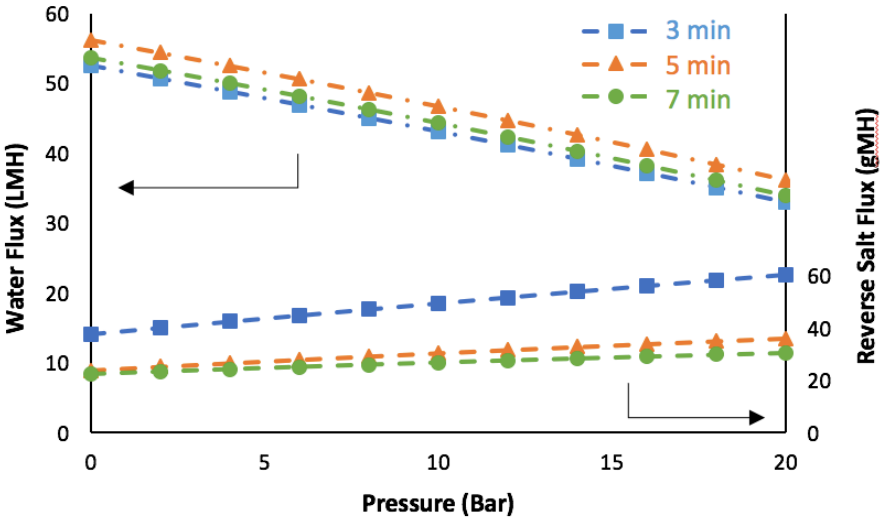

Figure 7.8 Modelled PRO performance at different circulation times of the MPD solution

To determine the optimal circulation time, the A and B values were input into a PRO model developed in our previous studies [2, 28]. The simulated PRO water flux and reverse salt flux as a function of pressure are plotted in Figure 7.8. At 3 min, even though the A value is higher, the water flux is the lowest because of the significantly higher reverse salt flux and the resulting enhanced concentration polarization [29-32]. When the MPD circulation time increases from 3 min to 5 min, the water flux is increased by 4.2% despite of a 4% decrease in the A value. This flux enhancement results from a 39.2% decrease in reverse salt flux and less concentration polarization in the PES substrates. A further increase in the MPD circulation time to 7 min only results in slight drops in both water flux and reverse salt flux. Therefore, the optimal duration to circulate the MPD solution is 5 min, which yields the highesst water flux and a moderately low reverse salt flux.

TMC Time (min)	A (LMH/bar)	B (LMH)
5	2.3	0.5
7	2.3	0.5
9	2.2	0.5

Table 7.2 Pure water permeability (A) and salt permeability (B) at different TMC solution circulation times

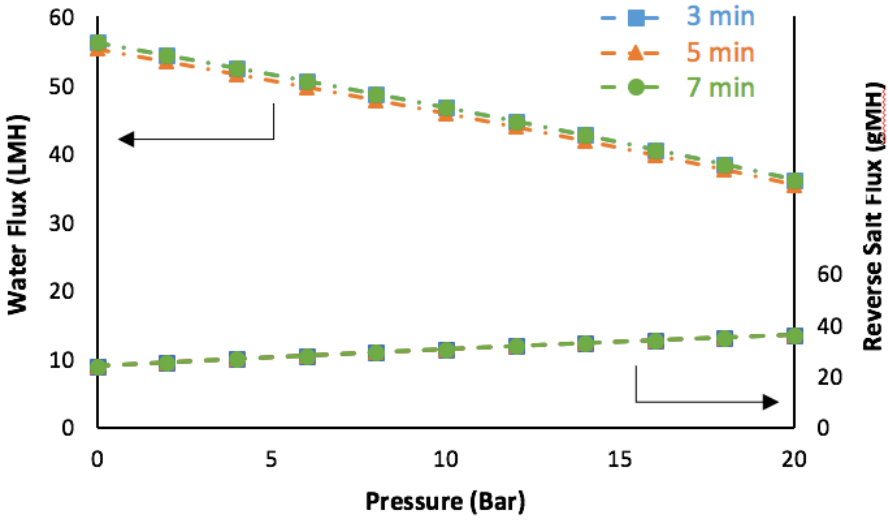

Figure 7.9 Modelled PRO performance at different circulation times of the TMC solution

Similarly, the optimal circulation time of the TMC solution is determined by maintaining the MPD circulation time at 5 min. Table 7.2 tabulates the A and B values, while Figure 7.9 shows the calculated water flux and reverse salt flux as a function of pressure. They do not vary much when the TMC circulation time increases from 5 to 9 min. This is because after 5 min, the polyamide layer is thick enough to prevent contact of the reactants and stops the polyamide layer from growing [33]. Therefore, the optimal TMC circulation time is 5 min.

7.3.3. PRO performance of hollow fiber modules

Three types of modules with packing densities of 2%, 30% and 50% were prepared. They contain 3, 180 and 300 pieces of hollow fibers, respectively. Figure 7.10 displays the evolution of their water fluxes, power densities and reverse salt fluxes as a function of pressure from 0 bar to 20 bar. In all three cases, the water flux drops at higher pressures as the driving force, defined as the difference between the osmotic pressure difference and hydraulic pressure difference, diminishes. The power densities increase continuously with increasing pressure and peak at 20 bar. Theoretically, the maximal power density can be achieved at one-half of the osmotic pressure difference, which is 24 bar when the feed pair of 1M NaCl solution and DI water is used.

The 2% packing density mini-module containing 3 hollow fibers yields the highest water flux of 66.5 LMH at 0 bar and 43.4 LMH at 20 bar. In contrast, the water flux is reduced by 13.5% on average when the packing density is increased to 30%, and it further drops by another 4.5% when the packing density is increased to 50%. As a consequence, the peak power density at 20 bar drops to 20.0 W/m^2 and 19.4 W/m^2 at 30% and 50% packing, respectively. The reasons of reductions in water flux and power density are threefold, less effective interfacial polymerization for more hollow fibers, less efficient mass transfer on the shell side at increased packing density, and loss of membrane area due to epoxy wicking.

First, it is much more challenging to ensure uniform flow distribution of the MPD and TMC solutions during interfacial polymerization in large modules

than small modules [34]. This lead to variations in the formation of polyamide selective layers. This phenomenon is also indicated by the significant higher reverse salt flux at higher packing densities as shown in Figure 7.10 (b). The reverse salt flux increases with pressure and becomes more than doubled when the packing density is increased to 30% and 50%.

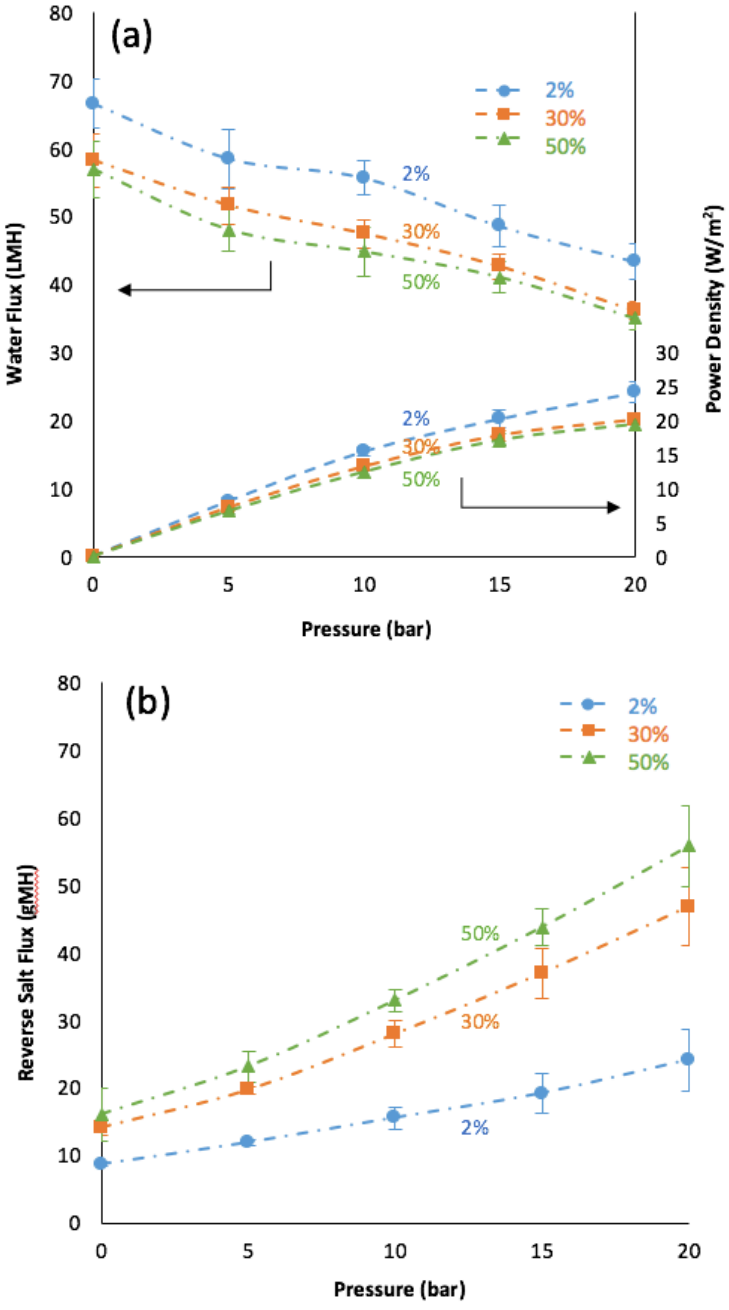

Figure 7.10 (a) water flux and power density and (b) reverse salt flux of modules with 2%, 30% and 50% packing densities under PRO tests

Moreover, the mass transport on the shell side becomes less effective at higher packing densities [17-19]. As a result, the salt accumulated in the substrates cannot be effectively washed out, causing severer concentration polarization. The combined effects of the increased reverse salt flux and the less effective mass transfer on the shell side cause the reductions of water flux and power density at higher packing densities.

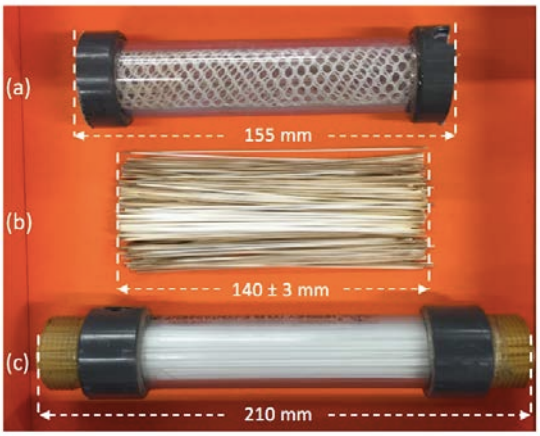

Figure 7.11 (a) the apparent effective length (used in calculations), (b) true effective length and (c) module length

Autopsy of the hollow fiber modules shows that wicking of epoxy reduces the effective membrane areas. After injecting epoxy into the potting mold, the epoxy will climb up to 8 mm on each end of the hollow fiber bundle due to the capillary actions. To measure the true effective length of the module, we dissembled the module and took out the hollow fiber bundle. The bundle was then cut off by 1mm slices until the space between hollow fibers was no more filled with epoxy. The true effective length of the module is 140 ± 3 mm, 9.7% shorted than the apparent length of 155 mm used in the calculations of water flux and power density. The loss of effective membrane area is presented in Figure 7.11, contributing to reductions in water flux and power density in the semi-pilot-scale hollow fiber modules as shown in Figure 7.10 (a). Therefore,

the water fluxes and power densities of the 30% and 50% packing modules can be improved by 9.7% if wicking of epoxy is eliminated. It is worth noting that wicking of epoxy can be less restrictive if the modules are enlarged to commercial scales, as the percentage loss of membrane areas becomes negligible.

7.3.4. Distribution of broken hollow fibers

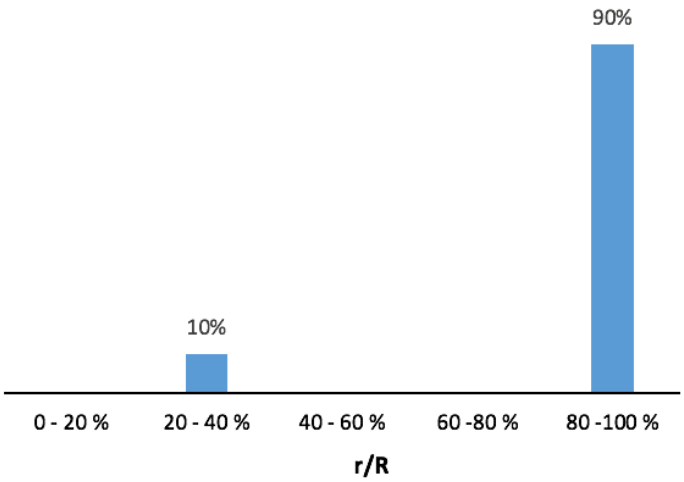

Figure 7.12 The radial distribution of broken hollow fibers in the module

Some hollow fibers may be damaged during handling and testing of the modules. Methods in Figure 7.5 (a) and (b) were employed to find out which hollow fiber was broken and which portion along the hollow fiber was broken, respectively. Figure 7.12 shows the radial distribution of broken membranes in the hollow fiber bundle. The x-axis is the relative location of the bundle with 0% being the center and 100% being the outermost edge of the bundle. 90% of the broken fibers are on the outer region of the hollow fiber bundles. The broken membranes are probably caused by damages during handling and the damaged areas become the weak points of the membranes. They may burst under high pressure tests.

The axial distribution of the broken spots is shown in Figure 7.13. Most of the modules are broken in the middle areas. This may arise from the fact that the hollow fiber bundle is axially compressed and radially expanded during insertion into the housing. It not only forms an expanded belly region in the middle of the bundle but also being pushed against the housing, thus it gets damaged due to abrasion. This also explains why most broken fibers are on the outermost region of the bundle.

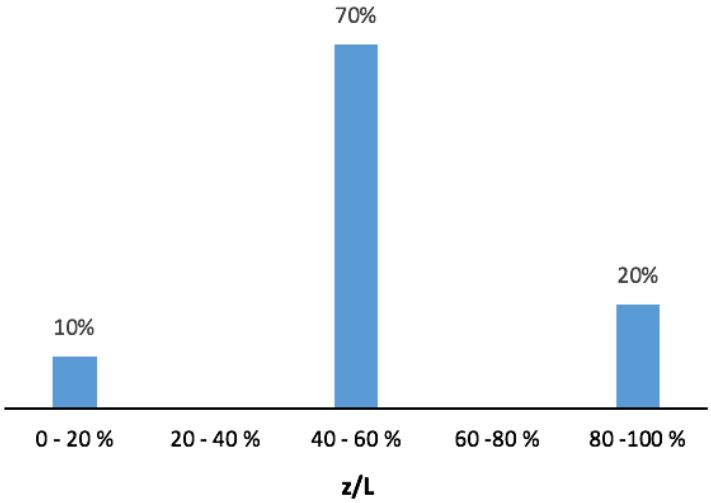

Figure 7.13 The axial distribution of leakages in the module

This problem is solved by wrapping the bundle with protective net during insertion into the housing. The net needs to be porous and flexible to prevent introducing addition resistance to the flow or hurt the hollow fiber membranes. Figure 7.14 (a) and (b) show the modules with and without the protective net, respectively. This method can prevent the bundle from expanding and protect the fibers from abrasion. In addition to the 70% damage in the middle portion of the hollow fiber bundle, a total of 30% damages are observed on the two ends of the bundle. Because the two ends contact with the tubesheets are partially coated with epoxy due to epoxy wicking, this portion of the fibers becomes

brittle and fragile. They can be easily damaged by the impact force of water and fluctuating pressure and flowrate.

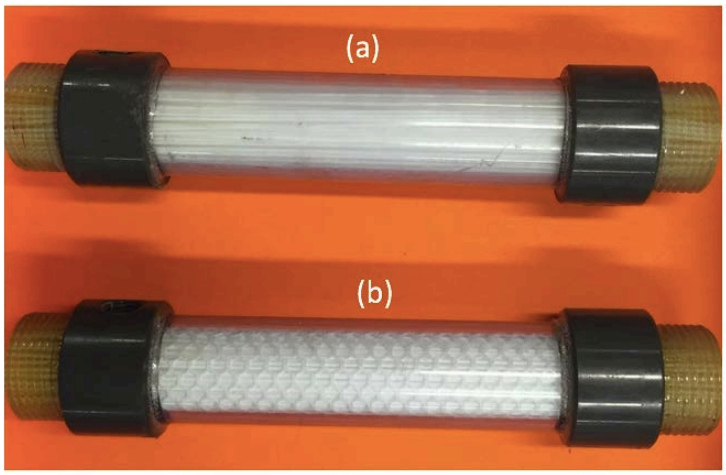

Figure 7.14 hollow fiber modules (a) without and (b) with the protective net

7.3.5. Modules repaired by epoxy-coated fillers and injection of epoxy

The damaged hollow fiber modules were then repaired by using epoxy-coated fillers and injection of epoxy. Figure 7.15 (a) and (b) show the comparisons of their PRO performances with undamaged ones. Modules repaired with fillers have a peak power density of 18.4 W/m^2, 9% lower than 20.0 W/m^2 of the undamaged modules, while those repaired with injection of epoxy only have a peak power density of 14.0 W/m^2 at 15 bar. In summary, modules repaired with fillers have a 12.3% higher power density and a 55.6% lower reverse salt flux than those repaired with epoxy injection. This indicates that the injection of epoxy still leaves some small unsealed defects on the membranes. Moreover, the mechanical strength of the modules repaired with epoxy injection is weaker and can only sustain a pressure of 15 bar. Clearly, injection of epoxy is less effective because the injected epoxy may flow out from the fibers through the small broken area and contact other fiber. The fibers contacted with epoxy will become brittle and break under vibration and impact. Therefore, insertion of the

epoxy-coated fillers is the more effective method. This repair method is also less tedious because it required to identify the broken hollow fibers from only one end of the modules instead of both ends. The fillers need to have good adhesion with epoxy and a slightly bigger dimension than the inner diameter of the hollow fibers to ensure an effective sealing.

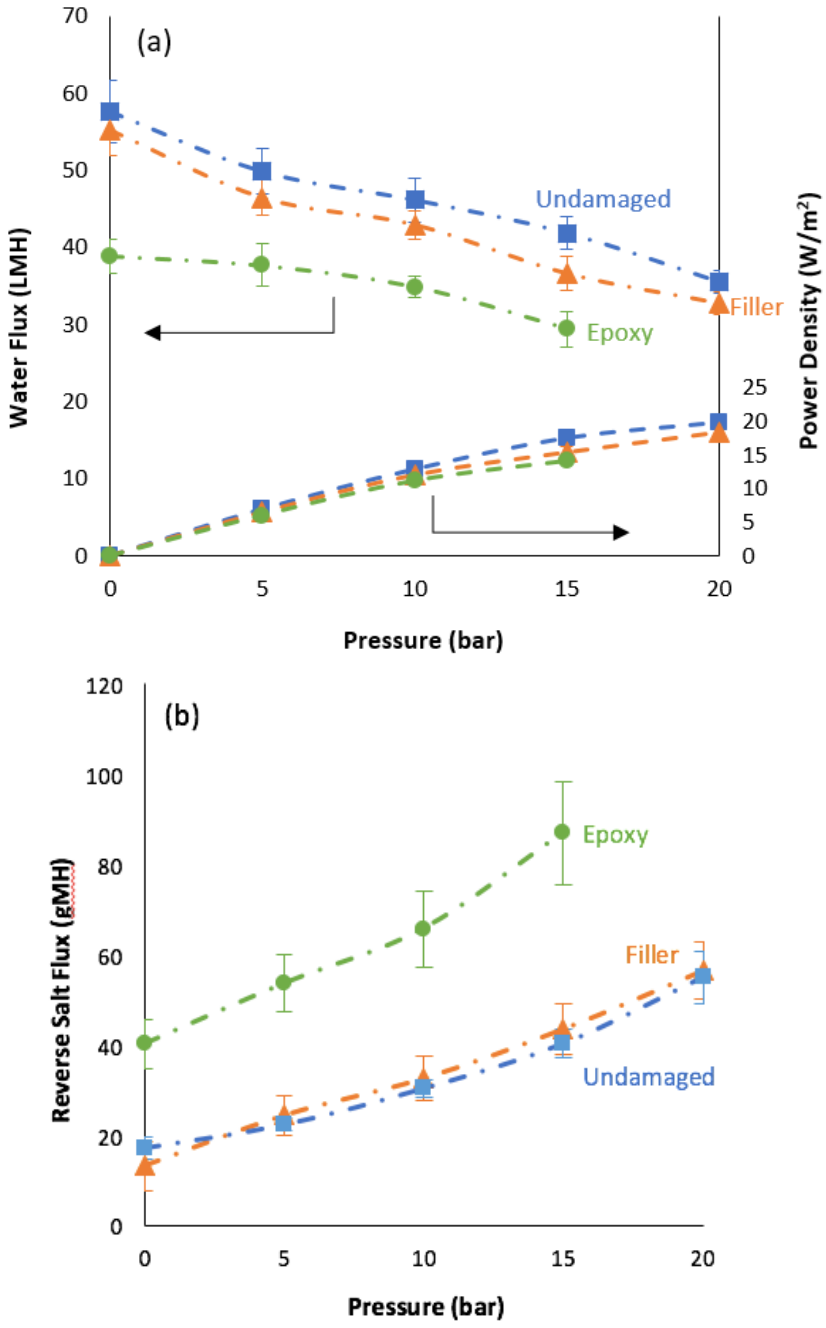

Figure 7.15 (a) water flux and power density and (b) reverse salt flux of 30% packing hollow fiber modules (undamaged and damaged but being repaired by epoxy or fillers)

7.4. Conclusions

For the first time, the protocol to fabricate semi-pilot-scale hollow fiber modules, conduct interfacial polymerization, identify and repair leakages is developed. TFC-PES hollow fiber modules with 30% structured packing and 50% random packing are successfully prepared. When the packing of hollow fibers is loose, it is important to arrange the hollow fibers in an orderly structure to achieve uniform distribution of hollow fibers. The optimal packing density of the TFC-PES hollow fiber modules will be determined by different flow, fouling conditions and economic factors. The respective peak power densities of a 30% packing module and a 50% packing modules at 20 bar using 1M NaCl solution and DI water as feed pair are 20.0 W/m^2 and 19.4 W/m^2, respectively. Even though they are lower than the value of 24.1 W/m^2 when only three coupons of hollow fiber membranes are tested, the power densities achieved are the highest among scalable PRO modules under the same testing condition. Broken hollow fiber membranes can be effectively plugged with epoxy-coated filler to restore the PRO performance. The performance of the PRO modules can be improved by further optimizing the interfacial polymerization conditions, promote mixing on the shell side and prevent wicking of epoxy onto the hollow fiber membranes. Other engineering issues, such as enhancement of the mechanical strength and durability of the modules, need to be addressed before making of commercial scale TFC-PES hollow fiber modules.

References:

[1] S. Zhang, P. Sukitpaneenit, T.S. Chung, Design of robust hollow fiber membranes with high power density for osmotic energy production, J. Chem. Eng. 241 (2014) 457-465.

[2] C.F. Wan, T.S. Chung, Osmotic power generation by pressure retarded osmosis using seawater brine as the draw solution and wastewater brine as the feed, J. Membr. Sci. 479 (2015) 148-158.

[3] N.C. Mat, Y. Lou, G.G. Lipscomb, Hollow fiber membrane modules, Curr. Opin. Chem. Eng. 4 (2014) 18-24.

[4] S. Sarp, Z. Li, J. Saththasivam, Pressure retarded osmosis (PRO): past experiences, current developments, and future prospects, Desalination (2016).

[5] A.P. Straub, A. Deshmukh, M. Elimelech, Pressure-retarded osmosis for power generation from salinity gradients: is it viable?, Energy Environ. Sci. 9 (2016) 31-48.

[6] E. Sivertsen, T. Holt, W. Thelin, G. Brekke, Pressure retarded osmosis efficiency for different hollow fibre membrane module flow configurations, Desalination 312 (2013) 107-123.

[7] D. F. Li, R. Wang, T. S. Chung, Fabrication of lab-scale hollow fiber membrane modules with high packing density, Sep. Purif. Technol. 40 (2004) 15-30.

[8] M.M. Teoh, S. Bonyadi, T.S. Chung, Investigation of different hollow fiber module designs for flux enhancement in the membrane distillation process, J. Membr. Sci. 311 (2008) 371-379.

[9] X. Yang, R. Wang, A.G. Fane, Novel designs for improving the performance of hollow fiber membrane distillation modules, J. Membr. Sci. 384 (2011) 52-62.

[10] K. L. Chong, N. Peng, Y. Hang, G. G. Lipscomb, T. S. Chung, Food sustainability by designing and modelling a membrane controlled atmosphere storage system, J. Food Eng. 114 (2013) 361–374.

[11] S. Zhang, T.S. Chung, Minimizing the instant and accumulative effects of salt permeability to sustain ultrahigh osmotic power density, Environ. Sci. Technol. 47 (2013) 10085-10092.

[12] J.K. Niermeyer, Thermoplastic hollow fiber membrane module and method of manufacture, US Patent 5,695,702 (1997).

[13] E.A. Philip, J.C. Schletz, J.A. Jensvold, W.E. Tegrotenhuis, W. Allen, F.L. Coan, S. K.L., D.O. Clark, V.W.J. Wait, Loom processing of hollow fiber membranes, US Patent 5,598,874 (1997).

[14] A. Azran, G. Dagan, Method for potting or casting inorganic hollow fiber membranes into tube sheets, US Patent 6,270,714 B1 (2001).

[15] J.M. Maxwell, W.E. Moore, R.D. Rego, Fluid separation process and apparatus, US Patent 3,339,341 (1967).

[16] G. Han, T.S. Chung, Robust and high performance pressure retarded osmosis hollow fiber membranes for osmotic power generation, AIChE J. 60 (2014) 1107-1119.

[17] L. Bao, G.G. Lipscomb, Mass transfer in axial flows through randomly packed fiber bundles with constant wall concentration, J. Membr. Sci. 204 (2002) 207-220.

[18] L. Bao, G.G. Lipscomb, Effect of random fiber packing on the performance of shell-fed hollow-fiber gas separation modules, Desalination 146 (2002) 243-248.

[19] L. Bao, G.G. Lipscomb, Well-developed mass transfer in axial flows through randomly packed fiber bundles with constant wall flux, Chem. Eng. Sci. 57 (2002) 125-132.

[20] A.A. Merdaw, A.O. Sharif, G.A.W. Derwish, Mass transfer in pressure-driven membrane separation processes, part I, J. Chem. Eng. 168 (2011) 215-228.

[21] J. Wu, V. Chen, Shell-side mass transfter performance of randomly packed hollow fiber modules, J. Membr. Sci. 172 (2000) 59-74.

[22] E. Sivertsen, T. Holt, W. Thelin, G. Brekke, Modelling mass transport in hollow fibre membranes used for pressure retarded osmosis, J. Membr. Sci. 417-418 (2012) 69-79.

[23] D. Xiao, W. Li, S. Chou, R. Wang, C.Y. Tang, A modeling investigation on optimizing the design of forward osmosis hollow fiber modules, J. Membr. Sci. 392-393 (2012) 76-87.

[24] S.C. Chen, G.L. Amy, T.S. Chung, Membrane fouling and anti-fouling strategies using RO retentate from a municipal water recycling plant as the feed for osmotic power generation, Water Res. 88 (2016) 144-155.

[25] S.C. Chen, C.F. Wan, T.S. Chung, Enhanced fouling by inorganic and organic foulants on pressure retarded osmosis (PRO) hollow fiber membranes under high pressures, J. Membr. Sci. 479 (2015) 190-203.

[26] A.K. Ghosh, E.M.V. Hoek, Impacts of support membrane structure and chemistry on polyamide-polysulfone interfacial composite membranes, J. Membr. Sci. 336 (2009) 140-148.

[27] X. Li, K.Y. Wang, B. Helmer, T.S. Chung, Thin-film composite membranes and formation mechanism of thin-film layers on hydrophilic

cellulose acetate propionate substrates for forward osmosis processes, Ind. Eng. Chem. Res. 51 (2012) 10039-10050.

[28] C.F. Wan, T.S. Chung, Energy recovery by pressure retarded osmosis (PRO) in SWRO–PRO integrated processes, Appl. Energ. 162 (2016) 687-698.

[29] Q. She, X. Jin, C.Y. Tang, Osmotic power production from salinity gradient resource by pressure retarded osmosis: effects of operating conditions and reverse solute diffusion, J. Membr. Sci. 401-402 (2012) 262-273.

[30] A. Achilli, J.L. Prante, N.T. Hancock, E.B. Maxwell, A.E. Childress, Experimental results from RO-PRO: a next generation system for low-energy desalination, Environ. Sci. Technol. 48 (2014) 6437-6443.

[31] A. Achilli, T.Y. Cath, A.E. Childress, Power generation with pressure retarded osmosis: an experimental and theoretical investigation, J. Membr. Sci. 343 (2009) 42-52.

[32] A.A. Merdaw, A.O. Sharif, G.A.W. Derwish, Mass transfer in pressure-driven membrane separation processes, part II, J. Chem. Eng. 168 (2011) 229-240.

[33] M. Liu, Y. Zheng, S. Shuai, Q. Zhou, S. Yu, C. Gao, Thin-film composite membrane formed by interfacial polymerization of polyvinylamine (PVAm) and trimesoyl chloride (TMC) for nanofiltration, Desalination 288 (2012) 98-107.

[34] J.K. Park, H.N. Chang, Flow distribution in the fiber lumen side of a hollow-fiber module, AICHE J. 32 (1986) 1937-1947.

Chapter 8: Recommendation and future works

Based on the experimental results and conclusions obtained from current research, the following recommendations may provide further insight for future work related to the development of membrane materials with high separation properties and the fabrication of high performance membranes for engineered osmosis processes.

8.1. SWRO-PRO life cycle assessment

Based on our previous studies in Chapter 5 and 6, integration of PRO with SWRO can achieve 40% energy saving for a 25% recovery SWRO plant and 45% energy saving for a 50% recovery SWRO plant. This integration can potentially double the operating profit of desalination. However, incorporation of PRO to existing SWRO systems requires additional equipment, piping and instrument, and membrane. A full life cycle assessment, including capital expenditure (Capex) and operating expenditure (Opex), is imperative to investigate the economic feasibility of SWRO-PRO.

8.2. Antifouling Strategy

A big hurdle to commercialize the PRO technology is the fouling upon and within the porous membrane substrate, especially when the NEWater reject is used as the feed solution. Fouling will not only reduce the power density of the membrane but also incur additional costs associated with cleaning chemicals and equipment. More than 75% drops in water flux and power density are observed when the feed solution is changed from deionized water to the NEWater reject. This is because the porous structure of the substrate is plugged

by the foulants from the NEWater reject. Ultrafiltration and nanofiltration are used to pretreat the NEWater reject, but only marginal improvements are seen. The team discovers that the inorganic fouling of hydroxyapatite $Ca_5(PO_4)_3(OH)$ is the main reason for the power density reduction. By reducing the pH of the NEWater reject to 5.5, the formation of hydroxyapatite is prohibited and only 2.3% reduction in power density is observed after 200 minutes of operation. Ethylenediaminetetraacetic acid (EDTA) is also used to further mitigate the hydroxyapatite and silica fouling. In addition to the pretreatments of the NEWater reject, molecularly designed anti-fouling hollow fiber membranes have been prepared by grafting a layer of hyper-branched polyglycerol (HPG) or zwitterionic copolymer on the porous substrates. The anti-fouling membranes only have a reduction of ~30% in power density as compared to the 60%-70% reduction of the unmodified membranes. Moreover, fouling is more reversible on the anti-fouling membranes, which show 98% water flux recovery after cleaning.

However, UF and NF pretreatments can only marginally mitigate fouling and recovery the power density of the PRO membrane. High dosage of acid for HP adjustment and anticipant renders this approach uneconomic and unpractical. Development of anti-fouling membrane involves complicated synthesis and modification of the TFC-PES membrane. More effects should be focuses the development a practical and effective combined strategy of pretreatment, chemical dosage and membrane modifications to reduce scaling and fouling on the PRO membrane. Eventually a long term test and a full life cycle assessment are necessary to determine the best anti-fouling strategy.

8.3. SWRO-PRO pilot testing

The PRO pilot system, as presented in Figure 8.1, was built and commissioned in March 2016. This pilot plant was designed for 100W power generation/recovery. 60 1-inch modules in 6 groups of 10 modules with a total membrane area of ~5.6 m^2 are required to reach a total power density of 100W. A SWRO unit was incorporated in the system to generate the concentrated seawater brine for PRO. The pressurized brine is subsequently diluted in the PRO unit and drive the PX to pressurize the seawater feed to SWRO, in order to reduce the energy consumption of SWRO.

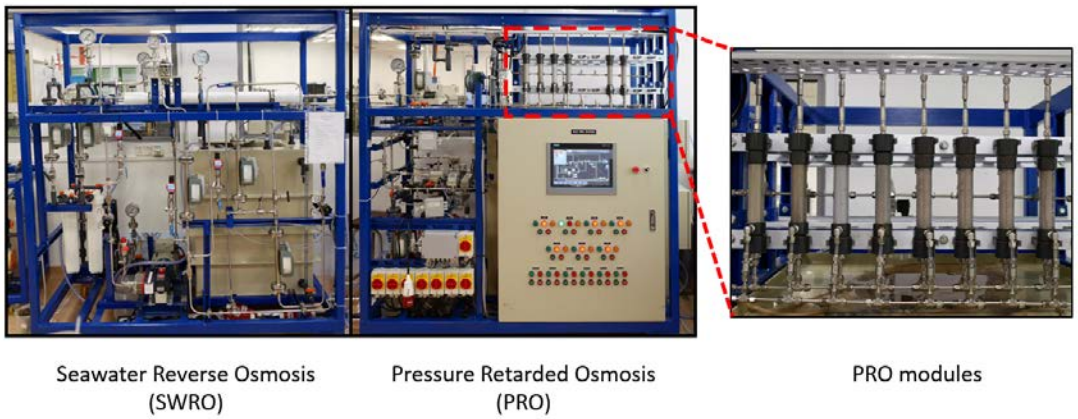

Figure 8.1 SWRO-PRO integrated pilot system in NUS

With the SWRO-PRO pilot system, the following aspects are to be investigated.

(1) Long term performance and stability of the PRO membrane/modules;

(2) The effects of feed solution recovery and draw solution dilution;

(3) The optimal operating conditions to minimize the energy consumption；

(4) The antifouling and cleaning strategy to maintain constant performance.

(5) The feasibility to fully scale up the SWRO-PRO system.

A list of publications

[1] **C.F. Wan**, B. Li, T. Yang, T.S. Chung, Design and fabrication of inner-selective thin-film composite (TFC) hollow fiber modules for pressure retarded osmosis (PRO), Sep. Purif. Technol. 172 (2017) 32-42

[2] Z.L. Cheng, X. Li, Y Feng, **C.F. Wan**, T.S. Chung, Tuning water content in polymer dopes to boost the performance of outer-selective thin-film composite (TFC) hollow fiber membranes for osmotic power generation, J. Membr. Sci. 524 (2017) 97-107

[3] D. Zhao, G. Qiu, X. Li, **C.F. Wan**, K. Lu, T.S. Chung, Zwitterions coated hollow fiber membranes with enhanced antifouling properties for osmotic power generation from municipal wastewater, Water Res. 104 (2016) 389-396

[4] G. Han, J. Zhou, **C.F. Wan**, T. Yang, T.S. Chung, Investigations of inorganic and organic fouling behaviors, antifouling and cleaning strategies for pressure retarded osmosis (PRO) membrane using seawater desalination brine and wastewater, Water Res. 103 (2016) 264-275

[5] **C.F. Wan**, T.S. Chung, Maximize the operating profit of a SWRO-PRO integrated process for optimal water production and energy recovery, Renew. Energy 94 (2016) 304-313.

[6] W. Gai, X. Li, J.Y. Xiong, **C.F. Wan**, T.S. Chung, Evolution of micro-deformation in inner-selective thin film composite hollow fiber membranes and its implications for osmotic power generation, J. Membr. Sci. 516 (2016) 104-112

[7] J.Y. Xiong, Z.L. Cheng, **C.F. Wan**, S.C. Chen, T.S. Chung, Analysis of flux reduction behaviors of PRO hollow fiber membranes: Experiments, mechanisms and implications, J. Membr. Sci. 505 (2016) 1-14.

[8] **C.F. Wan**, T.S. Chung, Energy recovery by pressure retarded osmosis (PRO) in SWRO–PRO integrated processes, Appl. Energ. 162 (2016) 687-698.

[9] T. Cai, X. Li, **C.F. Wan**, T.S. Chung, Zwitterionic polymers grafted poly (ethersulfone) hollow fiber membranes and their antifouling behaviors for osmotic power generation, J. Membr. Sci. 497 (2016) 142-152

[10] T.S. Chung, L. Luo, **C.F. Wan**, Y. Cui, G. Amy, What is next for forward osmosis (FO) and pressure retarded osmosis (PRO), Sep. Purif. Technol. 156 (2015) 856-860

[11] G. Han, J. Zuo, **C.F. Wan**, T.S. Chung, Hybrid pressure retarded osmosis–membrane distillation (PRO–MD) process for osmotic power and clean water generation, Environmental Science: Water Research & Technology 1 (2015) 507-515

[12] S.C. Chen, **C.F. Wan**, T.S. Chung, Enhanced fouling by inorganic and organic foulants on pressure retarded osmosis (PRO) hollow fiber membranes under high pressures, J. Membr. Sci. 479 (2015) 190-203.

[13] **C.F. Wan**, T.S. Chung, Osmotic power generation by pressure retarded osmosis using seawater brine as the draw solution and wastewater brine as the feed, J. Membr. Sci. 479 (2015) 148-158.